A Consensus Framework for Measuring Drug Synergy

By

Christian Thomas Meyer

Dissertation

Submitted to the Faculty of the

Graduate School of Vanderbilt University

in partial fulfillment of the requirements

for the degree of

DOCTOR OF PHILOSOPHY

in

Chemical and Physical Biology

March 31st, 2020

Nashville, Tennessee

Approved:

Professor Ken S. Lau, Ph.D.

Professor Vito Quaranta, M.D.

Professor Christopher V. Wright, Ph.D.

Professor Vivian Gama, Ph.D.

Professor Carlos F. Lopez, Ph.D.

This work is dedicated to Marlin Bidne, Genie Galbreth, John Gunther, Dawn Sandoval, Leah Stufflebam, John Williams, Cindy Post, and all those who await a cure.

ACKNOWLEDGMENTS

This work is the product of many hands and, though I cannot do justice to all of them, what follows is a poor attempt to acknowledge their impact on this work and my life.

First, I am the grateful to the funding sources which made this work possible. Specifically, I was funded by the National Science Foundation (NSF) through the Graduate Student Fellowship Program (GRFP; Award #1445197). The flexibility of this funding model was instrumental in the discoveries disclosed herein. Others who worked on this project were funded by NSF awards (MCB 1411482 and MCB 1715826) and awards from the National Institutes of Health (U54-CA217450, U01-CA215845, R01-186193). Finally, I am grateful for the VICB Armstrong award for research excellence which is funded by the Armstrong family. The honor of this award is reflective of the impact of Richard Armstrong on the Vanderbilt community.

This work would not exist without the outstanding mentorship I received during my tenure at Vanderbilt. Each member of my thesis committee contributed substantially the shape of this work. Dr. Vivian Gama was the genesis of the functional genomics screen work and I am grateful for the innate curiosity she brought to committee meetings. I am grateful to Dr. Ken Lau for chairing the committee and always working as my advocate during meetings. I am grateful to Dr. Carlos Lopez whose mentorship on the theoretical aspects of this work grounded this project on rigorous foundations. I am also much indebted to Dr. Chris Wright, who served as my co-mentor and tolerated my weekly presence at his lab meetings. His scientific acumen continues to provide guidance on how this work can translate into new biological insights. Finally, words cannot convey my gratitude to my mentor Dr. Vito Quaranta. Vito's gifts as a leader combine a brilliant mind for science with deep compassion for his trainees. I can only hope to pay his mentorship forward.

I have also had the privilege of working with a remarkable group of scientists at Vanderbilt and abroad who have been instrumental in this work. First and foremost, I would like to thank Dr. David Wooten, my co-conspirator in this work, without whom this work would have been fundamentally wrong ($\alpha_{12}^{h_1} = \alpha_{21}^{h_2}$). I am inestimably grateful to have such a brilliant colleague.

Additionally, the hard work of Dr. Joshua Bauer, Dr. Darren Tyson, Dr. Christine Lovly, and Dr. David Westover were instrumental in translating the equations on paper into experiments and subsequently potential therapeutic avenues. I am also the beneficiary of many conversations from members in the Quaranta, Lopez, and Wright labs. Specifically, Sarah Maddox Groves, Corey Hayford, Dr. Bishal Paudel, Dr. Alex Lubbock, Dr. Leonard Harris, Michael Ray, Dr. Brenda Jarvis, and Xiao-dun Yang all contributed time and thoughts which made this work better.

The broader support system at Vanderbilt has also been critical. Carolyn Berry and Beth Bowman in the BRET Office as well as Lois Alksninis, Neeru Paudel, Dr. Amanda Linkous, and Dr. Lourdes Estrada of the Quaranta Lab have all helped me navigate the many administrative and personal bumps along the path to a Ph.D. I am grateful to Mary Michael Woolman for her help in managing the NSF grant including the annual education supplement which was used to buy computer resources for this work. I would also like to thank members of the QCB and CPB programs for their continued support. In particular, I have been extraordinarily blessed by Patty Mueller and Dr. Bruce Damon who remain tireless in their advocacy for students. Finally, I would like to thank Dr. Dave Piston who first took a chance by recruiting a physics major with no biology since high school to the QCB program. Thank you.

Beyond Vanderbilt, I am grateful to colleagues around the world whose work has impacted my own. As Sir Isaac Newton said, "if I have seen farther, it is because I stood on the shoulders of Giants." In particular Dr. Chris Austin, Dr. Matt Hall, and Dr. Lu Chen at the National Center for Advancing Therapeutics (NCATS) have been early advocates for this work. Additionally, I am grateful to the Dr. Ernesto Andrianantoandro and Dr. Kusumika Mukherjee, the editors at *Cell Systems* and *Trends in Pharmacological Sciences*, respectively. Their guidance and insights were critical to the publishing this work—which I consider by far my greatest accomplishment.

It has been exceedingly gratifying to see some of the technology developed in this work transitioned to the cooperate sector. For this I have to thank my colleagues at Parthenon Therapeutics, Dr. Laurent Audoly, Dr. Amanda Linkous, Olga Granaturova, and Jérõme Windsor who inspire me daily. In particular, I would like to thank Laurent for his visionary approach to impacting patients'

lives. I look forward to seeing this family grow.

Finally, there are so many personal connections which have sustained and supported me through this work. I would like to thank Drs. Abbie and Steve Freeman for their unwavering support and encouragement. They reside at the germinal center behind the idea of getting a Ph.D. I am also inestimably grateful for Mamma Lisa (Bealhen) and Channah Edwards who are family to me. Their support and prayers have never faltered. I have been continuously blessed by my dear sister-in-laws Emma Franklin, Anna Veers, and (soon to be Dr.) Maggie Veers. Now having both, I think sisters are much preferred to brothers...except when the brothers are Carl, Peter, and Eric Meyer. Brothers, I love you so much and I am excited to see your stars on the horizon. I am also grateful to you guys for bringing such wonderful new sisters, Kyra Jensen and Maggie Meyer, into my family.

In addition, I would like to thank Dr. Marvin and Sonja Meyer (Grandma and Grandpa) along with Holli and Michael Giebler for the endless support and love they continue to shower on me and my family even away from Colorado. Also I would like to thank Rosetta Bidne (Grandma Zetta) for her support and and prayers. She has always believed great things of her grandchildren.

To my in-laws Dr. Paul and Karen Veers (Oma and Opa), thank you for your love and prayers which have filled these six years. Christ has given you as excellent examples of His image and I aspire to give the same grace you have given me.

To my own parents, having children of my own has made it incredibly clear how much of what I have originated from you. God blessed me abundantly with you as my parents. Thank you for loving, diapering, cheering, driving, teaching, wrestling, laughing (at), and feeding me. I can only hope my sons feel for me (someday) as I do for you (right now)—grateful.

To my beautiful wife, Elisabeth, and sons, Elijah (Paul) and Caleb (Thomas), no words can convey, no heart can contain the riches of your love in my life. Without you this work is empty and meaningless. With you my life is full of hope, peace, and love. From my deepest heart, thank you.

And finally, to the God to whom the glory belongs, to the Son to whom I belong, and to the Spirit whose movement inspired this work on a warm bike ride home in June, thank you.

TABLE OF CONTENTS

LIST OF TABLES

LIST OF FIGURES

LIST OF ABBREVIATIONS

Abbreviation

AIC Akaike information criterion

CCLE Cancer Cell Line Encyclopedia

CI Combination Index

cpm counts per million

DEG Differentially Expressed Gene

DEP Dose Equivalence Principle

EDM Effective Dose Model

EOB Excess Over Bliss

GPCR G-Protein Coupled Receptor

HSA Highest Single Agent

MCMC Monte Carlo Markov Chain

MSP Multiplicative Survival Principle

MuSyC Multidimensional Synergy of Combinations

NSCLC Non-Small Cell Lung Cancer

ODE Ordinary Differential Equation

PDE Partial Differential Equation

RT-qPCR quantitative Reverse Transcription Polymerase Chain Reaction

TCGA The Cancer Genome Atlas

Genes

BRAF serine/threonine-protein kinase B-Raf

EGFR Epidermal Growth Factor Receptor

HDAC Histone deacetylase

MEK MAP2K1

NOX5 NAPDH oxidase 5

Symbols

α_{12} Fold change in the potency (C_2) of $[d_2]$ induced by drug 1.

α_{21} Fold change in the potency (C_1) of $[d_1]$ induced by drug 2.

β Percent increase (or decrease) in max effect with both drugs over the most efficacious single drug ($\beta := \frac{min(E_1,E_2)-E_3}{E_0-min(E_1,E_2)}$).

γ_{12} Fold change in the cooperativity (h_2) of $[d_2]$ induced by drug 1.

γ_{21} Fold change in the cooperativity (h_1) of $[d_1]$ induced by drug 2

$A_{1,2}$ Percent of affected by both drug 1 and drug 2.

A_1,A_2 Percent of affected by drug 1 and drug 2, respectively.

C_1,C_2 The concentration of drug required to achieve 50% of the maximal effect (*i.e.*, EC_{50}).

d_1, d_2 Drug concentrations for drug pair.

E_0 The basal effect $E_d(d1 = d2 = 0)$.

E_1,E_2 Maximal efficacy of drugs 1 and 2 in isolation. (*i.e.*, E_{max})

E_3 Maximal efficacy of the combination of drugs 1 and 2.

E_d Measured effect at (d_1, d_2).

h_1,h_2 Hill coefficients for dose response curves of drug 1 and 2 in isolation.

U Percent Unaffected.

Chapter 1

Charting the Fragmented Landscape of Drug Synergy

1.1 Introduction

Even as the clinical impact of drug combinations continues to accelerate, no consensus on how to quantify drug synergy has emerged. Rather, surveying the landscape of drug synergy reveals the persistence of historical fissures regarding the appropriate domains of conflicting synergy models—fissures impacting all aspects of the discovery and deployment of combination therapy. Herein I chronicle the impact of these divisions on: 1) the design, interpretation, and reproducibility of high-throughput combination screens; 2) the performance of algorithms to predict synergistic mixtures; and 3) the search for higher-order synergistic interactions. Further progress in each of these subfields hinges on reaching a consensus regarding these long-standing rifts in the field.

1.2 The fragmented foundations of drug synergy

Experiments with medicinal combinations stretch back to antiquity. The concept of synergy can be found in Aristotle's musings in his metaphysics book 8, "the totality is not, as it were, a mere heap, but the whole is something besides the parts" a sentiment which has subsequently been distilled into the more familiar colloquial expression "the whole is more than the sum of its parts." However, the quantitative model considered to be the foundation of modern efforts to quantify synergy was advanced recently, by comparison, in 1926 by Loewe (Loewe, 1926, 1927). Loewe proposed what is now called the Dose Equivalence Principle (DEP) which asserts if the effect of reducing one drug's concentration can be compensated for by adding a second drug at a constant ratio, there is no synergy (also called additivity). This definition leads to the classic linear isobols of Loewe Additivity. Observed deviations from this expected ratio signify synergy or antagonism. The second principle, the Multiplicative Survival Principle (MSP), was first proposed by Bliss in 1939 (Bliss, 1939) then later independently by Webb (Webb, 1963). In contrast to the DEP,

the MSP takes a probabilistic approach to synergy asserting the probability of being unaffected by each drug individually (U_1, U_2) is independent. Therefore, the probability of being unaffected by the combination (U_{12}) is equal to the product of the single drug probabilities ($U_{12} = U_1 * U_2$). This equation has been termed Bliss Independence. If the percent of the population unaffected for the combination is less or more than this product, the combination is synergistic or antagonistic, respectively. A third major synergy principle was proposed by Gaddum in 1940, which defined synergy as the difference between a combination's effect and the most efficacious single agent (Gaddum, 1940). This model is commonly called Highest Single Agent (HSA). Together, these three principles, (DEP, MSP, and HSA) comprise the foundations of almost all subsequent synergy frameworks (Figure 1.1A, Foundational Principles). Several excellent reviews on the mathematical basis of these foundational principles are (Tallarida, 2001, 2011; Foucquier and Guedj, 2015).

In the 1980s, two equations—one satisfying the MSP and the other the DEP—were derived from a mass action model of drug effect by Chou and Talalay (Figure 1.1A, Mass Action Interpretation) (Chou et al., 1983; Chou and Talalay, 1984). Because the mass-action based equations for MSP and DEP are not equivalent, Chou recommended using the DEP equation which assumes the inhibitors are mutually exclusive. This equation is called the Combination Index (CI). However, the existence of multiple paradigms for calculating drug synergy became increasingly problematic in the late 1980s and early 1990s as systematic comparisons between methods emerged. These comparisons highlighted the frequent contradictory results between the MSP and DEP frameworks (Berenbaum, 1989; Greco et al., 1995)—inconsistencies that have been subsequently documented as recently as 2019 (Vlot et al., 2019). Amidst these comparisons, a conference was convened in Saariselkä, Finland in 1993 seeking consensus for the field. The resolutions of the attendees were documented in what was termed the Saariselkä Agreement (Greco et al., 1992; Tang et al., 2015) (Figure 1.1A, Seeking Consensus). The agreement concluded,

> "It is clear that the adherents of Loewe additivity and Bliss independence have heard all the most compelling arguments for and against each model, and cannot be persuaded to switch allegiances. Thus…I propose that both models be tentatively accepted…This recommendation is made even though predictions of

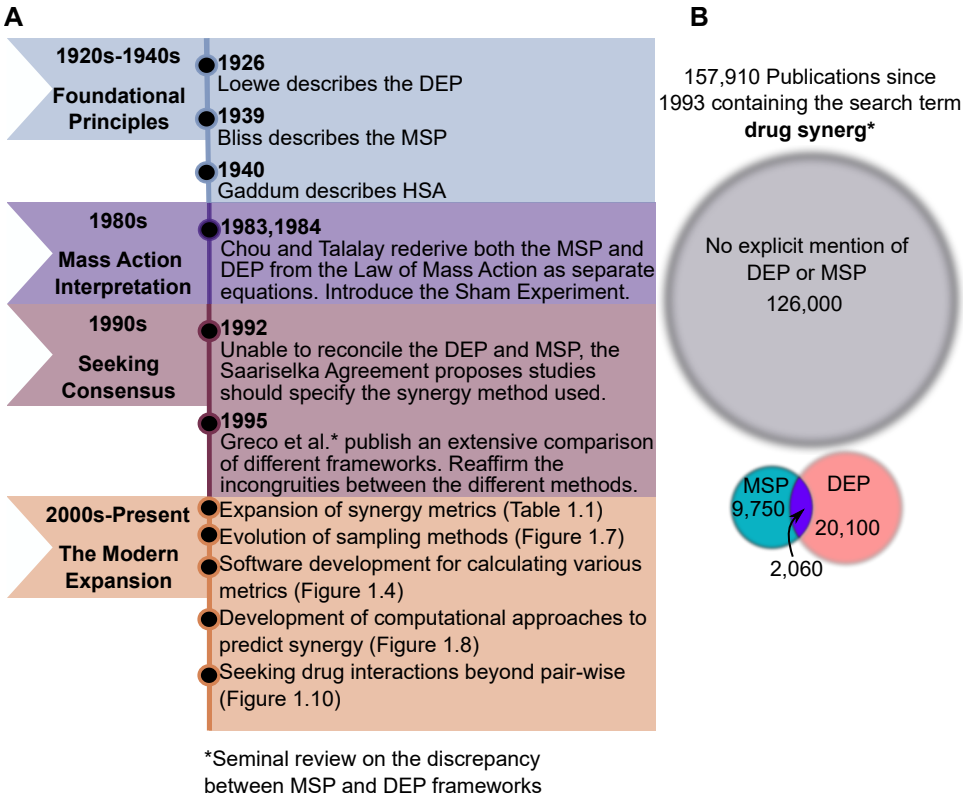

Figure 1.1: Timeline of developments in drug synergy highlights the persistence of historical rifts in the field. A) Developments in drug synergy span four distinct epochs. During the Foundational Principles period, the major drug synergy principles were first described. Subsequent work in the 1980s rederived the DEP and MSP based on a mass-action model of drug effect resulting in two equations. The DEP-based equation became known as the Combination Index (CI). A series of studies during a critical period in the 1990s highlighted the incongruence of the DEP and MSP culminating in the recommendation studies should explicitly state how synergy was calculated. The modern era is characterized by an expansion of synergy models that seek to extend the DEP and MSP (Table 1.1). Substantial developments have also occurred in related subfields (Software-Figure 1.4, Sampling Methods Figure 1.8, Computational Prediction-Figure 1.9, Higher-Order Interactions-Figure 1.11). B) Publications (in Web of Science) which include the term "drug synerg*" where * is a wild card to encompass terms such as "synerg-y" and "synerg-istic." Publications are grouped by those mentioning MSP (blue), DEP (red), both (purple), or neither (gray). The subset containing TOPIC: ("dose equivalence principle" OR isobol* OR Loewe OR "combination index") were considered to reference DEP frameworks while papers matching TOPIC: ("multiplicative survival principle" OR bliss OR "fractional product method") were considered to reference MSP frameworks.The time span included was: 1993-2019. The databases included: SCI-EXPANDED, SSCI, A&HCI, CPCI-S, CPCI-SSH, BKCI-S, BKCI-SSH, ESCI, CCR-EXPANDED, IC. Over 80% of publications continue to use the term synergy without referencing a particular model. Of those that do, $< 7\%$ acknowledge the existence of multiple frameworks.

combined-effects based on each of the rival reference models may be quite different"

Symptomatic of this internal division in the field, the preponderance of papers using variations of the term "drug synergy" since 1993 (approximately 80%) do not reference either the DEP or MSP (Figure 1.1B). Further, the adherents of the MSP- or DEP-based frameworks remain firmly entrenched in their respective camps—DEP-based studies being roughly twice as common as MSP-based—with $< 7\%$ of studies explicitly mentioning both (Figure 1.1B).

Nevertheless, this lack of consensus has not slowed the development of combination screening technology which has outpaced the analytical tools necessary to translate its potential for therapeutic discovery. Seeking to address this gap, an assortment of synergy frameworks have been postulated in recent years (Yadav et al., 2015; Twarog et al., 2016; Zimmer et al., 2016; der Borght et al., 2017; Schindler, 2017; Wicha et al., 2017; Sinzger et al., 2019) (Figure 1.1A, Modern Expansion). In the next section, I review these recent advances and highlight how the persistence of divisions between the MSP and DEP identified at Saariselkä continue to impact all aspects of synergy studies in the modern era.

1.3 Recent advances building on fractured foundations

Over the last decade, there has been an explosion of synergy frameworks, almost all of which continue to derive from either the MSP or DEP (Figure 1.1A, Modern Expansion). However, the implicit assumptions and limitations of each new framework often go unnoted and there are no standardized criteria for comparison. Table 1.1 catalogs the most critical features of all frameworks. These features can broadly be grouped into implicit assumptions of the equation (Table 1.1, Equation Assumptions) and restrictions on the types of data that can be analyzed (Table 1.1, Data Assumptions).

Commensurate with the expansion of computational resources, most modern frameworks have transitioned to fitting parametric equations to calculate synergy (Table 1.1 Parametric). ZIP and Effective Dose Model (EDM) (Yadav et al., 2015; Zimmer et al., 2016) are parameterized models

for the MSP while BRAID, Hill PDE, and BIGL (Twarog et al., 2016; der Borght et al., 2017; Schindler, 2017) are the same for the DEP. The GPDI model (Wicha et al., 2017) fits two different equations, one for the DEP and one for the MSP, in an approach similar to the CI. All of these methods assume a Hill-like dose-response curve for each single-drug, an assumption first used by Chou (Chou et al., 1983), which is not an original assumption of Bliss, Loewe, or HSA (Table 1.1 Hill Approx). Finally, the recently rediscovered Hand model (Sinzger et al., 2019) is also a parameterized version of the DEP which only requires the dose-response function to be differentiable and invertible and therefore could be applied with non-Hill dose-response curves, though it was not considered in these instances.

Which form of the Hill equation (Figure 1.2A) these methods are derived from constrains the range and type of drug effects for which they are applicable (Figure 1.2B). The EDM, Hill PDE, CI, and BIGL are derived with a 2-parameter Hill equation with parameters only for cooperativity (also known as the Hill slope) and the potency, measured as the concentration of drug required to achieve the half-maximal effect (EC_{50}). This 2-parameter form assumes a minimum and maximum effect of 100% and 0% (Figure 1.2B). For dose-response data for which the maximal effect does not reach 0%, these methods can result in poor fits (Figure 1.3A,C). In contrast, ZIP, and BRAID all use the 4-parameter Hill equation as their base making them generally applicable to non-percent data with arbitrary effect ranges (Table 1.1 Non-% Data). Because the 2-parameter Hill equation is a special case of the 4-parameter equation (Figure 1.2B), these methods are also applicable to percent data. The distinction between the 2- and 4-parameter equations stems from the distinction between the percent affect and the percent effect of a drug. While MSP frameworks assume the measurement is the percent affect (*e.g.* percent of affected cells), most phenotypic screens measure the percent effect (*e.g.* percent change in cell count relative to control). As a result, it is common to observe maximal effects which saturate above 0% (Figure 1.3). In a Chapter 2, Section 2.4 (page 51), I shown this distinction between effect and affect can result in a systematic bias toward antagonism when applying Bliss to drugs with intermediate effects (e.g. saturate between 35% and 65%). Comparing an anti-cancer dataset (O'Neil et al., 2016) and an anti-malarial dataset (Mott et al.,

Table 1.1: Comparison of drug synergy frameworks.

	Equation Assumptions					Data Assumptions			Citation
	Dose-independent	Parametric (#Parameters)	# Synergy Variables	Hill Approx.	Not Sham Compliant	>2 drugs	Non-% data	Unbounded Drug Effect	Original Citation
MSP									
Bliss			1		✓	✓			(Bliss, 1939)
EOB			1		✓		✓	✓	(Niepel et al., 2019)
ZIP		✓(10)	1	✓	✓		✓	✓	(Yadav et al., 2015)
EDM	✓	✓(6)	2	✓	✓	✓			(Zimmer et al., 2016)
DEP									
Loewe			1			✓	✓		(Loewe, 1926)
CI*		✓(4)	1	✓					(Chou et al., 1983)
Hill PDE		✓(6)	1	✓					(Schindler, 2017)
Hand			1	✓		✓	✓	✓	(Sinzger et al., 2019)
BIGL			1	✓	✓		✓	✓	(der Borght et al., 2017)
BRAID	✓	✓(10)	2	✓			✓	✓	(Twarog et al., 2016)
Other									
HSA			1		✓	✓	✓	✓	(Gaddum, 1940)
GDPI_LA	✓	✓(12)	4	✓			✓	✓	(Wicha et al., 2017)
GDPI_BI	✓	✓(12)	4	✓	✓			✓	(Wicha et al., 2017)

* CI is the DEP-based eq. in (Chou and Talalay, 1984).
✓indicates property is satisfied

2015) shows the prevalence of such drugs is assay/model dependent (Figure 1.3B,D). Therefore, careful investigation of the single-drug dose-response curves should precede any use of methods derived with a 2-parameter Hill equation (Table 1.1 Unbounded Drug Effect). Both Excess Over Bliss (EOB) (Niepel et al., 2017) and BIGL (der Borght et al., 2017) propose rescaling arbitrary drug effects to range between 0% and 100% in order to apply Bliss and Loewe respectively; however, it is unclear how this rescaling impacts synergy calculations when comparing combinations with different maximal efficacy.

In summary, the modern expansion of drug synergy frameworks has increased confusion, rather than clarified, the appropriate domain of each synergy model. This has stemmed in part from the unstated limitations and assumptions of each model (Table 1.1). Careful consideration of the assay read-out, the single-drug dose-response curves, and the assumptions of a particular synergy framework is therefore critical to avoiding systematic biases and improving reproducibility.

1.4 A field divided

Due to the lack of a consensus regarding the best synergy framework, several software packages, including SynergyFinder (Ianevski et al., 2017) and Combenefit (Di Veroli et al., 2016), have been developed which calculate multiple synergy metrics, commonly including Bliss, Loewe, and HSA. Other software has been developed to directly couple synergy calculations with image analysis in high throughput studies which also calculates multiple metrics (Chantzi et al., 2019, 2018). However, I find that even on the same dataset, SynergyFinder and Combenefit can give opposite results for the same synergy metric (Figure 1.4A,B). This likely stems from different data transformations, normalizations, and manipulations which are not standardized in the field. I find divergent predictions to be the case for up to 36% of combinations comparing between SynergyFinder and Combenefit for Bliss in an anti-malaria dataset (Mott et al., 2015) (Figure 1.4C, green bars).

The difficulty in comparing software calculations is augmented by the lack of consensus on what summary statistics should be used for these dose-dependent models of synergy. In the anti-malarial dataset, I find the top 5% of antagonistic combinations by the mean are all in the top 32%

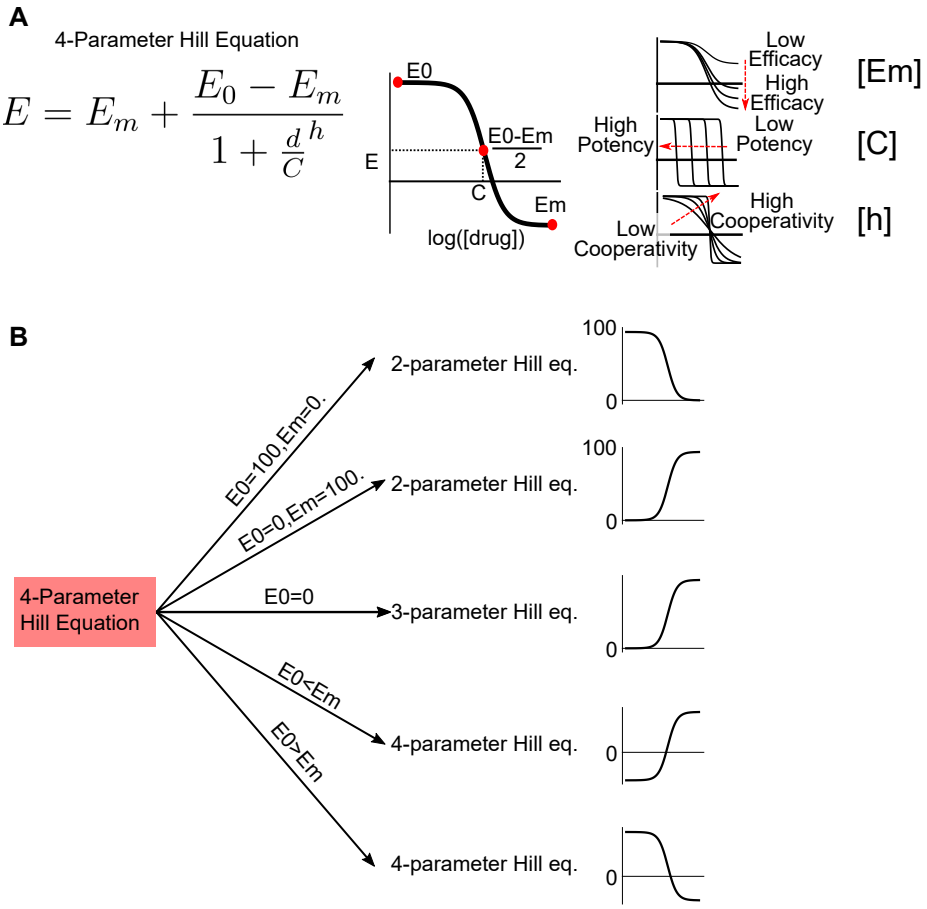

Figure 1.2: Different Forms of the Hill Equation. A) The general 4-parameter Hill equation describes a sigmoidal dose-dependence of an arbitrary effect with parameters for a drug's efficacy ($E_m - E_0$), potency (C), and cooperativity (h) also called the Hill slope. The potency is the concentration of drug required to achieve a half-maximal effect ($\frac{E_0 - E_m}{2}$) (dotted line). Dose-response data are commonly plotted on a log scale to assess the sigmoidicity of the curve. Because the zero concentration goes to negative infinity when logged, E_0 (effect at zero concentration of drug) is commonly plotted at 10-fold lower than the smallest non-zero concentration tested. B) The 4-parameter equation can be simplified to many different forms. The 2-parameter Hill equations are commonly thought to quantify percent affect/unaffected. This form is commonly assumed in drug synergy frameworks that do not account for differential maximal efficacy between different therapeutics.

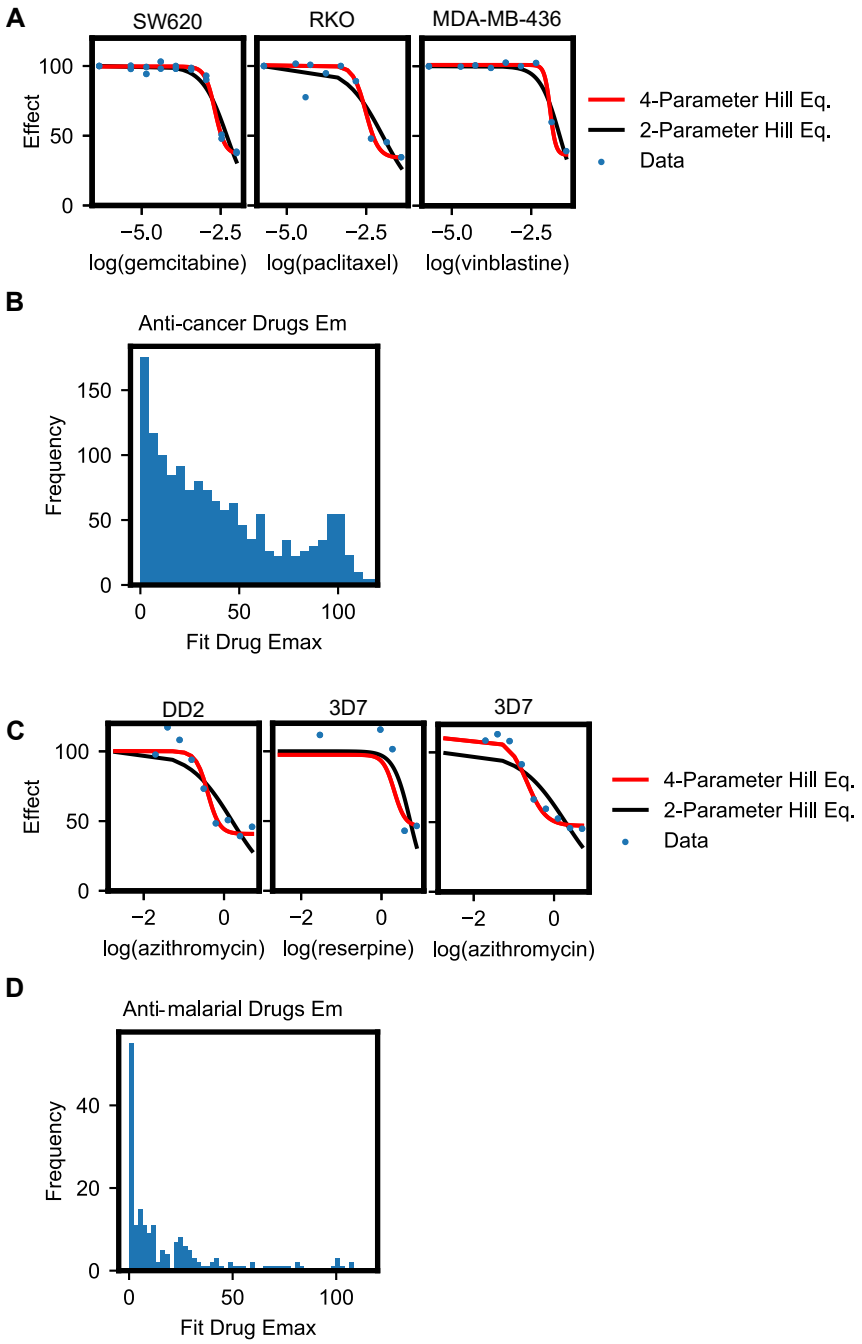

Figure 1.3: Prevalence of drug effects that saturate above 0% is assay/model dependent. A) Three examples of anti-cancer drugs that have maximal effects >20% according to the 4-parameter Hill fit. The data is in blue, the fit using the 4-parameter equation is in red, and the fit using the 2-parameter equation (asserting E_0=100 and E_m=0) is in black. The cell line targeted is noted on top of each panel. B) Distribution of the fitted maximal efficacy in the (O'Neil et al., 2016) anti-cancer dataset. C) Three examples of anti-malaria drugs targeting different malarial strains (annotated top of each panel) which have fitted maximal effects >20%. D) There is a lower frequency of drugs with effects that saturate before 0% in the (Mott et al., 2015) anti-malarial dataset compared to the anti-cancer dataset.

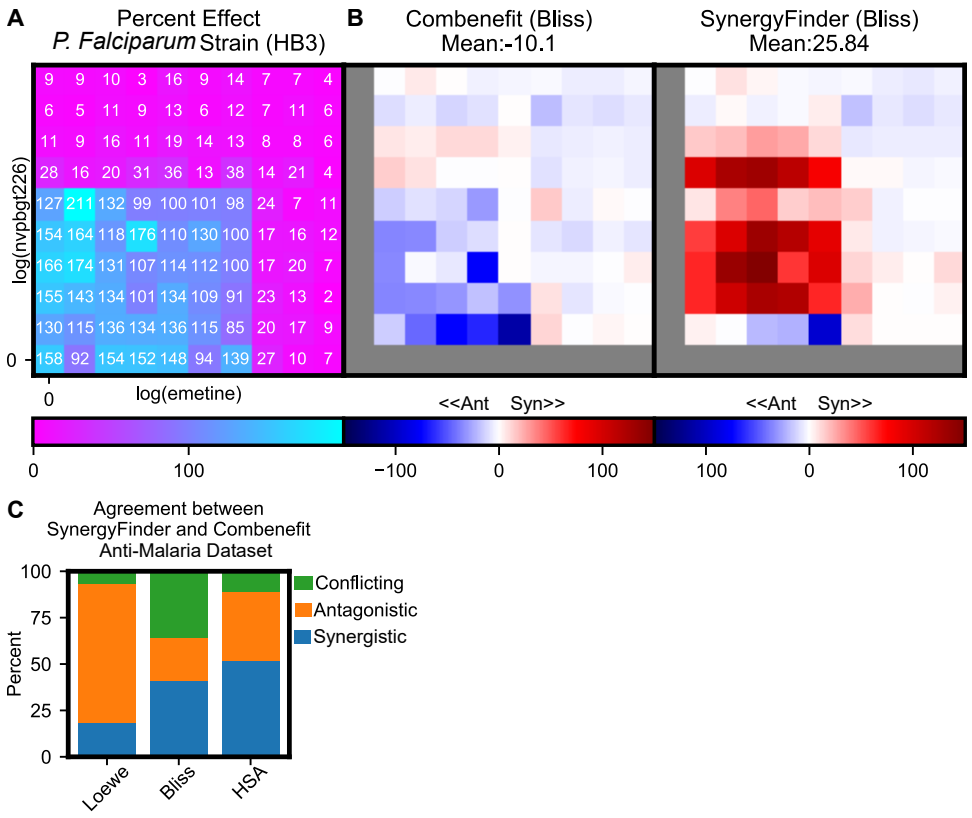

Figure 1.4: Conflicting results between synergy software suites impair reproducibility. A) Percent effect (color-bar bottom, numbers in boxes) of nvpbgl226 (PI3K/mTor inhibitor) and emetine (anti-protozoal) against HB3 strain of malaria. Data from Mott et al. (Mott et al., 2015). The percent effect can be greater than 100% because static endpoint measures of drug effect rely on normalization to untreated controls. If the treated condition has more cells than the control, the normalized percent effect is >100%. This highlights the difference between percent affect (which can never exceed 100%) and percent effect. (See Section 2.4) B) Combenefit and SynergyFinder calculate Bliss (color scale bottom)—which assumes percent affect—for this combination differently resulting in conflicting synergy classification based on the mean across the surface. Gray boxes are undefined as synergy is only calculated for combination conditions. Syn=synergy, Ant=Antagonism. The color scale is the same for both heatmaps. This disparity may arise from different approaches to deal with effects >100%. C) The frequency of agreement between SynergyFinder and Combenefit in the anti-malarial dataset depends on which synergy metric is calculated.

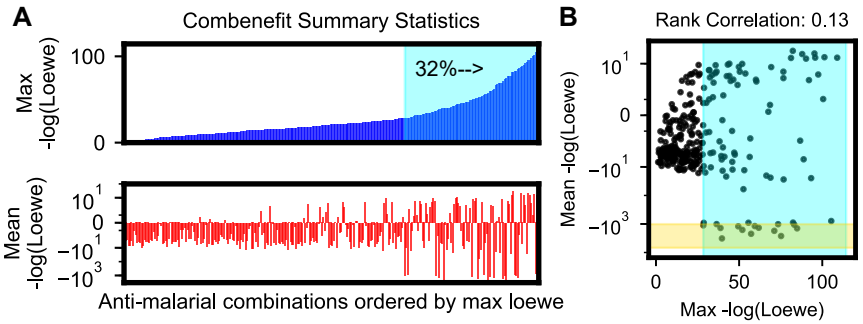

Figure 1.5: Dose-dependent synergy frameworks perform inconsistently when using summary statistics. A) Different summary statistics for dose-dependent synergy metrics (Table 1, Dose-Independent) prioritize different combinations for follow-up. Anti-malarial combinations are ranked from left to right in order of increasing maximum observed Loewe (calculation by Combenefit). Combinations with high maximum synergy are often antagonistic by mean (red lines bottom panel). The top 5% of antagonistic combinations by the mean fall in the top 32% of synergistic combinations by the max. -log(Loewe) values <0 are antagonistic and >0 are synergistic. B) Scatterplot of the Loewe summary statistics shows Spearman correlation of 0.13 between the mean over the surface and maximum observed Loewe for the anti-malaria dataset.

of synergistic combinations by the maximum observed synergy (Figure 1.5A,B Spearman rank correlation=0.13). This is because dose-dependent synergy frameworks, such as Bliss and Loewe, were not designed to compare different drug combinations, but rather different doses of the same combination. For example, I find anti-malarial combinations where 3 samples at different doses are all antagonistic by Bliss (Figure 1.6) and Loewe (Figure 1.7), while the combination is synergistic by the mean over the whole dose-response surface. The discrepancy points to a philosophic quagmire regarding whether synergy is a property of drug pairs or drug dose pairs—one of many outstanding questions in the field (Outstanding Questions, pg 14). If synergy is a property of drug pairs, then the optimal drug concentrations should be determined based on maximizing efficacy with as little drug as necessary. However, if synergy is a property of particular drug concentrations, then there is no basis for choosing one summary statistic over another when comparing drug combinations. The implications of these divergent worldviews have not been previously discussed, yet they represent a critical fault-line in the field with far-reaching ramifications for the discovery and deployment of combination therapy.

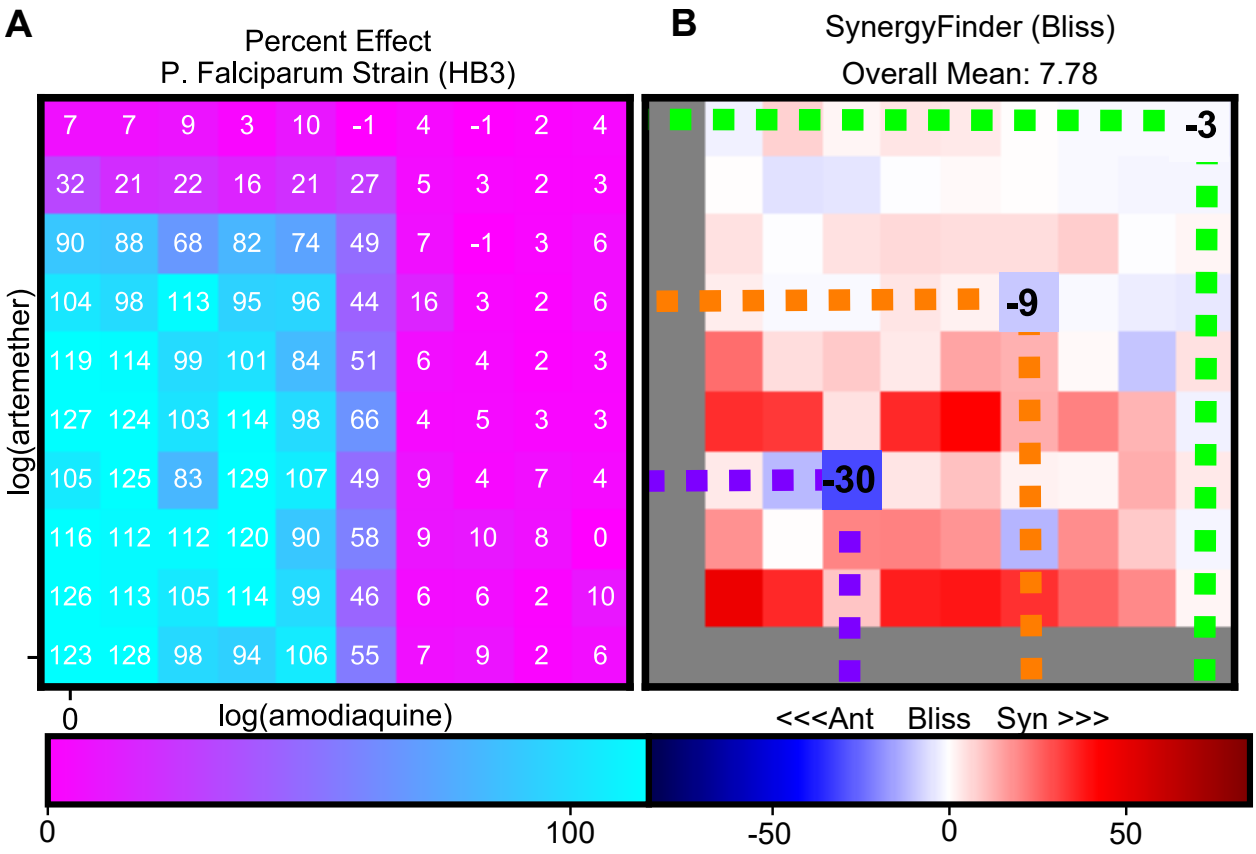

Figure 1.6: Dose-dependent Bliss calculations conflict with summary statistics. A) Percent effect (color scale bottom, numbers in boxes) of amodiaquine (polymerase inhibitor) and artemether (proposed to function by inhibiting anti-oxidant enzymes) on the HB3 strain of malaria. B) The combination is antagonistic (Ant) by Bliss (color scale bottom) according to SynergyFinder at three different combination doses (purple, orange, green lines); however, the combination is synergistic (Syn) by mean over the surface. Gray boxes are undefined as synergy is only calculated at combination conditions.

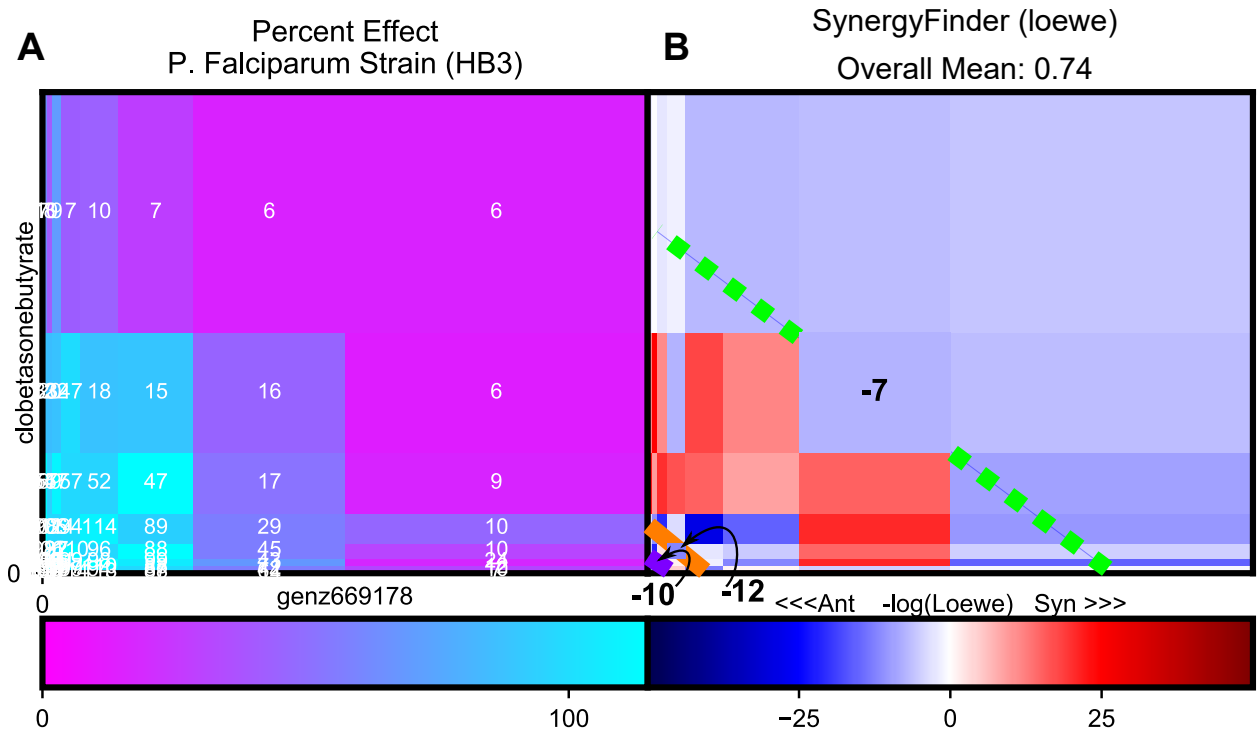

Figure 1.7: Dose-dependent Loewe calculations conflict with summary statistics. A) Percent effect (color scale bottom) of genz669178 (plasmodium dihydroorotate dehydrogenase inhibitor) and clobetasone butyrate (synthetic glucocorticoid corticosteroid) on the HB3 strain of malaria. The drug scale is linear on both axes. B) The combination is antagonistic by Loewe (color scale bottom) according to SynergyFinder at three different doses (at the midpoint of purple, orange, and green lines); however, the combination is synergistic by mean over the surface.

1.5 Outstanding Questions

Surveying the field resolves the following outstanding questions.

- **DEP vs MSP:** The appropriate domains for each principle is still in need of consensus.
- **Dose-Dependent Synergy:** Whether synergy is dose-dependent or a property of each unique combination has not been extensively discussed. Subsequent work should avoid methods that assume synergy is dose-dependent when comparing combinations as the summary statistic or dose selection strongly impacts the results of such comparisons (Figure 1.5).
- **Data Pre-processing:** An increase in the transparency of the data pre-processing (*e.g.* normalization, removing data, interpolating missing values) should be required for subsequent studies to improve reproducibility. The lack of standards results in disparate calculations between different software packages (Figure 1.4).
- **Data Format:** Drug combination data is commonly reported in matrix form or in list form. While the matrix form is more common, I recommend moving to a list format as it is more flexible for alternative sampling schemes (*e.g.* CSS or DiaMOND Figure 1.8) as well as for reporting combinations of $>= 3$ drugs.
- **Parameter Names:** Theoretical comparisons of different parameterized synergy models is challenging due to the various naming conventions. However, given most frameworks share a core set of variables (*e.g.* Hill slope), I recommend parameters, as noted in Symbols section of Abbreviations, should be used in subsequent derivations. These names are sufficiently parsimonious to be used in large equations and flexible enough for frameworks that expand readily to quantifying synergy in mixtures of three or more drugs.
- **Sampling Methods:** The sampling scheme impacts the applicable synergy frameworks (Figure 1.8). I recommend subsequent screens should test several sampling strategies to estimate the trade-off in precision and cost for an assay's noise profile before depending on a particular strategy.

- **Comparison Data:** Most recent frameworks compare their method with others using one dataset. However, this precludes understanding the broader applicability of each new method. The notable development of drug combination databases (Zagidullin et al., 2019) should facilitate more comprehensive comparisons in the future.

- **Higher-Order Interactions:** The nature and existence of higher-order interactions remain debated (Figure 1.11). Careful consideration of the metrics of drug effect, assay noise, synergy metrics, and the selected drugs will be critical for advances in our understanding of high order mixtures.

- **Sham Experiment:** The criticality of satisfying the sham experiment for new frameworks remains contentious. However, given evidence that satisfying the sham experiment introduces a Hill-slope dependent bias (Section 2.5, page 57), I recommend discarding sham compliance as a sanity test for subsequent frameworks.

In summary, not only do the oft-cited contradictions between synergy models persist, but even the same metric can be contradictory between different software packages. Reliance on summary statistics to compare drug combinations for dose-dependent synergy frameworks (Table 1.1) further compounds this problem. Such conflicts undermine the reproducibility and translatability of synergy studies and therefore should motivate concerted efforts toward establishing data handling standards in the field.

1.6 Tackling the combinatorial complexity of synergy studies

One challenge, common to all synergy studies, is the looming curse of dimensionality (Cokol et al., 2017; Zimmer et al., 2017; Tekin et al., 2018). Each additional drug exponentially increases the requisite number of conditions to measure making an exhaustive search of combinatorial space intractable. Three subfields have evolved to deal with the inflationary cost of combination screens. First minimal sampling designs have been proposed for both MSP and DEP frameworks. Second, computational algorithms are increasingly being developed to predict synergy. And finally, the

existence and nature of synergistic interactions beyond pair-wise remains an active area of study. The lack of such interactions would mean the effects of >2-drug mixtures could be predicted from pair-wise measurements substantially reducing the number of conditions required for higher-order combinations.

1.6.1 Minimalistic sampling heuristics

The most direct way to decrease costs of combination screens is to reduce the number of data points required to calculate synergy. Several minimalistic sampling schemes have been proposed (Figure 1.8) (Zimmer et al., 2017; Fang et al., 2017; Cokol et al., 2017; Huang et al., 2018; Amzallag et al., 2019; Cokol-Cakmak et al., 2018; Malyutina et al., 2019); however, not all sampling methods are equally appropriate for different frameworks. Specifically, the particularly stringent sampling patterns annotated Minimal MSP and DEP in Figure 1.8, require only 3 data points per combination, but can only be analyzed by Bliss/HSA or Loewe, respectively. Synergy studies should therefore carefully consider a framework's limitations before depending on a sampling scheme (Table 1.1). Additionally, as discussed above, the selection of dose becomes critical for these minimalistic sampling schemes (Figures 1.6,1.7).

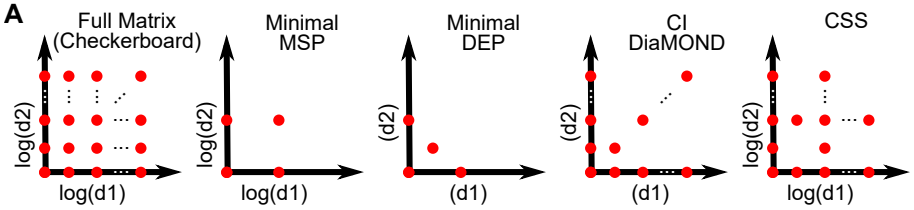

Figure 1.8: Minimal sampling designs. A) Data sampling recommendations for different frameworks.

An alternative approach to reduced sampling schemes is the use of scaling laws to infer effects for under-sampled combinations (Wood et al., 2014). These scaling laws have been used to calculate drug response in resistant mutants based on responses of sensitive cells. However, this

approach is sensitive to the level of experimental noise for a given assay. Further, it implicitly assumes that drug interactions are unidirectional (i.e. drug A changes the potency of drug B, but drug B does not change drug A's potency). Bidirectional synergistic potency has subsequently been assumed by several groups (Yadav et al., 2015; Twarog et al., 2016; Zimmer et al., 2016; Wicha et al., 2017).

In summary, because the robustness of synergy calculations to different sampling strategies has not been rigorously addressed and depends on intrinsic experimental noise, I recommend subsequent screens should sample the full matrix of combinations when possible for greater versatility and robustness.

1.6.2 Predicting synergy

In silico algorithms to predict synergy are a potential method to expand the pool of "tested" combinations and have seen significant recent activity including two DREAM challenges (Bansal et al., 2014; Menden et al., 2019). Broadly, the algorithms can be grouped into either machine learning (statistical) methods or mechanistic models.

Two excellent reviews on common types of machine learning algorithms employed in predicting drug synergy as well as available databases for training models are (Bulusu et al., 2015; Tang, 2017). Machine learning algorithms can be categorized as network-based, gene expression-based, drug-centric, or some combination thereof. However, because each algorithm has different input data, it is challenging to compare performance between methods. The most recent DREAM challenge found combining information about gene expression with information on drug-target interaction improved predictivity (Menden et al., 2019) suggesting combining data modalities as potentially profitable.

However, an understudied aspect of these approaches is how each algorithm's performance depends on which synergy metric is used to measure synergy. The first DREAM challenge (Bansal et al., 2014) used Bliss while the most recent challenge (Menden et al., 2019) was based on Loewe (calculated by Combenefit). When I predicted Bliss, Loewe, or HSA synergy for anti-cancer com-

binations using DeepSynergy (Preuer et al., 2018)—a neural network algorithm which uses drug and gene expression information as input—I found a 12% overlap in the top 1,000 predicted combinations with no overlap in the top 5 (Figure 1.9A). The first overlap between all three occurred at the 263rd combination by Loewe ranking (Figure 1.9A). Further, the physicochemical drug features (Figure 1.10A) and expressed genes (Figure 1.10B) with the largest influence on synergy/antagonism (as assessed by mean SHAP value (Lundberg and Lee, 2017) over 1,000 combinations) had a rank correlation between the different synergy metrics of <0.04 for all comparisons (Figure 1.10). This potentially stems from the different sensitivity of Bliss, Loewe, and HSA to different mechanisms of joint action as described by Gilvary and colleagues (Gilvary et al., 2019). Given the historical discrepancy between these metrics, a more customized approach is warranted.

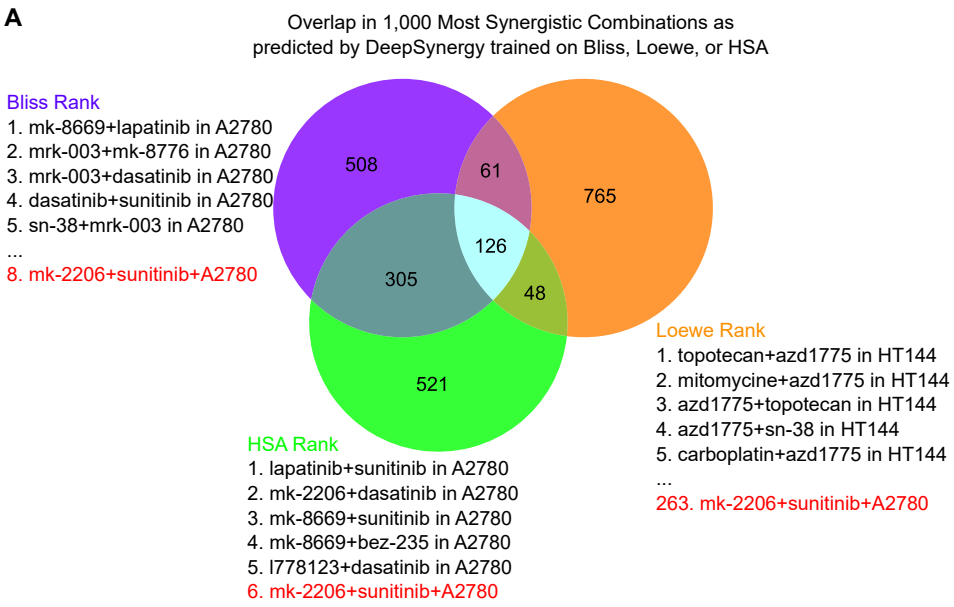

Figure 1.9: Top machine learning-predicted combinations depend on the synergy metric. A) I trained DeepSynergy (Preuer et al., 2018), a machine-learning algorithm to predict drug synergy from gene expression and drug physicochemical properties, on the O'Neil et al. anti-cancer dataset with Bliss (purple), HSA (green), or Loewe (orange) as the measure of synergy. The top-predicted synergistic combinations were different depending on which metric was used. mk-2206 (AKT inhibitor) plus sunitinib (tyrosine kinase inhibitor) in A2780 cells was the first combination present in the rank-orderings of all three metrics at the 6th, 8th, and 263rd position for HSA, Bliss, and Loewe respectively (red highlight). The top 5 predicted synergistic interactions in Loewe are all in HT144 cells (malignant melanoma) while in Bliss and HSA all are in A2780 (ovarian carcinoma).

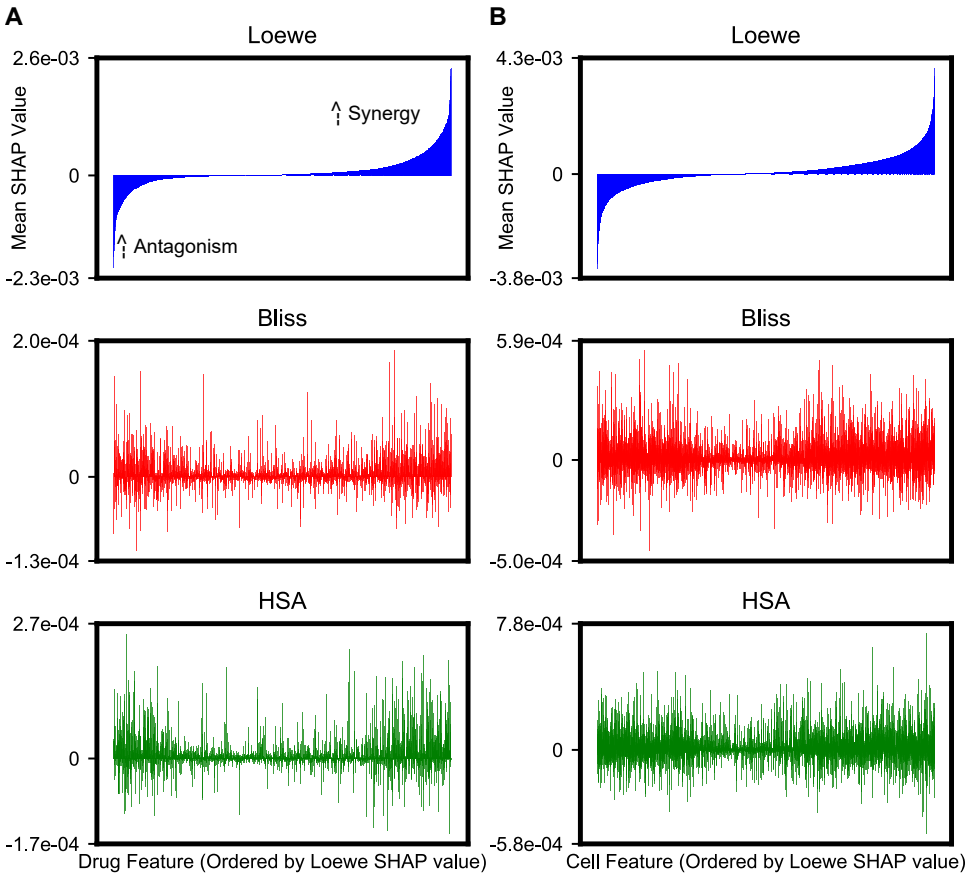

Figure 1.10: Physicochemical and cell features which increase the synergy of a combination in a cell line depends on the synergy metric. A) The mean SHAP value across the top 100 predicted synergistic combinations for 2,431 drug physicochemical features for Loewe (top), Bliss (middle), and HSA (bottom). Features are ranked-ordered from left to right by increasing SHAP values based on the Loewe model. SHAP values ¿0 indicate a feature tends to increase the synergy while SHAP values ¡0 indicate features that tend to increase antagonism. Drug features predicted to have the greatest contribution to synergy or antagonism vary depending on which synergy metric is used (spearman rank correlation ¡0.04 for all pairs). B) Cell features (gene expression of 6,415 genes) contribution to synergy or antagonism of a combination as measured by the mean SHAP value.

In contrast to statistical models, mechanistic approaches to predict synergy are based on models of biological processes. An early example of this, coPIA, used an ordinary differential equation (ODE) based model to predict combination effects in breast cancer cells (Nelander et al., 2008). A more recent ODE model of the HGF/Met signaling pathway was used to identify personalized combinations in hepatocellular carcinoma (Jafarnejad et al., 2019). Another example used

dynamic logic models of phosphorylation cascades to predict colorectal cancer response (Eduati et al., 2017). Even in the absence of kinetic parameters necessary for an ODE model, purely topological models have been used to predict with 80% accuracy perturbation impacts on gene expression (Santolini and Barabási, 2018) in a chemotaxis model of bacteria. Such topological models have also been applied in cancer to identify the synergistic interaction of Aurora B and ZAK in triple-negative breast cancer (Tang et al., 2019). The predictivity of such approaches tends to leverage the sparsity of biological networks.

Finally, a hybrid approach constraining the architecture of an artificial neural network to match biological networks has been shown to be predictive of growth dynamics in budding yeast (Ma et al., 2018) and could be used to predict collateral dependencies in biological networks. While it remains enticing to understand the mechanistic basis of synergy, no unifying theme from these studies has emerged and which synergy model should be coupled to the mechanistic models or statistical models remains an open question.

1.6.3 Higher-order interactions

There has been substantial interest in predicting the effects for mixtures of three or more drugs based on pair-wise effects (Wood et al., 2012; Zimmer et al., 2016; Russ and Kishony, 2018; Tekin et al., 2018; Tendler et al., 2019). See (Tekin et al., 2017) for a more in-depth review of recent work. In a seminal paper on this topic, Wood et al. did not find evidence for higher-order interactions in 3-drug combinations in *Escherichia coli* (Wood et al., 2012). Specifically, they could predict the effects of 3-drug combinations using an MSP-based, Isserlis-like formula that depended only on pair-wise and single drug effects. A series of follow-up comparisons were done between EDM, the Isserlis-like formula, and Bliss to predict multi-drug effects for combinations up to 10 drugs (Zimmer et al., 2016, 2017; Katzir et al., 2019). This is unsurprising, as neither the Isserlis nor Bliss formula have parameters to fit to data, unlike the EDM. Regardless, these studies reinforced the absence of higher-order interactions as first postulated by Wood et al.

However, these findings were challenged by two papers that found emergent synergy for multi-

drug combinations in E. coli based on Bliss (Beppler et al., 2016; Tekin et al., 2018). This trend toward synergy was also observed by Russ and Kishony (Russ and Kishony, 2018), though less pronounced, in a study that directly compared the scaling of Loewe and Bliss. They found the null models for Loewe and Bliss diverge for increasingly higher-order combinations with Bliss becoming more synergistic (in agreement with (Beppler et al., 2016; Tekin et al., 2018) and Loewe becoming more antagonistic. Cokol and colleagues also found evidence for higher-order interactions according to Loewe for combinations of anti-tuberculosis compounds, though no trend as a function of the number of drugs was observed (Cokol et al., 2017). In my comparison of the trends in the three datasets ((Russ and Kishony, 2018; Tekin et al., 2018; Katzir et al., 2019)), I find a trend toward antagonism as the number of drugs increases for Loewe in all datasets (Figure 1.11A). The trend for Bliss, however, is contradictory between the three datasets (Figure 1.11B). Given my work demonstrating bias in Bliss toward antagonism for drugs with maximal effects $>0\%$ (see Section 2.4 page 51), I corrected the Katzir et al. data to account for this bias and found the emergent antagonism substantially decreases (Figure 1.12A). I find a higher proportion of drugs with maximal effects $>0\%$ in the Katzir et al. data than the Russ et al. data (Figure 1.12B) explaining why this bias was more prevalent in the former data.

In the end, the presence or absence of higher-order synergy does not preclude the deployment of mixtures of 3 or more drugs, as gains in efficacy can still be achieved, as shown in a recent study in colorectal cancer (Horn et al., 2016). Indeed, the possible existence of a synergy-efficacy trade-off (Gupta and Dixit, 2018; Sen et al., 2019) emphasizes the search for synergistic combinations should not be solely focused on optimizing synergy, but rather high efficacy at tolerable doses.

In summary, the existence and nature of higher-order interactions remain controversial. Clearly delineated studies on the role of assay, metric, drug selection, model system, etc. are needed to better address this question. Nevertheless, what is clear is the discrepancies between the MSP and DEP are further exacerbated by the scaling to higher numbers of drugs amplifying the need for a consensus approach synergy before tackling this problem.

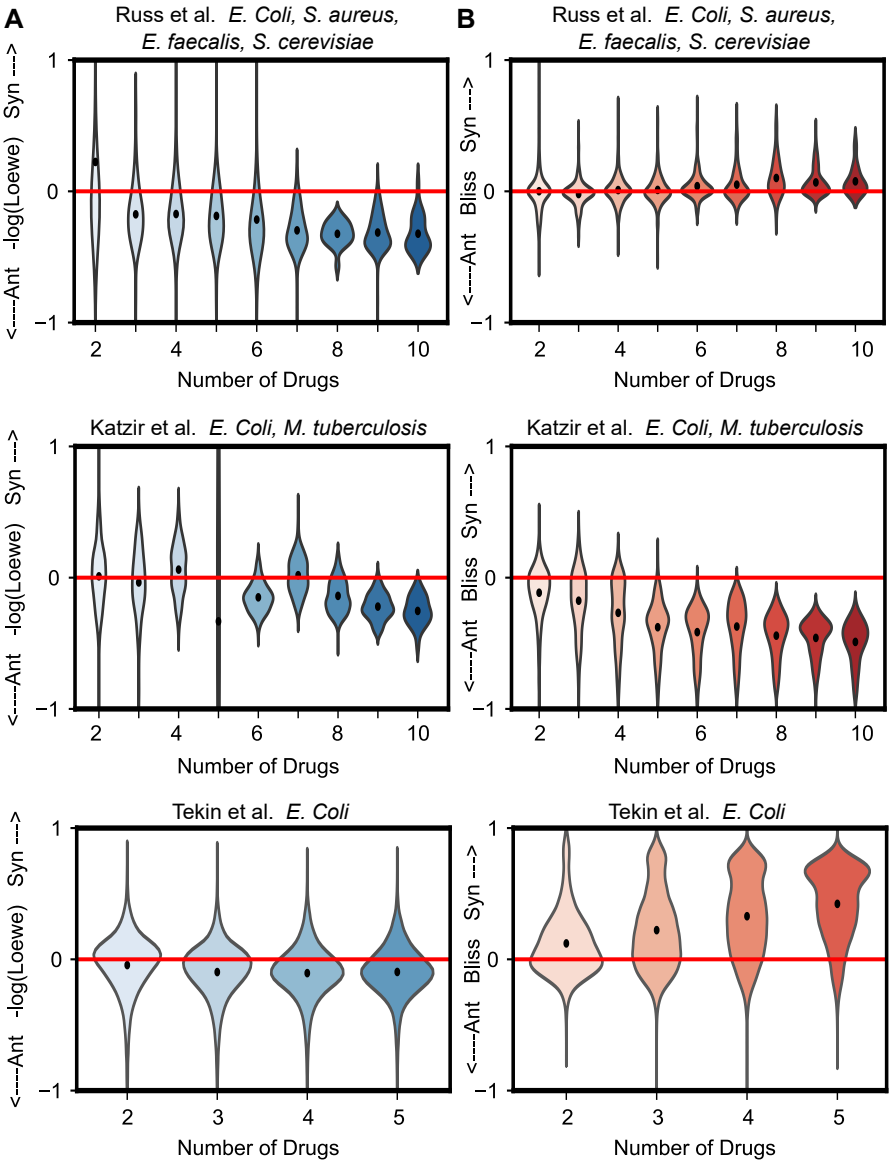

Figure 1.11: Seeking consensus on the existence and nature of higher-order interactions. A) Average Loewe synergy decreases for an increasing number of drugs in three datasets ((Russ and Kishony, 2018; Tekin et al., 2018; Katzir et al., 2019)). The black dot is the mean value of the distribution. Red-line demarcates synergy (Syn) from antagonism (Ant). The species tested in each paper are indicated in the panel title. B) Distribution of Bliss synergy as a function of increasing numbers of drugs. Accounting for the difference between percent effect and percent affect reduced the bias toward antagonism for ultra-high order combinations in the Katzir et al. data (Figure 1.12).

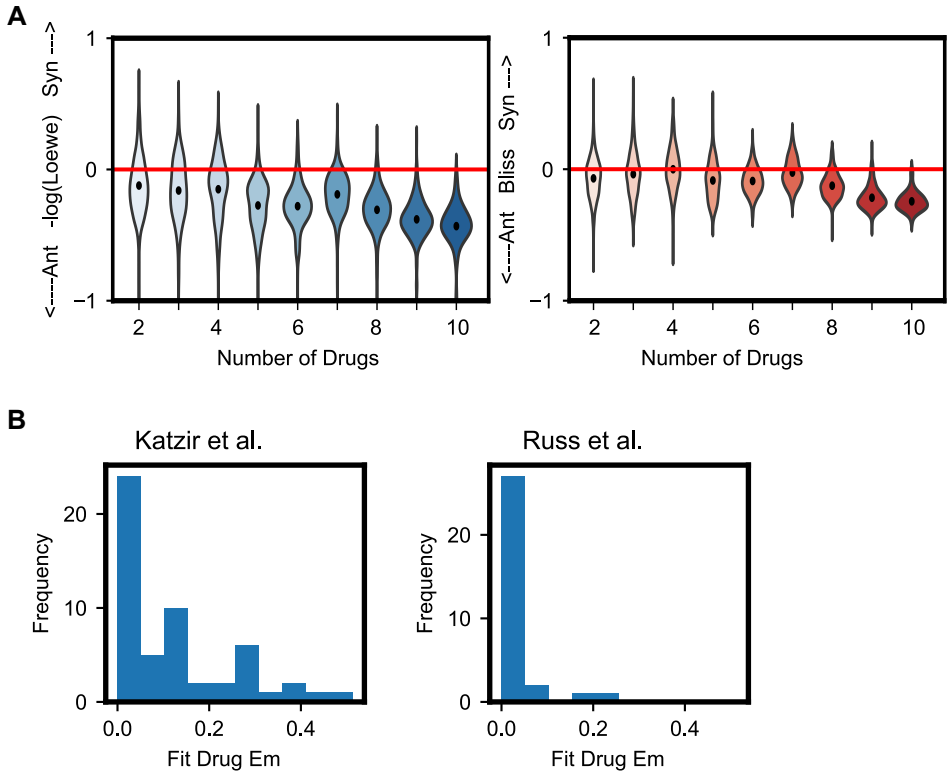

Figure 1.12: Correcting for the antagonistic bias in Bliss calculations for drugs with maximal effects $> 0\%$ decreases the bias toward antagonism for combinations of ultra-high order combinations. A) Distributions of Loewe and Bliss synergy as a function of the number of drugs in the Katzir et al. dataset based on percent affect. To calculate the percent affect from percent effect data, the data were fit using a 4-parameter Hill equation (Figure 1.2). The fitted Hill slope and EC_{50} from the 4-parameter equation were used in the 2-parameter Hill equation to calculate the percent affect at a given concentration. This is equivalent to renormalizing each combination to fall within E_0=1 to E_m=0. Syn=Synergy, Ant=Antagonism. B) The distribution of fitted E_m in the Katzir et al. and Russ et al. datasets. Bin sizes are equivalent in the two plots.

1.7 Synergy in new contexts

Despite the persistent historical fissures in the field, there are exciting developments that continue to add new dimensions to the quantification of combination pharmacology. One interesting development is the study of synergy in temporally staggered treatments (Koplev et al., 2017), which are known to impact in vivo efficacy (Bulman et al., 2016). These dosing programs better mimic patient combinations which are not commonly given simultaneously—an often-ignored assumption of all Hill-equation based frameworks (Table 1.1, Hill Approx.). Koplev et al. take a geometric additivity approach similar to the MSP (Russ and Kishony, 2018) and find several anti-cancer combinations with temporally dependent synergy in pancreatic cancer. Related to this, a recent study by Dean et al. has investigated how synergy is related to the short-term development of resistance (Dean et al., 2019). They found the rate of adaptation in *E. faecalis* is not related to the synergy of the combination, but rather was a function of the overlap in mechanism between the drugs. In related work, (Maltas and Wood, 2018) found the collateral effects of a single drug are pervasive but drug-specific. Therefore, the optimal combinations to reduce the development of resistance are likely drug-dependent, though the connection between collateral effects of a single drug and synergy is not well understood.

Another rapidly evolving concept is the translation of synergy between different scales (Dry et al., 2016; Palmer and Sorger, 2017). Palmer et al. used a Bliss model to show most clinical combinations can be explained by variable sensitivity in a population rather than true pharmacologic interaction. While they did not prove the existence of the two patient populations with a different drug, they demonstrated such population variance was sufficient to explain the additive benefit of most clinical combinations. A conceptually similar idea was the basis of DRUG-NEM (Anchang et al., 2018), an MSP-based framework for identifying combinations that maximize coverage of a heterogeneous cell population measured by CyTOF. Overall, these studies highlight the role of heterogeneity at every scale on our understanding of drug synergy.

Another developing area of research is the use of multi-parametric read-outs from combination experiments to prioritize drug combinations. For example, SynToxProfiler (Kononov et al.) and

CSS (Malyutina et al., 2019) both calculate synergy as well as total efficacy. Toxmatrix instead quantifies toxicity, or protection against toxicity, due to a combination (Tong et al., 2018). These multi-parametric approaches to drug synergy better captures the clinical trade-offs between therapeutic efficacy and tolerable dose. However, it is unclear how much the in vitro measures of efficacy, toxicity, and synergy correlate to clinical axes of interest (*e.g.* side effects and clinical efficacy). Furthermore, the optimal trade-off between these different parameters is unknown though Pareto optimization would appear appropriate.

Finally, the rapid evolution of chemical-genomics screens is only beginning to impact the search for drug combinations. Examples include recent studies in *M. tuberculosis* (Johnson et al., 2019) and *E. coli* (Nichols et al., 2011) which identified mutant-specific classes of inhibitors and suggest mutation mimicking drug combinations as a promising path forward. Another study used a CRISPR-based double knockout screen to identify synergistic combinations against leukemia cells (Han et al., 2017). However, as gene knock-outs and mutations are fundamentally different than molecular inhibition, the relationship between synthetic lethal and drug synergy is likely to be case dependent. Notably, Cokol et al. did not find an increase in Loewe synergy in targeting synthetic lethal genes compared to random (Cokol et al., 2011). While the historical overlap between functional genomics and drug synergy has been small, these recent efforts are beginning to bridge these disciplines.

1.8 The need for consensus

Throughout the preceding century, two dominant principles have been used to quantify synergy of drug combinations: the Dose Equivalence Principle (DEP), introduced by Loewe (Loewe, 1926, 1927) and expanded by Chou (Chou et al., 1983), and the Multiplicative Survival Principle (MSP), introduced by Bliss (Bliss, 1939). Discrepancies between these two principles, however, have resulted in divergent conclusions between synergy studies (Greco et al., 1995). This led to the Saariselkä Agreement, which recommended drug combination studies explicitly state how synergy was calculated (Greco et al., 1992; Tang et al., 2015) (Figure 1.1A).

More recently, a proliferation of synergy models, derived as extensions of either the DEP or MSP, has further splintered the field (Zimmer et al., 2016; Yadav et al., 2015; Schindler, 2017; Foucquier and Guedj, 2015; Geary, 2013; Twarog et al., 2016) (Figure 1.1A). In the absence of a consensus framework for drug synergy, discovery efforts for combinations often calculate all available synergy metrics (Ianevski et al., 2017; Flobak et al., 2017; He et al., 2018) (Figure 1.4). However, even these software packages conflict and there remains no basis for choosing one metric over another, which becomes particularly problematic when synergy metrics are in conflict. This "calculate everything" paradigm thus hampers reproducibility between studies, delays progress in the discovery of truly synergistic drug combinations, and negatively impacts the translatability of combination discovery efforts.

Despite the lack of consensus on how to quantify synergy, drug combination screens remain essential to both pharmaceutical and academic discovery efforts, as shown in recent challenges by AstraZeneca and the NCI-DREAM consortia (Bansal et al., 2014; Menden et al., 2019), as well as combinatorial CRISPR screens (Han et al., 2017). Yet, the paucity of successful clinical combinations explicable by true pharmacological interaction, rather than patient-to-patient variability (Palmer and Sorger, 2017), is symptomatic of the challenges facing the field. Therefore, the need identified at Saariselkä still exists: a consensus framework to interpret drug combination pharmacology.

In the next chapter, I present a mass action based theory of drug synergy, termed MuSyC, which generalizes the DEP and MSP, thereby unifying the field of drug synergy, as sought at Saariselkä (Section 2.2). I further map the landscape of current synergy metrics, including: Bliss Independence (Bliss, 1939), Loewe Additivity (Loewe, 1926), Combination Index (CI) (Chou et al., 1983), Highest Single Agent (HSA) (Gaddum, 1940), Effective Dose model by Zimmer et al. (Zimmer et al., 2016), ZIP (Yadav et al., 2015), a partial differential equation (PDE) Hill model by Schindler (Schindler, 2017), and BRAID (Twarog et al., 2016). In mapping relationships between these various metrics, I identified systematic differences impacting the interpretation of synergy in drug combination experiments. Specifically, I found: (1) the conflation of different types of

drug interactions (Section 2.3); (2) MSP frameworks are biased toward antagonism for drugs with intermediate efficacy (Section 2.4); and (3) DEP frameworks contain a Hill-slope dependent bias (Section 2.5). The Hill-slope bias results from satisfying the famous "sham" combination thought experiment, arguing against the merit of sham-compliance as a measure of validity for synergy frameworks. Using two large combination datasets (O'Neil et al., 2016; Mott et al., 2015), MuSyC identifies real-world examples where the conflicting assumptions of previous drug synergy frameworks misleads or impedes drug discovery efforts through these pervasive and predictable biases. I therefore propose MuSyC as a consensus framework to interpret combination pharmacology and signify its broad applicability to the study of drug mixtures.

Chapter 2

A Consensus Framework Unifies Multi-Drug Synergy Metrics

2.1 MuSyC: A mass action framework to measure synergistic effects

The 4-parameter Hill equation is commonly used to fit dose-response data from *in vitro* and *in vivo* assays (see Section 2.2 eq. (2.3) for derivation and Table 2.5 for parameter annotation). This equation can be derived from the equilibrium of a 2-state model of drug effect based on the Law of Mass Action (Figure 2.1A left). Traditionally, the parameters of the Hill equation are interpreted as a drug's efficacy ($E_0 - E_1$), potency (C), and cooperativity (h), also known as the Hill slope. These parameters correspond to three possible geometric transformations of a dose-response curve (Figure 2.1A right). To generalize this one-drug formalism to two concurrent drugs, I propose a 4-state mass-action model of combination pharmacology (Figure 2.1B left). From this model, I derived a two-dimensional (2D) Hill equation for two drugs (equation 2.8) defining a dose-response surface (Figure 2.1B middle). The derivation is as follows.

Consider a reversible transition between an unaffected population (U) and an affected population (A) governed by

$$U \underset{r_{-1}}{\overset{r_1 \cdot d^h}{\rightleftharpoons}} A \tag{2.1}$$

where d is the concentration of the drug, h is the Hill slope, often called cooperativity, and r_1 and r_{-1} are constants corresponding to the reaction rate (Figure 2.1A). Applying the Law of Mass Action, steady state ratios of U and A are determined to be

$$\frac{\mathrm{d}U}{\mathrm{d}t} = A \cdot r_{-1} - U \cdot r_1 d^h \equiv 0$$

$$\frac{A}{U} = \frac{r_1 d^h}{r_{-1}}$$

When $d = \frac{r_{-1}}{r_1}^{\frac{1}{h}}$, then $(A = U)$. This dose is commonly called the EC50 (herein denoted as C).

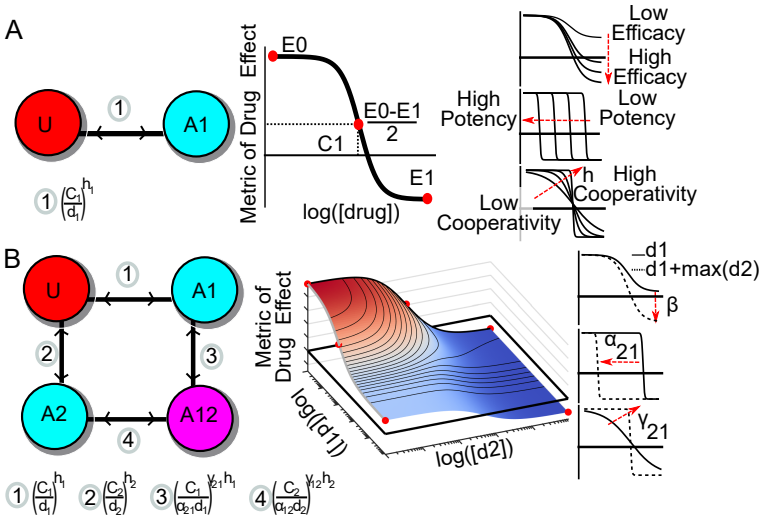

Figure 2.1: MuSyC mass action model of drug combination synergy. A) Single-drug model: The traditional equation for fitting dose-response relationships (middle) is the 4-parameter Hill equation. This equation can be derived using the Law of Mass Action from a two state model of drug effect (left). Edge notation is equal to the ratio of states at equilibrium ($\frac{A_1}{U}$). The Hill equation contains parameters measuring a drug's efficacy ($E_0 - E_1$), potency (C), and cooperativity (h). Each parameter corresponds to distinct geometric transformations of the dose-response curve (right). B) Two-drug model: MuSyC is derived from a four-state mass-action model of combination pharmacology (left) and results in a 2D Hill-like equation describing a dose-response surface (middle). Edge notation denotes the ratio of the connected corners for the boundary condition. For example, edge #3 annotation means $\frac{A_{12}}{A_1} \rightarrow \frac{C_1}{\alpha_{21} d_1}^{\gamma_{21} h_1}$ when $d_2 \rightarrow$ inf. Beyond the parameters of the single Hill equation, the 2D Hill equation has additional parameters (β, α, γ) corresponding to distinct transformations of the dose-response surface (right). These transformations directly measure the changes in a single drugs' efficacy, potency, and cooperativity due to the combination, and, therefore, are interpreted as synergistic efficacy (β), synergistic potency (α), and synergistic cooperativity (γ). There are two values for α and γ because each drug can independently modulate the potency and cooperativity of the other (Zimmer et al., 2016; Yadav et al., 2015) (edge 3 vs. edge 4 of the state transition model). In contrast, the single β parameter describes the percent increase in maximal effect due to both drugs (effect at A12). See Figure 2.2 for MuSyC extension to three drugs.

Because 100% of the population is either unaffected or affected, I also have the condition $U + A = 1$. This leads to the 2-parameter 1D Hill equation

$$U = \frac{C^h}{C^h + d^h} = \frac{1}{1 + \left(\frac{d}{C}\right)^h} \tag{2.2}$$

If the U and A differ by an observed effect (such as proliferation rate (Harris et al., 2016)), the measured effect E at dose d will be a weighted average

$$E = U \cdot E_0 + A \cdot E_1,$$

where E_0 and E_1 are the the effects characteristic of the U and A, respectively. From this I find the final form of a 4-parameter Hill equation:

$$E = E_1 + \frac{E_0 - E_1}{1 + \left(\frac{d}{C}\right)^h} \tag{2.3}$$

To extend the Hill equation to considering a system of two drugs, consider a phenomenological model with 4 possible states, U, A_1, A_2, and $A_{1,2}$ corresponding to populations that are unaffected, affected by drug 1 alone, affected by drug 2 alone, or affected by both drugs, respectively. The corresponding reactions between these states are:

$$\begin{aligned}
U &\underset{r_{-1}}{\overset{r_1 \cdot d_1^{h_1}}{\rightleftharpoons}} A_1 \\
U &\underset{r_{-2}}{\overset{r_2 \cdot d_2^{h_2}}{\rightleftharpoons}} A_2 \\
A_1 &\underset{r_{-2}^{\gamma_{12}}}{\overset{r_2^{\gamma_{12}} \cdot (\alpha_{12} d_2)^{\gamma_{12} h_2}}{\rightleftharpoons}} A_{1,2} \\
A_2 &\underset{r_{-1}^{\gamma_{21}}}{\overset{r_1^{\gamma_{21}} \cdot (\alpha_{21} d_1)^{\gamma_{21} h_1}}{\rightleftharpoons}} A_{1,2}
\end{aligned} \tag{2.4}$$

Here, the α parameters quantify the modulation of one drug's EC50 (potency) due to the other

drug. Similarly, the γ parameters measure the change of a drug's Hill slope (cooperativity) due to the other drug.

As in the 1D case, finding the steady state of the system leads to the following system of equations

$$\begin{aligned}
\frac{\mathrm{d}U}{\mathrm{d}t} &= -U \cdot \left(r_1 d_1^{h_1} + r_2 d_2^{h_2}\right) + A_1 \cdot r_{-1} + A_2 \cdot r_{-2} \\
\frac{\mathrm{d}A_1}{\mathrm{d}t} &= -A_1 \cdot \left(r_{-1} + r_2^{\gamma_{12}} (\alpha_{12} d_2)^{\gamma_{12} h_2}\right) + U \cdot r_1 d_1^{h_1} + A_{1,2} \cdot (r_{-2})^{\gamma_{12}} \\
\frac{\mathrm{d}A_2}{\mathrm{d}t} &= -A_2 \cdot \left(r_1^{\gamma_{21}} (\alpha_{21} d_1)^{\gamma_{21} h_1} + r_{-2}\right) + U \cdot r_2 d_2^{h_2} + A_{1,2} \cdot (r_{-1})^{\gamma_{21}} \\
\frac{\mathrm{d}A_{1,2}}{\mathrm{d}t} &= -A_{1,2} \cdot \left(r_{-1}^{\gamma_{21}} + r_{-2}^{\gamma_{12}}\right) + A_1 \cdot r_2^{\gamma_{12}} (\alpha_{12} d_2)^{\gamma_{12} h_2} + A_2 \cdot r_1^{\gamma_{21}} (\alpha_{21} d_1)^{\gamma_{21} h_1}
\end{aligned} \tag{2.5}$$

At equilibrium, the equations 2.5 must all be equal to zero; however, the system only defines a rank 3 matrix. Taking the first three equations from 2.5 with the constraint $U + A_1 + A_2 + A_{1,2} = 1$, I define

$$\mathbf{M} := \begin{bmatrix}
-\left(r_1 d_1^{h_1} + r_2 d_2^{h_2}\right) & r_{-1} & r_{-2} & 0 \\
r_1 d_1^{h_1} & -\left(r_{-1} + r_2^{\gamma_{12}} (\alpha_{12} d_2)^{\gamma_{12} h_2}\right) & 0 & (r_{-2})^{\gamma_{12}} \\
r_2 d_2^{h_2} & 0 & -\left(r_1^{\gamma_{21}} (\alpha_{21} d_1)^{\gamma_{21} h_1} + r_{-2}\right) & (r_{-1})^{\gamma_{21}} \\
1 & 1 & 1 & 1
\end{bmatrix} \tag{2.6}$$

such that

$$\mathbf{M} \cdot \begin{bmatrix} U & A_1 & A_2 & A_{1,2} \end{bmatrix}^T = \begin{bmatrix} 0 & 0 & 0 & 1 \end{bmatrix}^T$$

or, solving for the proportions of each state,

$$\begin{bmatrix} U & A_1 & A_2 & A_{1,2} \end{bmatrix}^T = \mathbf{M}^{-1} \cdot \begin{bmatrix} 0 & 0 & 0 & 1 \end{bmatrix}^T \tag{2.7}$$

If I again consider distinct effects E_0, E_1, E_2, and E_3 distinguishing populations U, A_1, A_2, and $A_{1,2}$, I find the equation for the dose response surface to be

$$E = \begin{bmatrix} E_0 & E_1 & E_2 & E_3 \end{bmatrix} \cdot \mathbf{M}^{-1} \cdot \begin{bmatrix} 0 & 0 & 0 & 1 \end{bmatrix}^T \tag{2.8}$$

As $d1 \to \infty$ the equation reduces to

$$E = E_3 + \frac{E_1 - E_3}{1 + \left(\frac{\alpha_{12} d2}{C2}\right)^{\gamma_{12} h2}} \tag{2.9}$$

by which I can see the 2D equation reduces to a 1D Hill equation at the boundaries. The proof is as follows.

When $d_1 \to \infty$, then the 4 state reduces to 2 states transition model between A1 and A12.

$$A_1 \underset{r_{-2}^{\gamma_{12}}}{\overset{r_2^{\gamma_{12}} \cdot (\alpha_{12} d_2)^{\gamma_{12} h_2}}{\rightleftharpoons}} A_{1,2} \tag{2.10}$$

At equilibrium

$$\frac{A_{1,2}}{A_1} = \frac{r_2^{\gamma_{12}} (\alpha_{12} d_2)^{\gamma_{12} h_2}}{r_{-2}^{\gamma_{12}}} \tag{2.11}$$

When $A_1 = A_{1,2}$ this is the EC50 for drug 2 given saturating concentrations of drug 1 (C_2'). This dose can be found by solving the above.

$$C_2' = \frac{1}{\alpha_{12}} \left(\frac{r_2}{r_{-2}}\right)^{1/h_2} = \frac{C_2}{\alpha_{12}} \tag{2.12}$$

The boundary then reduces to a Hill equation of the form

$$E = E_3 + \frac{E_1 - E_3}{1 + \frac{\alpha_{12} d_2}{C_2}^{\gamma_{12} h_2}} \tag{2.13}$$

The 2D Hill equation (eq. 2.8) contains five additional parameters, not present in the single-drug Hill equation, which measure different types of drug interactions. These additional parameters measure changes in a drug's efficacy (β), potency (α_{12} and α_{21}), and cooperativity (γ_{12} and γ_{21}) in a combination —representing three distinct types of synergy (Figure 2.1B right, Table 2.5). I therefore term these parameters as synergistic efficacy, synergistic potency, and synergistic cooperativity. As I show in Section 2.2, these parameters are conflated in traditional synergy metrics

obscuring the true origin and magnitude of drug synergy or antagonism.

Following the cubic geometry of the mass action model in (Figure 2.1B) it is trivial to continue to expand to increasing numbers of drugs. Figure 2.2 shows the extension to three drug system resulting in a cube. For combinations of 4 drugs, the geometry is a tesseract. In general, MuSyC can describe combinations N-drug combinations by considering 2^N possible states with transitions defining the edges of an N-dimensional hypercube. Dose-response surfaces generalize to N-dimensional scalar functions. In the most general case, for N drugs there are $2^N - N - 1$ distinct β parameters (one for each state characterized by the action of at least 2 drugs), and $n \cdot \left(2^{n-1} - 1\right)$ distinct α and γ parameters (one for each edge, excluding edges connected to the undrugged state, which correspond only to single-drug potency and cooperativity). Thus, MuSyC can account for higher-order synergies (*e.g.*, synergy that emerges from a combination of three drugs, but is not evident in any pairwise combination of those drugs); however, the rapid growth of the number of synergy parameters with N suggests that significant quantities of data, or confident knowledge of pairwise synergies, would be needed to measure such higher-order synergies.

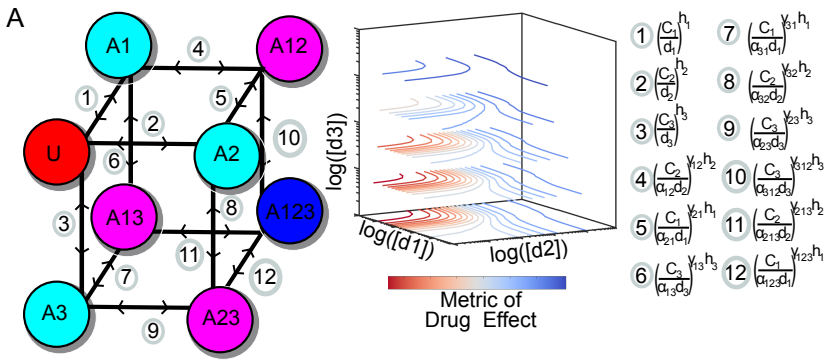

Figure 2.2: Extension of MuSyC to combinations of three drugs. A) Following the cubic geometry of Figure 2.1B, combinations of 3 drugs result in a cube. Numbered notation next to each edge corresponds to the ratio of the connected corners at equilibrium for the boundary conditions. For example, edge #10 annotation means $\frac{A_{123}}{A_{12}} \rightarrow \left(\frac{C_3}{\alpha_{23} d_3}\right)^{\gamma_{312} h_3}$ as $d_1 \rightarrow \text{inf}$, $d_2 \rightarrow \text{inf}$.

2.2 A bridge between DEP and MSP maps existing synergy approaches onto a common landscape

In recent years, several alternative synergy models have been proposed. Broadly, these models are derived from one of two guiding principles: the Multiplicative Survival Principle (MSP) and the Drug Equivalence Principle (DEP) (Table 2.6). Prior work has shown contradictory results when comparing between MSP and DEP frameworks (Greco et al., 1995), and there remains a lack of consensus on the commonality between the two principles (Greco et al., 1992; Yadav et al., 2015; Twarog et al., 2016; Foucquier and Guedj, 2015). Here I show MuSyC satisfies both the DEP and MSP under certain conditions (Figure 2.3A,B), thereby unifying the foundational principles of drug synergy.

2.2.1 MuSyC subsumes the Multiplicative Survival Principle

The MSP was first described by Bliss (Bliss, 1939) and is the foundation of the Bliss Independence framework. MSP assumes the probability of a cell surviving treatment by drug 1 (U_1) is independent of the probability of the same cell surviving treatment by drug 2 (U_2). Therefore, the probability of surviving both Drug 1 and Drug 2 is $U = U_1 \cdot U_2$ (Bliss, 1939). Synergy or antagonism occur when $U \neq U_1 \cdot U_2$. MuSyC satisfies the MSP under the following conditions: (1) the effect metric is expressed as a percent ($E_0 = 1$, and $E_3 = E_1E_2$), (2) there is no potency synergy ($\alpha_{12} = \alpha_{21} = 1$), and (3) there is and no cooperativity synergy ($\gamma_{12} = \gamma_{21} = 1$) (Figure 2.3A).

To show this, let each drug in isolation have a 1D hill response

$$U_i = \frac{1}{1 + \left(\frac{d_i}{C_i}\right)^{h_i}} \tag{2.14}$$

where U_i reflects the portion of cells unaffected by drug i alone. For the 2D case, when $\alpha_{12} = \alpha_{21} = 1$ and $\gamma_{12} = \gamma_{21} = 1$, each edge in Figure 2.1B satisfies detailed balance and therefore the

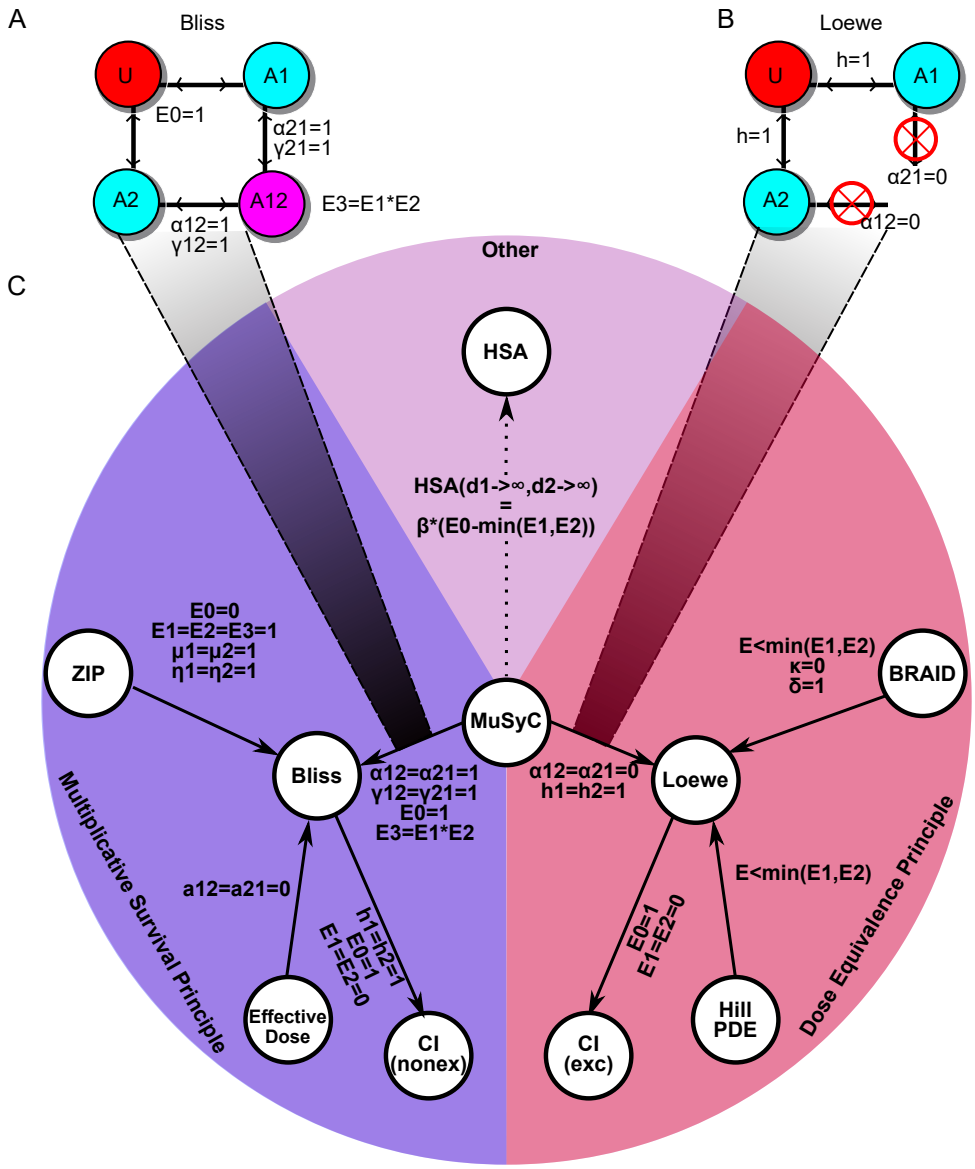

Figure 2.3: Unifying MSP and DEP with MuSyC, and mapping the landscape of drug synergy. A) The Bliss null model, the base model for all MSP frameworks, emerges from MuSyC when $E_0 = 1$, $\alpha_{12} = \alpha_{21} = \gamma_{12} = \gamma_{21} = 1$, and $E_3 = E_1 E_2$. B) The Loewe null model, the base model for all DEP frameworks, emerges from MuSyC when $h_1 = h_2 = 1$ and $\alpha_{12} = \alpha_{21} = 0$. The constraint on α indicates the drugs' activities are mutually exclusive (*i.e.*, the double-drugged state $A_{1,2}$ does not exist). C) Network of relationships between synergy frameworks (nodes) grouped by their underlying principle (colors). The notation next to solid edges signifies conditions under which source model reduces to end model's null model. The dotted edge indicates MuSyC synergistic efficacy (β) is proportional to HSA as $d_1 \to \infty, d_2 \to \infty$. Where possible, parameters from each framework were translated in terms of the dose-response parameters defined for MuSyC (Table 2.5) to facilitate comparison.

state occupancy is given by

$$A_1 = \left(\frac{d_1}{C_1}\right)^{h_1} U$$
$$A_2 = \left(\frac{d_2}{C_2}\right)^{h_2} U$$
$$A_{1,2} = \left(\frac{d_2}{C_2}\right)^{h_2} A_1$$

Because $U + A_1 + A_2 + A_{1,2} = 1$, the MuSyC mass action model gives

$$U = \frac{1}{1 + \left(\frac{d_1}{C_1}\right)^{h_1} + \left(\frac{d_2}{C_2}\right)^{h_2} + \left(\frac{d_1}{C_1}\right)^{h_1}\left(\frac{d_2}{C_2}\right)^{h_2}} \tag{2.15}$$
$$A_1 = \frac{\left(\frac{d_1}{C_1}\right)^{h_1}}{1 + \left(\frac{d_1}{C_1}\right)^{h_1} + \left(\frac{d_2}{C_2}\right)^{h_2} + \left(\frac{d_1}{C_1}\right)^{h_1}\left(\frac{d_2}{C_2}\right)^{h_2}}$$
$$A_2 = \frac{\left(\frac{d_2}{C_2}\right)^{h_2}}{1 + \left(\frac{d_1}{C_1}\right)^{h_1} + \left(\frac{d_2}{C_2}\right)^{h_2} + \left(\frac{d_1}{C_1}\right)^{h_1}\left(\frac{d_2}{C_2}\right)^{h_2}}$$
$$A_{1,2} = \frac{\left(\frac{d_1}{C_1}\right)^{h_1}\left(\frac{d_2}{C_2}\right)^{h_2}}{1 + \left(\frac{d_1}{C_1}\right)^{h_1} + \left(\frac{d_2}{C_2}\right)^{h_2} + \left(\frac{d_1}{C_1}\right)^{h_1}\left(\frac{d_2}{C_2}\right)^{h_2}}$$

From this, it is easy to verify that $U = U_1 \cdot U_2$ where $U_1 = 1 - (A_1 + A_{1,2})$ and $U_2 = 1 - (A_2 + A_{1,2})$ which is equivalent to the Bliss Independence null model.

Furthermore, given $E_0 = 1$

$$E = U + A_1 E_1 + A_2 E_2 + A_{1,2} E_3 \tag{2.16}$$

I define $\overline{U_i}$, $\overline{A_i}$, and $\overline{E_i} = \overline{U_i} + \overline{A_i} E_i$ to be the fraction of unaffected cells, fraction of affected cells, and observed effect for treatment due to the single drug i, as described by equation 2.14. The overline distinguishes affects attributable to each drug, such that $\overline{A_1}$ includes cells affected either by drug 1 alone, or by both drug 1 and drug 2, while A_1 only includes cells affected by drug 1, but

not drug 2 (*i.e.*, $\overline{A_1} = A_1 + A_{1,2}$). Then

$$\begin{aligned}\overline{E_1} \cdot \overline{E_2} &= \left[\overline{U_1} + (1 - \overline{U_1}E_1)\right]\left[\overline{U_2} + (1 - \overline{U_2}E_2)\right] \\ &= \overline{U_1U_2} + E_1(\overline{U_2} - \overline{U_1U_2}) + E_2(\overline{U_1} - \overline{U_1U_2}) + E_1E_2(1 - \overline{U_1})(1 - \overline{U_2})\end{aligned}$$

From 2.15, I know $U = \overline{U_1} \cdot \overline{U_2}$, and $A_{1,2} = \overline{A_1} \cdot \overline{A_2}$, leading to

$$= U + E_1(\overline{U_2} - U) + E_2(\overline{U_1} - U) + E_1E_2A_{1,2}$$

Similarly, it is simple to show $A_1 = \overline{U_2} - U$, and similarly for A_2

$$= U + E_1A_1 + E_2A_2 + E_1E_2A_{1,2}$$

If $E_3 = E_1 \cdot E_2$, then this is equivalent to equation (2.16). Therefore, given $\alpha_{12} = \alpha_{21} = 1$, $\gamma_{12} = \gamma_{21} = 1$, $E_0 = 1$, and $E_3 = E_1 \cdot E_2$, MuSyC predicts $\overline{E_1} \cdot \overline{E_2} = E$. Thus, while Bliss was derived purely within the scope of "percent affected", MuSyC shows that the Bliss model may be appropriately extended to any measure of effect for which $E_0 = 1$ and effects are expected to be multiplicative. Nevertheless, for effects which do not satisfy these criteria, the Bliss model cannot be reliably used, while MuSyC may still be used for arbitrary effects.

2.2.2 MuSyC subsumes The Dose Equivalence Principle

The DEP was first established by Loewe (Loewe, 1926, 1927) and subsequently expanded by Chou and Talalay (Chou and Talalay, 1984). This approach assumes that for a given effect E—achievable either by dose d_1 of Drug 1 alone, or dose d_2 of Drug 2 alone—there is a constant ratio $R = \frac{d_1}{d_2}$ such that using Δd_2 less of Drug 2 can always be compensated for with $\Delta d_1 = R\Delta d_2$ more of Drug 1 to achieve the same effect (Foucquier and Guedj, 2015). This definition leads to the linear isoboles (contours of equal effect) characteristic of the Loewe null model (Figure 2.4 left panel). Synergy occurs when less one drug is required to compensate for a decrease in the other

than expected by DEP.

Chou and Talalay first showed that linear isoboles emerge when the two drugs are mutually exclusive (Chou and Talalay, 1981), meaning that the double-drugged state ($A_{1,2}$ in Figure 2.1B) is unreachable. In MuSyC, this requires setting $\alpha_{12} = \alpha_{21} = 0$, which reduces the 2D Hill equation (eq. (2.8)) to

$$(E - E_0) + (E - E_1)\left(\frac{d_1}{C_1}\right)^{h_1} + (E - E_2)\left(\frac{d_2}{C_2}\right)^{h_2} = 0 \tag{2.17}$$

From this equation it is easy to see when $h_1 = h_2 = 1$, the conic section reduces to a line, resulting in the canonical linear isoboles of Loewe Additivity and the CI null models. Further from equation (2.17), I find the slope of isoble is equal to $-\frac{C_2}{C_1}$ as shown by:

$$\frac{\partial}{\partial E}\left((E - E_0) + (E - E_1)\left(\frac{d_1}{C_1}\right) + (E - E_2)\left(\frac{d_2}{C_2}\right)\right) = 0$$

$$d_2 = -d_1\frac{C_2}{C_1} - C_2$$

Therefore the constant R in the statement of the Dose Equivalence Principle is revealed by MuSyC to be equal to the ratio of the two drugs' EC50. There is no dependence on β or γ because those parameters relate to the $A_{1,2}$ state, which is blocked here. For fixed values of E, equation (2.17) results in linear isoboles only when $h_1 = h_2 = 1$. Thus, given these conditions on α and h, MuSyC reproduces the DEP. However, when $h \neq 1$ nonlinear isoboles result (Figure 2.4 middle and right panel), suggesting that DEP is an inappropriate expectation for such drugs (see Section 2.5 on page 57 for further investigation into this issue).

Therefore, MuSyC satisfies the DEP under the following conditions: (1) the drugs are mutually exclusive ($\alpha_{12} = \alpha_{21}$=0) and (2) $h_1 = h_2 = 1$ (Figure 2.3B).

2.2.3 Mapping the global landscape of drug synergy frameworks

From the literature, I identified several prominent synergy models beyond Bliss and Loewe including: CI (Chou et al., 1983), HSA (Gaddum, 1940), Effective Dose model (Zimmer et al., 2016), ZIP (Yadav et al., 2015), and Hill PDE (Schindler, 2017). Table 2.6 compares key features

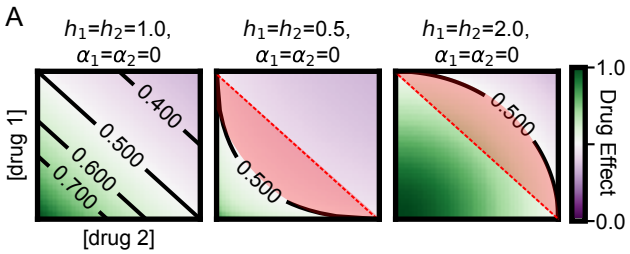

Figure 2.4: Loewe bias results from non-linear isobles when the Hill slope does not equal one. A) When $h = 1$ and $\alpha = 0$, MuSyC results in linear isoboles (contours of equivalent effect) characteristic of DEP models. When $h < 1$ (middle panel), the isoboles bend inward such that DEP models will misclassify the red region as synergistic, biasing DEP calculations toward synergy for $h < 1$. Conversely when $h > 1$, isoboles bend outward (right panel) and DEP models will misclassify the red region as antagonistic, biasing Loewe toward antagonism for $h > 1$.

and assumption of the different synergy models. Each of these methods, as well as MuSyC, defines synergy based on the experimental deviation from a null (additive) dose-response surface. Because almost all synergy frameworks are founded on either the DEP or MSP, I standardized relationships between the various models, mapping the global landscape of drug synergy (Figure 2.3C). The details for each method is as follows:

Effective dose model (Zimmer *et. al.*)

Zimmer *et. al.* (Zimmer et al., 2016) introduced the EDM as a parameterized extension of Bliss, and were the first to account the asymmetric potency synergy, which is also present in MuSyC. The effective dose model is constructed by fitting the dose response of each single drug to a two-parameter 1D Hill equation in which E_0 and E_{max} are fixed at 1 and 0, respectively

$$g(d_{1,eff}) = \frac{1}{1+(\frac{d_{1,eff}}{C_1})^{h_1}} \qquad (2.18)$$
$$g(d_{2,eff}) = \frac{1}{1+(\frac{d_{2,eff}}{C_2})^{h_2}}$$

To model combination synergy, the authors propose transforming the doses d_i to "effective doses" via a system of equations coupling effective doses to one another via a Michaelis-Menten term in the denominator scaled by a synergy parameter a.

$$d_{1,eff} = \frac{d_1}{1 + a_{12}\left(\frac{1}{1+\left(\frac{d_{2,eff}}{C_2}\right)^{-1}}\right)} \tag{2.19}$$
$$d_{2,eff} = \frac{d_2}{1 + a_{21}\left(\frac{1}{1+\left(\frac{d_{1,eff}}{C_1}\right)^{-1}}\right)}$$

Table 2.1: Translating the EDM. Where possible, the original variable names from Zimmer *et. al.* have been translated to the equivalent variable names used in this manuscript, for ease of readability.

Original variable name	MuSyC variable name
n_1	h_1
$D0_1$	C_1
n_2	h_2
$D0_2$	C_2

The parameter a_{12} represents how drug 2 modifies the effective dose synergistically ($a_{12} < 0$) or antagonistically ($a_{12} > 0$) drug 1. Note that as $a_{12} \to -\left(\frac{1+d_{2,eff}/C_2}{d_{2,eff}/C_2}\right)$, $d_{1,eff} \to +\infty$, and as $a_{12} \to +\infty$, $d_{1,eff} \to 0$, which defines the bounds over which a_{12} is defined. The authors then fit the a parameters using a surface model based on MSP

$$E_d = g(d_{1,eff}) \cdot g(d_{2,eff}) \tag{2.20}$$

Thus the EDM reduces to the Bliss null model when $a_{12} = a_{21} = 0$. There are obvious similarities between EDM's a parameters and MuSyC's α values, as both reflect a potency transformation; however, the exact details are slightly different. For example, EDM assumes each drug has a Michaelis-Menten like effect on the potency of the other drugs (eq. (2.19)), whereas MuSyC

can account for non-Michaelis-Menten effects (when $h \neq 1$). Furthermore, by using equation 2.18, EDM explicitly assumes the measured drug effect ranges from 100% to 0%, and fit the data with this constraint. Their model is unable to accurately describe combinations where the two drugs either have unequal maximum effects, or the combination has a greater effect than the drugs can achieve alone, features which are commonly observed (Fallahi-Sichani et al., 2013) (Figure 2.12). In contrast, MuSyC is able to fit dose response surfaces with arbitrary effect ranges.

ZIP

Table 2.2: Translating ZIP. Where possible, the original variable names from Yadav *et. al.* (Yadav et al., 2015) have been translated to the equivalent variable names used in this manuscript, for ease of readability. Note I found an erratum flipping x_2 and m_2 in the step from equation 13 to equation 14 in Yadav *et. al.* which is propagated through to equation 19. Our analysis uses the intended form.

Original variable name	Translated variable name
m_1	C_1
m_2	C_2
$m_{1\to2}$	$\mu_1 \cdot C_2$
$m_{2\to1}$	$\mu_2 \cdot C_1$
λ_1	h_1
λ_2	h_2
$\lambda_{1\to2}$	$\eta_1 \cdot h_2$
$\lambda_{2\to1}$	$\eta_2 \cdot h_1$
x_1	d_1
x_2	d_2
δ	δ

In contrast to the Effective Dose Model, ZIP, accounts for changes in both the Hill slope and the potency across the dose-response surface. In ZIP, these changes are integrated into a single number (δ), given by

$$\delta = \frac{1}{2}\left(\frac{\frac{1}{1+\frac{d_2}{C_2}^{h_2}} + \frac{d_1}{\mu_2 C_1}^{\eta_2 h_1}}{1+\frac{d_1}{\mu_2 C_1}^{\eta_2 h_1}} + \frac{\frac{1}{1+\frac{d_1}{C_1}^{h_1}} + \frac{d_2}{\mu 1 C_2}^{\eta 1 h_2}}{1+\frac{d_2}{\mu_1 C_2}^{\eta_1 h_2}}\right) - \left(\frac{1}{1+\frac{d_1}{C_1}^{-h_1}} + \frac{1}{1+\frac{d_2}{C_2}^{-h_2}} - \frac{1}{1+\frac{d_1}{C_1}^{-h_1}}\frac{1}{1+\frac{d_2}{C_2}^{-h_2}}\right) \tag{2.21}$$

ZIP is formulated for arbitrary E_0 and E_{max}; however, it assumes E_{max} is the same for both drugs, as well as the combination ($E_1 = E_2 = E_3$). To calculate δ, the ZIP method fixes the concentration of one drug, then fits a Hill-equation dose response for the other drug. However, for combinations with efficacy synergy or antagonism, slices of the dose-response surface can have non-Hill, and even non-monotonic shapes. In these cases, ZIP parameter fits may not be meaningful. Because MuSyC accounts explicitly for efficacy synergy, its surfaces are able to describe such complex drug combination surfaces where ZIP cannot.

Nevertheless, ZIP parameters μ and η are closely related to MuSyC parameters α and γ. In the absence of synergistic efficacy, slices of MuSyC dose-response surfaces are sigmoidal, though in general do not perfectly follow a Hill equation, and so the ZIP model is still not identical to MuSyC. However, at saturating concentrations of one or the other drug, MuSyC does reduce to the Hill equation. In these saturating cases, ZIP's δ can be related analytically to MuSyC's α and γ by

$$\lim_{d_2\to\infty}\delta(d_1,d_2) = \frac{1}{2}\left(\frac{1}{1+\left(\frac{d_1}{\alpha_{21}C_1}\right)^{\gamma_{21}h_1}}\right)$$

$$\lim_{d_1\to\infty}\delta(d_1,d_2) = \frac{1}{2}\left(\frac{1}{1+\left(\frac{d_2}{\alpha_{12}C_2}\right)^{\gamma_{12}h_2}}\right)$$

BRAID

BRAID (Twarog et al., 2016) is an extension of the DEP to effects exceeding the weaker drug and consequently reduces to Loewe under particular conditions (Figure 2.3). The authors propose three BRAID models with increasing complexity, with eBRAID capable of describing the most general dose-interaction surfaces. I focus my analysis on eBRAID, which assumes that each drug alone has a Hill-like response, and constructs an Hill-like equation for the combination

$$E = E_0 + \frac{E_3 - E_0}{1 + D^{-\delta \cdot \sqrt{h_1 h_2}}} \tag{2.22}$$

where

$$D = D1^{\frac{1}{\delta \cdot \sqrt{h_1 h_2}}} + D2^{\frac{1}{\delta \cdot \sqrt{h_1 h_2}}} + \kappa \sqrt{D1^{\frac{1}{\delta \cdot \sqrt{h_1 h_2}}} D2^{\frac{1}{\delta \cdot \sqrt{h_1 h_2}}}}$$

$$D1 = \frac{\frac{E_1 - E_0}{E_3 - E_0} (\frac{d_1}{C_1})^{h_1}}{1 + (1 - \frac{E_1 - E_0}{E_3 - E_0})(\frac{d_1}{C_1})^{h_1}}$$

$$D2 = \frac{\frac{E_2 - E_0}{E_3 - E_0} (\frac{d_2}{C_2})^{h_2}}{1 + (1 - \frac{E_2 - E_0}{E_3 - E_0})(\frac{d_2}{C_2})^{h_2}}$$

The BRAID equation (eq. (2.22)) uses a dose parameter, which combines the doses of both individual drugs, using a parameter κ and a parameter for the Hill slopes δ which acts as a multiplicative of the geometric mean hill slope $h = \sqrt{(}h_1 h_2)$. This formalism, like Loewe, is sham compliant under certain conditions, namely when $\kappa = 2^{\frac{-1}{\delta h}} - 2^{-h}$. By adjusting κ, BRAID is able to fit complex drug combination surfaces, including non-monotonic responses, unlike ZIP. Additionally, because BRAID fits the whole combination surface using a single parameter, it can be used to make unambiguous statements about whether the combination is synergistic or antagonistic. Nevertheless, BRAID does not account for differences in synergy due to efficacy, potency, and cooperativity, whereas I find many combinations that are synergistic with respect to one, but antagonistic with respect to the other (Figure 2.6C). Though κ and δ are related to the potency and cooperativity respectively, their biochemical interpretation is not straightforward.

Highest Single Agent

Highest single agent (HSA) (Gaddum, 1940) is a parsimonious model that defines synergy as the

Table 2.3: Translating the BRAID model. Based on eBRAID model set of equations in the supplement. Note I corrected a typo in equation for $\tilde{D}_A$ where $ID_{M,B}$ is suppose to be $ID_{M,A}$

Original variable name	Translated variable name
D_A	d_1
D_B	d_2
$\tilde{D}_{AB}$	D
$\tilde{D}_A$	$D1$
$\tilde{D}_B$	$D2$
E_0	E_0
E_f	E_3
$E_{f,A}$	E_1
$E_{f,B}$	E_2
E_{AB}	E_d
n_a	h_1
n_b	h_2
$ID_{M,A}$	C_1
$ID_{M,B}$	C_2
δ	δ
κ	κ

net difference between the combination response and the stronger single-drug response

$$HSA = min(E_d(d_1,0), E_d(0,d_2)) - E_d(d_1,d_2) \tag{2.23}$$

This form assumes that drug decreases E, though it can also be defined for drugs that increase E. At high concentrations of d_1 and d_2, equation (2.23) becomes proportional to our definition of efficacy synergy (β) as shown in equation 2.24 and Figure 2.3. Nevertheless, at intermediate doses, HSA will conflate synergy of potency, efficacy, and cooperativity (Figure 2.9) highlighting the importance of considering the whole dose-response surface when calculating synergy.

$$\lim_{d_1,d_2\to\infty} HSA(d_1,d_2) = \beta \cdot (E_0 - min(E_1,E_2)) \tag{2.24}$$

2D Hill PDE

$$E_d = \left(\frac{E_1(\frac{d_1}{C_1}) + E_2(\frac{d_2}{C_2})}{(\frac{d_1}{C_1}) + (\frac{d_2}{C_2})} \right) \left(\frac{1}{1 + ((\frac{d_1}{C_1}) + (\frac{d_2}{C_2}))^{-\left(\frac{h_1(\frac{d_1}{C_1}) + h_2(\frac{d_2}{C_2})}{(\frac{d_1}{C_1}) + (\frac{d_2}{C_2})} \right)}} \right) \tag{2.25}$$

Table 2.4: Translating the Schindler *et al.* model.

Parameter	Translated
m_a	d_1/C_1
m_b	d_2/C_2
a_{max}	E_1
b_{max}	E_2
α	h_1
β	h_2

The most recent framework is one by Schindler (Schindler, 2017) which interpolates a null dose-response surface from the single dose-response curves alone without any fit parameters. This was done by using PDE Hill equations and then imposing boundary conditions as well as sham compliance. It is therefore an extension of Loewe to effects greater than the least efficacious drug (Figure 2.3, Table 2.6). The boundary conditions enforce the null model's maximal effect of the combination (E_3) is equal to the mean of E_1 and E_2. This results in the non-intuitive scenarios such as if the maximal effect of one compound is 0.25 and the other is 0.75, then the null hypothesis for the maximal effect of the combination is 0.5 which is much less than achievable with a single drug.

In deriving this map, I uncovered potential sources of error when using MSP or DEP methods which impact interpretation of synergy studies. Specifically, I identified three recurrent considerations meriting attention from the field. 1) Previous synergy metrics conflate different synergy types (*i.e.* potency, efficacy, cooperativity) in ways that can mask synergistic and antagonistic interactions (Section 2.3). 2) The connection between MuSyC and the MSP-derived frameworks depend

on the single drugs' efficacy (E_1,E_2), and as a result, MSP frameworks are biased against the combination of moderately efficacious single agents (Section 2.4). 3) The connection between the DEP and MuSyC is constrained by single drugs Hill slopes (h) and therefore DEP frameworks impose a Hill-slope dependent bias, artificially inflating the synergy for drugs with low Hill slopes (Section 2.5). To assess impact of these considerations on synergy calculations in different fields, I analyzed two large publicly available datasets (Table 2.7) using MuSyC and other synergy frameworks (See Appendix 4.4 for methods). Note, while synergistic cooperativity (γ) is theoretically plausible (as initially postulated by (Yadav et al., 2015)), including it did not increase the fit quality (Figure 2.5) as measured by AIC and therefore I ignore synergistic cooperativity in subsequent analysis.

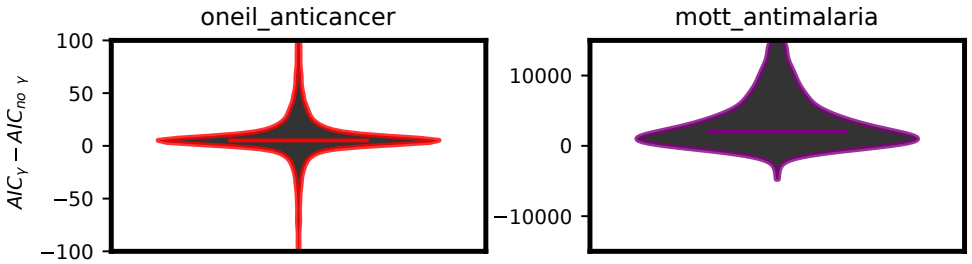

Figure 2.5: Fitting γ does not significantly improvement fits. A) Difference in the Akaike Information Criterion (AIC) values for MuSyC models including fitting synergistic cooperativity (γ_{12} and γ_{21}) or fixing γ to 1 thereby reducing the parameter count by two. Models which minimize AIC are preferred. The mean $AIC_\gamma - AIC_{no\gamma}$ for anti-cancer and anti-malarial datasets was 8 and 3312, respectively. The percent of combinations for which the model including γ had a lower AIC value was 18% and 5%, respectively.

Table 2.5: Annotation of MuSyC parameters.

U	Percent of unaffected population.
A_1,A_2	Percent of affected by drug 1 and drug 2, respectively.
$A_{1,2}$	Percent of affected by both drug 1 and drug 2.
d_1, d_2	Drug concentrations for drug pair.
E_d	Measured effect at (d_1, d_2).
C_1,C_2	The concentration of drug required to achieve 50% of the maximal effect (*i.e.*, EC_{50}).
h_1,h_2	Hill coefficients for dose response curves of drug 1 and 2 in isolation.
E_0	The basal effect $E_d(d1 = d2 = 0)$.
E_1,E_2	Maximal efficacy of drugs 1 and 2 in isolation.
E_3	Maximal efficacy of the combination of drugs 1 and 2.
β	Percent increase (or decrease) in max effect with both drugs over the most efficacious single drug ($\beta := \frac{min(E_1,E_2)-E_3}{E_0-min(E_1,E_2)}$).
α_{12}	Fold change in the potency (C_2) of $[d_2]$ induced by drug 1.
α_{21}	Fold change in the potency (C_1) of $[d_1]$ induced by drug 2.
γ_{12}	Fold change in the cooperativity (h_2) of $[d_2]$ induced by drug 1.
γ_{21}	Fold change in the cooperativity (h_1) of $[d_1]$ induced by drug 2.

Table 2.6: Comparing MySyC to traditional and modern frameworks for calculating synergy.

	DEP				MSP			Other	Both	
	Loewe	BRAID	Hill PDE	CI*	Bliss	EDM	ZIP	HSA	MuSyC	
Defined for arbitrary metrics of drug effect (not just percent data)	✓	✓					✓	✓	✓	
Does not require all drugs to be equally efficacious		✓	✓		✓			✓	✓	
Synergy is concentration independent		✓				✓			✓	
Synergy is related to traditional dose-response parameters						✓		✓	✓	
Satifies the sham experiment	✓	✓	✓	✓						

*CI has 2 equations for synergy in the original derivation (Chou et al., 1983)
for the mutually exclusive and mutually non-exclusive case.
The mutually exclusive case, which is equivalent to Loewe, has been widely adopted
and is the model compared here.

Table 2.7: Summary of the datasets used for validating theoretical predictions by MuSyC.

Model	# of Combinations	Metric of Drug Effect	Citation
P. falciparum Strains:3D7,HB3,Dd2	773	% Response	(Mott et al., 2015)
37 Cancer Cell Lines	22,738	% Viable	(O'Neil et al., 2016)

2.3 Conflating synergistic potency and efficacy masks synergistic interactions

To determine how conflation of distinct synergy types impacts the interpretation of drug-response data, I generated synthetic dose-response surfaces using MuSyC (eq. 2.8) across a range of α and β values and calculated the synergy according to Loewe, Bliss, and Highest Single Agent (HSA) at the EC50 of both drugs (Figures 2.6A,2.8A,2.9A). In each case, many distinct sets of $(\alpha_{12}, \alpha_{21}, \beta)$ are indistinguishable (*e.g.* the black contour line on the spheres).

Figure 2.6A shows that near the boundary between synergism and antagonism, Loewe is insensitive to changes in synergistic potency, tracking instead with synergistic efficacy. Consequently, in the anti-cancer dataset from O'Neil *et. al.* (O'Neil et al., 2016), Loewe misses potency antagonism in combinations with synergistic efficacy (Figure 2.6B middle distribution, see Figure 2.7 for an example surface). This reflects Loewe's assertion of infinite potency antagonism ($\alpha_{12} = \alpha_{21} = 0$, Figure 2.3A) in its null model. Therefore, combinations that are antagonistically potent ($\alpha < 1$) are all synergistic by Loewe in the absence of sufficient antagonistic efficacy (values above black contour in Figure 2.6A). Indeed, Loewe is frequently synergistic even in cases of antagonistic potency and efficacy (Figure 2.6B bottom distribution). As an example, the combination of methotrexate (targets folate synthesis) and erlotinib (EGFR inhibitor) in UWB1289 (BRCA1-mutant ovarian carcinoma) cells is antagonistically efficacious and potent by MuSyC, but synergistic by Loewe (Figure 2.6C).

Bliss synergy is classically thought to calculate synergistic potency. This is because assays where Bliss is appropriate ($E_0 = 1$ and $E1 = E2 = E3 = 0$) by definition have no synergistic efficacy. However, even in these cases, Bliss still conflates α_{12} and α_{21} such that asymmetric potency synergy is obfuscated (Figure 2.8A, black contour line through $\beta = 0$ plane). In the anti-malarial dataset from Mott *et. al.* (Mott et al., 2015), Bliss is consistently synergistic when $log(\alpha_{12}, \alpha_{21}) > 0$, and antagonistic if $log(\alpha_{12}, \alpha_{21}) < 0$; however, when $log(\alpha_{12}) < 0 < log(\alpha_{21})$, Bliss will strictly classify a combination as either synergistic or antagonistic (Figure 2.8B bottom distribution) despite the asymmetric interactions. As an example, Bliss conceals that halofantrine (inhibits polymerization of heme molecules) reduces the potency of mefloquine (targets phospho-

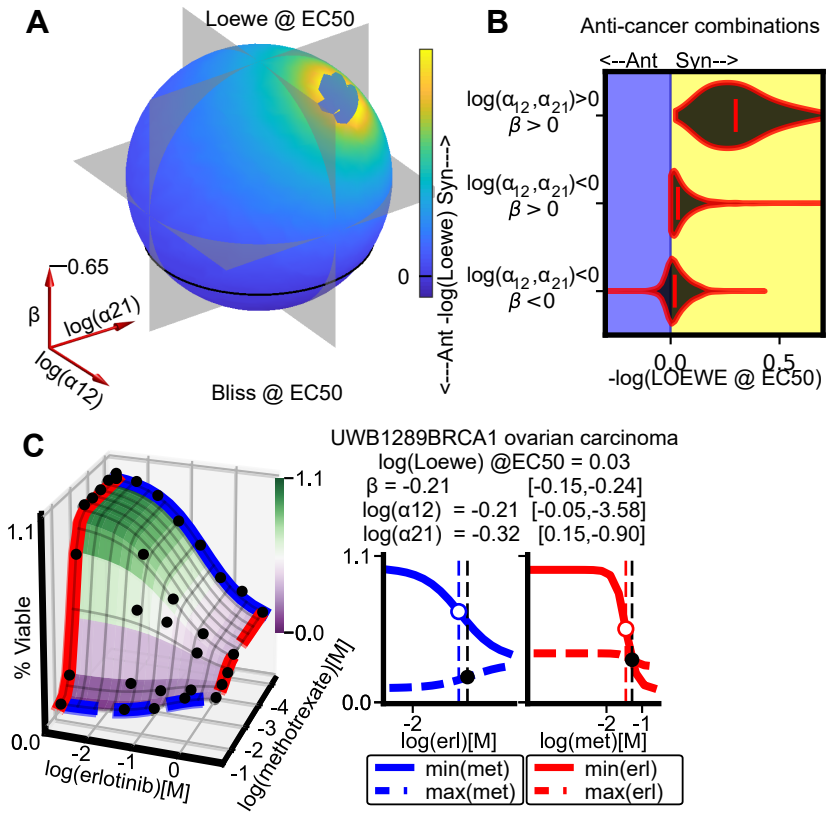

Figure 2.6: Loewe conflates potency and efficacy synergy masking synergistic interactions in large drug combination datasets. A) The colors on the sphere (radius on β axis bottom left) represent the value of Loewe (colorbar to right) for a drug combination with a MuSyC synergy profile (α_{12}, α_{21}, and β) (axes bottom left). For all combinations: $E_0 = 1$, $E_1 = E_2 = 0$, $h_1 = h_2 = 1$, $d_1 = d_2 = C_1 = C_2$, $\gamma_{12} = \gamma_{21} = 1$. The solid line marks the boundary between Loewe synergy and antagonism. Along this contour, which includes many different sets of (α_{12}, α_{21}, and β), Loewe is equivalent (-log(Loewe)= 0). Gray planes correspond to $\beta = 0$, $\log(\alpha_{12}) = 0$, and $\log(\alpha_{21}) = 0$. The hole in the upper-right quadrant represents sets for which Loewe is undefined. B) Distribution of Loewe for anti-cancer drug combinations grouped by their synergy profiles according to MuSyC. Loewe was calculated as detailed in Methods, including the Hill slope correction. C) The anti-cancer combination methotrexate and L-778123 is antagonistically potent and efficacious against HT29 cells, by MuSyC; however, it is designated by Loewe to be synergistic. Left panel shows the MuSyC-fitted dose-response surface, right panel shows the edges of the MuSyC surface. The open circle marks the EC50 for each drug in isolation, closed circle is the shifted EC50 due to antagonistic potency. Brackets are 95% confidence intervals for each parameter based on Monte Carlo sampling.

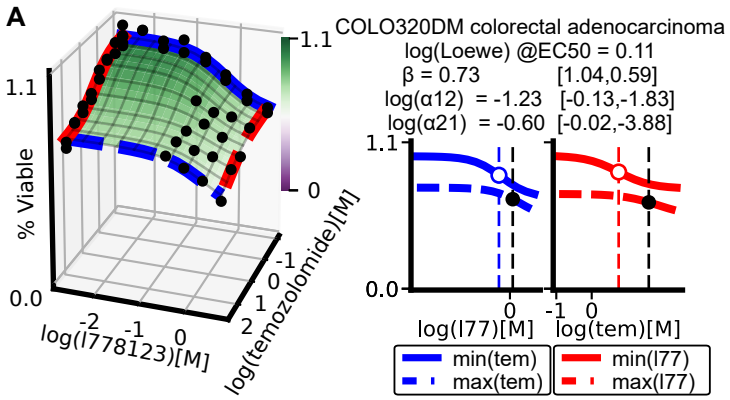

Figure 2.7: Loewe masks antagonistic potency. A) The combination of L778123 (a dual farnesyl and geranylgeranyl transferase inhibitor) and temozolomide (DNA alkylating agent) in COLO320DM cell lines is synergistically efficacious but antagonistically potent, and is an example where Loewe misses antagonistically potent interactions.

lipids) against the multi-drug resistant malaria strain HB3 (Figure 2.8C).

In contrast to Bliss, HSA is commonly thought to quantify synergistic efficacy. However, for antagonistically potent combinations, it cannot distinguish synergistic and antagonistic efficacy because it does not account for the topology of the dose-response surface (compare $(\log(\alpha_{12}), \log(\alpha_{21}), \beta) = (-,-,+)$ and $(-,-,-)$ quadrants of Figure 2.9A). In the anti-cancer combination dataset (O'Neil et al., 2016), I observe this trend (Figure 2.9B middle vs bottom distributions). As an example, the synergistically efficacious combination of dexamethasone (agonist of the glucocorticoid receptor) and mk-8669 (PI3K/mTOR dual inhibitor) in a colorectal adenocarcinoma cell-line is masked by HSA due to antagonistic potency (Figure 2.6C). Repressing glucocorticoid signalling has previously been shown to repress mTOR signalling (Wang et al., 2006) providing a potential molecular mechanism explaining the synergy.

2.4 MSP is biased against combinations of drugs with intermediate efficacy

MSP frameworks explicitly expect drug effects to measure the "percentage of cells affected," which is by definition bounded within the closed interval $E \in [0,1]$. Nevertheless, dose-response data is usually not a measure of percent *affect*, but rather of relative percent *effect*. Indeed, percent transformations are commonly applied to data in order to apply Bliss. In Bliss' original study,

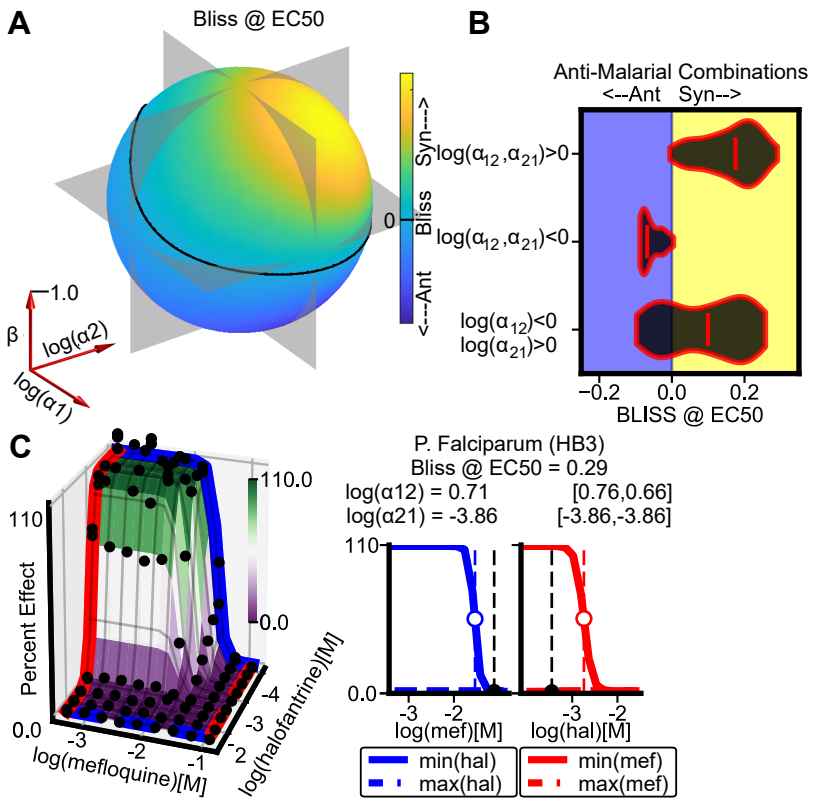

Figure 2.8: Bliss conflates potency and efficacy synergy masking synergistic interactions in large drug combination datasets. A) Sphere for Bliss as in Figure 2.6A. B) Distribution of Bliss for anti-malarial drug combinations. Combinations for which each drug alone achieves $E_{max} < 0.1$ were selected, ensuring $E_1 \cdot E_2 \approx E_3 \approx 0$. Under this condition, the differences between MuSyC and Bliss are due only to asymmetric potency synergy (all combinations fall near the $\beta = 0$ plane in (A)). C) Mefloquine increases the potency of halofantrine (red curves) but halofantrine decreases the potency of mefloquine (blue curves) in the HB3 strain of *P. falciparum*.

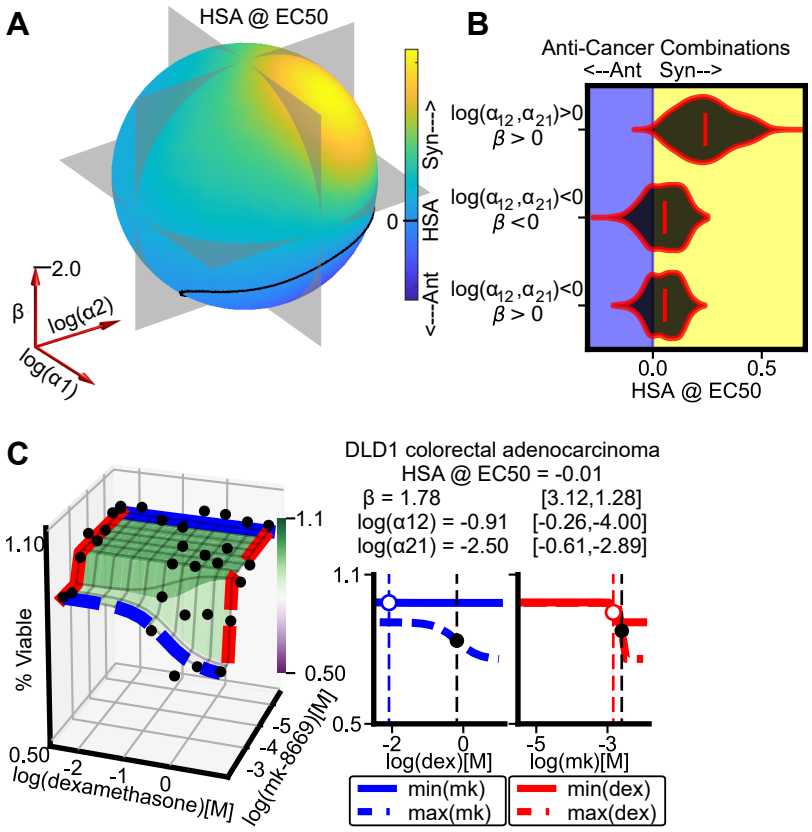

Figure 2.9: HSA conflates potency and efficacy synergy masking synergistic interactions in large drug combination datasets. A) Sphere for HSA as in Figure 2.6A. B) Distribution of HSA for anti-cancer combinations grouped by MuSyC synergy profile. In antagonistically potent combinations, HSA can miss synergistic efficacy. C) Combination of dexamethasone and mk-8669 in DLD1 cells is anagonistically potent, but synergistically efficacious.

drug effect was quantified as the percentage of eggs killed (the probability that each egg would die at a given toxin dose), but in all cases the measurement was a discrete event (death of an insect egg). Therefore, the metric of drug *effect* was the a percentage of affected eggs. However, to apply Bliss to more general measures of drug effect for which discrete counts cannot be obtained, it has been ubiquitous practice to normalize the drug effect as a percent relative to control (*e.g.*, percent viability in cancer research). Nevertheless, such normalization does not, in general, transform measures of efficacy into measures of percent affect.

As a thought experiment, suppose analyzing a drug treatment which actually caused the cells to grow slightly faster than control. By normalizing the drug effect to control, the percent viability is greater than 100% which cannot mean that $>100\%$ of the cells were *affected*.

Alternatively, consider the case when a cytostatic drug causes all treated cells to halt both proliferation and death. If the control population doubled twice over 72 hours, the percent viability would be $\frac{1}{2^3} = 16.25\%$. If the measure of percent viability was taken instead at 96 hours, the percent viability would be $\frac{1}{2^4} = 6.25\%$. At both time points the percent of affected cells was the same (100%); however, the percent of drug *effect* changes due to normalization.

The distinction between percent effect (E_x) and percent affect (U_x), maintained by MuSyC (see Section 2.1), is critical because percent effect data commonly saturates (*i.e.*, percent *affect* is near 100%) at intermediate effect (*i.e.*, relative percent *effect* is near 50%). For combinations of these moderately efficacious drugs, Bliss expects a large increase in effect over the single agents, even when each drug is administered at saturating concentrations (Figure 2.10A middle panel). In contrast, if combining drugs with high or low efficacy, Bliss expects a more modest increase (Figure 2.10A left and right panels).

Based on this expectation that $E_3 = E_1 \cdot E_2$ (Figure 2.3A), MuSyC predicts Bliss would be biased toward antagonism in combinations of moderately efficacious drugs (Figure 2.10B yellow shading around $E_1 = E_2 \approx 0.5$). As expected, the median Bliss score in the anti-cancer dataset is biased toward antagonism for moderately efficacious combinations $0.35 < (E1, E2) < 0.65$ (Figure 2.10C, cyan square). This bias persists even when looking at pan-cancer trends in the combination

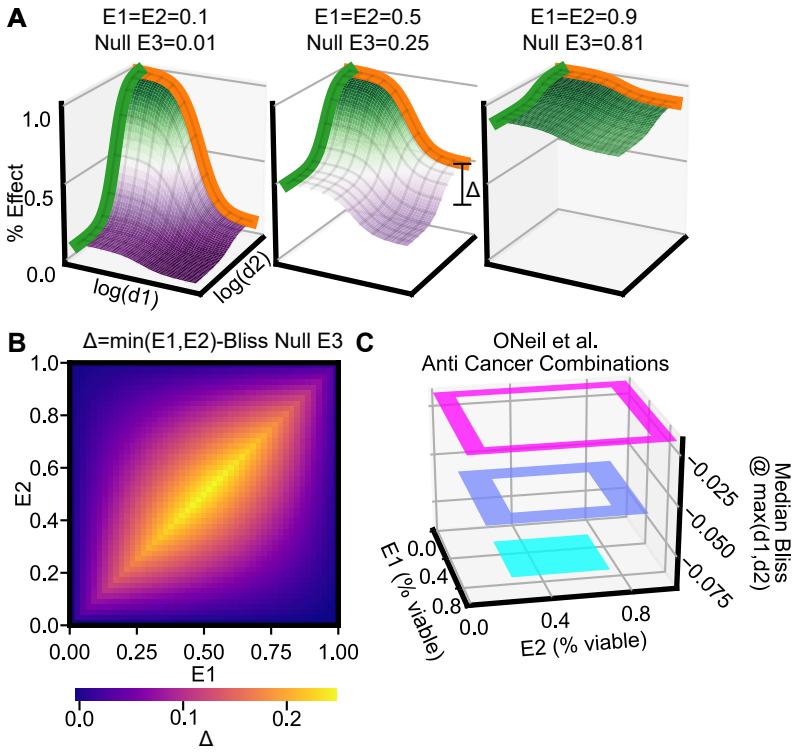

Figure 2.10: Bliss is biased against combinations of moderately efficacious drugs. A) The null Bliss surface for different maximal efficacy of single agents. Δ is defined as the expected increase in percent effect of the combination over the stronger single agent at saturating doses. The left and right panels have the same expected increase according to Bliss, $\Delta = 0.09$, while the combination of moderately efficacious drugs (middle panel) has a expected increase of $\Delta = 0.25$. B) Calculation of Δ (colorbar bottom) for surfaces with different pairings of $(E1, E2)$. C) Median Bliss for anti-cancer combinations grouped by the maximal efficacy of their single agents. Ranges for each square: cyan square: $[0.35, 0.65]$, blue square: $[0.1, 0.9]$ and magenta square: $[0.0, 1.0]$. Bliss is calculated at the maximum tested concentrations of both drugs.

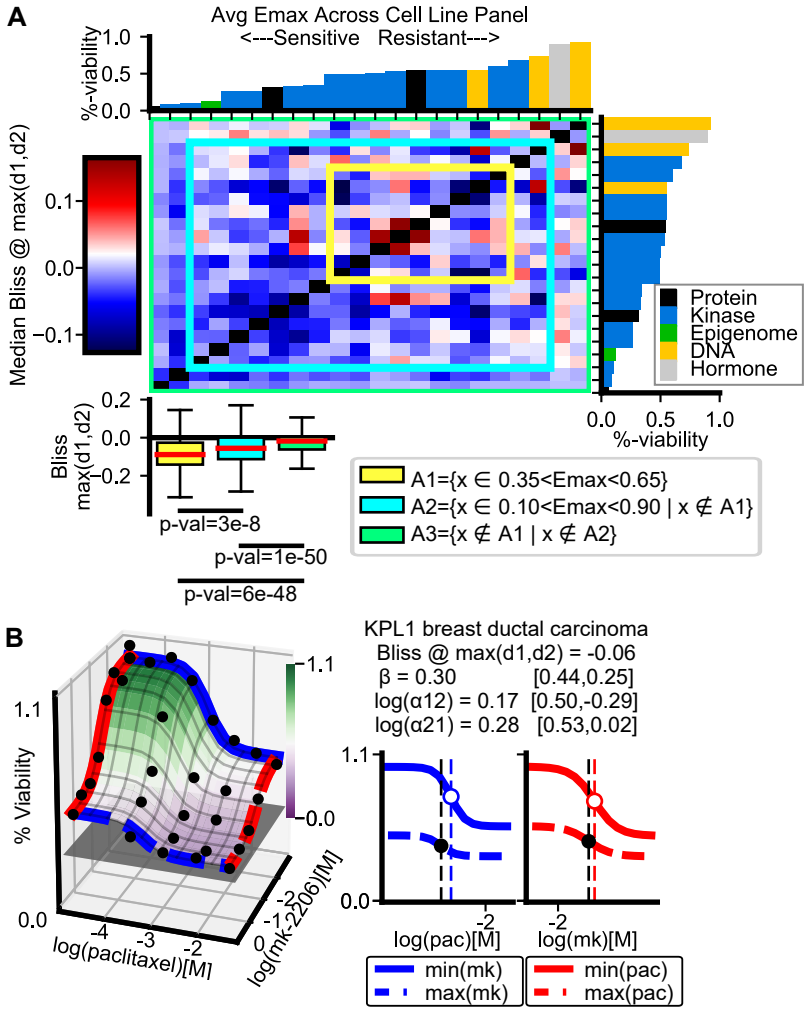

Figure 2.11: The Bliss efficacy bias results in pan-cancer drug combination trends A) Heatmap of the median Bliss score (colorbar left) for each combination across the cancer cell-line panel. Rows and columns are ordered by the average efficacy of each drug alone over all cell-lines (E_{max}) (bar graphs top and right). Colored boxes correspond to groupings denoted in the legend (bottom). Boxplots show Bliss trends toward antagonism for combinations of moderately efficacious drugs (green $\rightarrow$ blue $\rightarrow$ yellow) (2-sample, 1-sided t-test). B) Dose-response surface of paclitaxel and mk-2206 in KPL1 cells. Gray plane is the expected effect of the combination by Bliss at max(d1,d2).

of drugs which have, on average, intermediate effect over the entire cell line panel (Figure 2.11A). As a particular example, the synergistic efficacy of paclitaxel (targets microtubule stability) and mk-2206 (AKT inhibitor) in KPL1 cells is masked by Bliss's high expectation for moderately efficacious drugs (Figure 2.11B grey plane).

Additionally, some MSP methods, such as CI (nonexclusive) and the EDM, assume data measures percent *affect* and fit a simplified 2-parameter Hill equation enforcing $E_0 = 1$ and $E_1 = 0$ (Figure 1.2A page 8, Table 1.1 page 6). This assumption can lead to poor fits of percent *effect* data for moderately efficacious drugs, and thus invalid synergy scores (see Figure 2.12).

2.5 Re-examining the sham experiment.

A new synergy model's consistency is traditionally tested with the "sham" combination thought experiment. In a sham experiment, a single drug is considered as though it were a combination, with the expectation that the drug should be neither synergistic nor antagonistic with itself. However, MuSyC only satisfies the sham experiment when $h = 1$. When $h \neq 1$, the biochemistry of sham combinations (Figure 2.13A) is distinct from real combinations (Figure 2.13B), as states representing mixed-inhibition (black circles) are equivalent to single drug, complete-inhibition states (cyan circles) in sham combinations, but not in real combinations.

2.5.1 The sham biochemistry of the sham experiment

To simulate a sham experiment using MuSyC, there is no state $A_{1,2}$ (Figure 2.1B), which requires $\alpha_{12} = \alpha_{21} = 0$. Further, because drugs 1 and 2 are the same, $h_1 = h_2 = h$, $C_1 = C_2 = C$, and $E_1 = E_2$. Thus, the 2D Hill equation (eq. (2.8)) reduces to

$$E_d(d_1, d_2) = \frac{E_0 + E_1 \frac{d_1^h + d_2^h}{C^h}}{1 + \frac{d_1^h + d_2^h}{C^h}} \quad \text{MuSyC Sham} \tag{2.26}$$

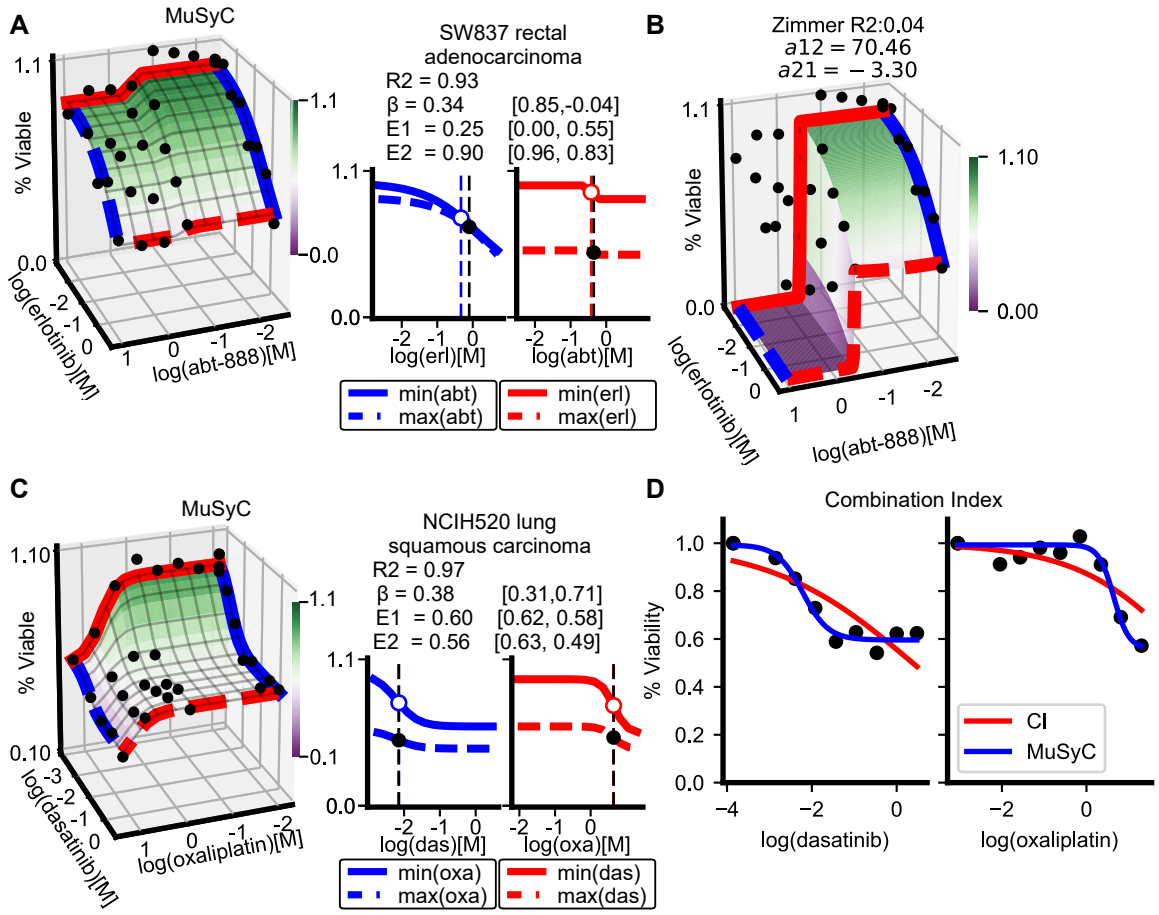

Figure 2.12: MSP based frameworks assume 2-parameter Hill equation leading to poor fits. A) Dose-response surface for combination erlotinib and abt-888 in SW837 cells. B) Dose response surface according to Effective Dose model, which enforces $E_0 = 1$ and $E_1 = E_2 = 0$. C) Dose-response surface for dasatinib and oxaliplatin in NCI-H520 cells. Both dasatinib and oxaliplatin have intermediate effects on this cell line (*i.e.* $E_1 \approx E_2 \approx 0.5$). D) CI single drug dose-response fits for dasatinib and oxaliplatin. Minimizing residuals while enforcing $E_0 = 1$ and $E_1 = E_2 = 0$ causes artificially low Hill slopes for both drugs ($h1 < h2 < 0.35$). For additional examples of poor CI fits see Figure 1.3, page 9.

In comparison, the true dose-response surface of a sham experiment can be analytically determined from the 1D Hill dose-response equation (eq. 2.3) as

$$\begin{aligned} E_d(d_1,d_2) &= E_{single}(d_1+d_2) \\ &= \frac{E_0+E_1\left(\frac{d_1+d_2}{C}\right)^h}{1+\left(\frac{d_1+d_2}{C}\right)^h} \quad \text{True Sham} \end{aligned} \tag{2.27}$$

Equations 2.26 and 2.27 are only equivalent when $h=1$. This makes sense, as the constraints on α and h are the conditions required for MuSyC to satisfy the DEP (Figure 2.3B). To see what happens when $h \neq 1$, consider, for instance, a molecule with three binding sites targeted by a small molecule inhibitor ($h=3$). For clarity, I assert $E_0=1$ and $E_1=0$, though the findings are valid more generally. The MuSyC sham surface follows

$$E_d(d_1,d_2) = \left(1+\frac{d_1^3}{C^3}+\frac{d_2^3}{C^3}\right)^{-1} \quad \text{MuSyC Sham}$$

In contrast, the true sham surface is

$$\begin{aligned} E_d(d_1,d_2) &= \left(1+\left(\frac{d_1+d_2}{C}\right)^3\right)^{-1} \\ &= \left(1+\frac{d_1^3}{C^3}+3\frac{d_1^2d_2}{C^3}+3\frac{d_1d_2^2}{C^3}+\frac{d_2^3}{C^3}\right)^{-1} \quad \text{True Sham} \end{aligned} \tag{2.28}$$

The two additional cross-terms in the true sham equation ($3\frac{d_1^2d_2}{C^3}$ and $3\frac{d_1d_2^2}{C^3}$) describe the six possible mixtures of drugs 1 and 2 that, together, fill all binding sites (Figure 2.13A, blue, green, and magenta paths show three possible mixtures). In a sham experiment, because drugs 1 and 2 are the same, the diagonal states (black and cyan circles) in Figure 2.13A are all equivalent, and fully inhibited.

Conversely, in non-sham combinations, drugs rarely target the same binding sites, or even the same molecule. Even when two drugs are mutually exclusive inhibitors of the same molecule *and*

have the same number of binding sites, the cross-terms describe non-equivalent, not fully inhibited states (Figure 2.13B). A commonly applied and physiologically supported approximation is that only fully bound molecules become (in)active (see reaction schemes 5-7 in (Weiss')). Partially bound cross-terms are therefore reasonably modeled as unaffected, and the absence of these cross-terms from equation (2.26) is justified for real (non-sham) combinations (see Discussion). Further, when the two drugs do not target the same molecule or are mutually exclusive or have the same number of binding sites, by far the preponderance of real combinations, the diagonal states are ill defined yet remain embedded in the sham equation.

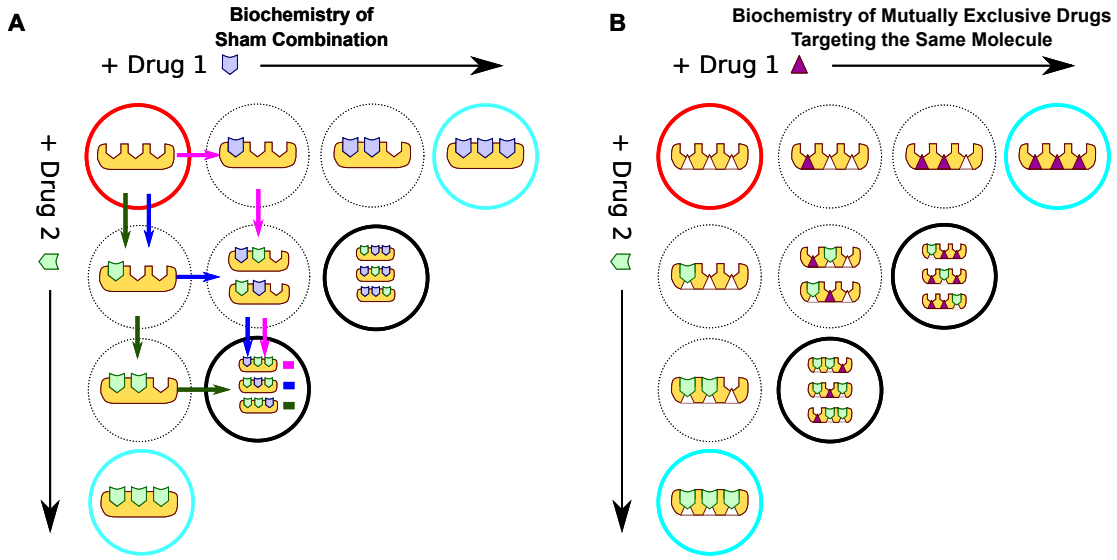

Figure 2.13: Unique biochemistry of the sham experiment discredits its general applicability A) An illustration of the unique biochemistry of the sham experiment. The red circle represents an undrugged molecule with 3 binding sites. In a sham experiment, a drug is treated as though it were two separate drugs (green and blue polygons). Mixed states in which the binding sites are bound by both green and blue drugs (black circles) are equivalent to fully drugged states (cyan circles). I highlight three paths (green, blue, magenta arrows) that can be followed to reach a mixed-drugged state. These three paths correspond to the coefficient of $3\frac{d_1 d_2^2}{C^3}$ in equation (2.28). B) In a combination of mutually exclusive drugs (triangle and polygon), targeting the same molecule, and with the same number of binding sites, the mixed states (black circles) are not equivalent to fully drugged (cyan circles) accounting for the discrepancy between MuSyC and the sham experiment.

2.5.2 Hill slope requirement of the sham experiment leads to systematic bias in DEP frameworks

The constraint on h leads to non-linear isoboles in MuSyC (Figure 2.4) when $h \neq 1$. Specifically, in the absence of synergistic potency ($\alpha_{12} = \alpha_{21} = 1$), MuSyC isoboles bend inward when $h < 1$, and outward when $h > 1$. Sham-compliant frameworks (Table 2.6) assume linear isoboles regardless of the Hill slope, and therefore classify combinations in the region between the linear and non-linear isoboles (red shading in Figure 2.4) as synergistic (middle panel) and antagonistic (right panel), respectively. MuSyC therefore predicts sham-compliant frameworks will overestimate synergy when $h < 1$, and underestimate when $h > 1$.

In combinations from the anti-cancer dataset, the average trend of Loewe synergy closely follows the Hill slope bias predicted by MuSyC (Figure 2.14A). Further, subtracting the MuSyC-predicted bias from Loewe values for each combination results in a distribution independent of Hill slope (bottom panel). The bias toward synergy is particularly large for drugs with low Hill slopes. As an example, both doxorubicin (DNA damaging agent) and mk-4827 (PARP inhibitor) have small Hill slopes when applied to MBA-MB-436 cells, and their combination is synergistic by Loewe. However, using MuSyC, I see this combination is both antagonistically efficacious and antagonistically potent (Figure 2.14B).

Therefore, satisfying sham compliance biases models toward synergy for drugs with low Hill slopes, regardless of with what these drugs are combined. This bias—which stems from enforcing a biochemical reaction scheme only appropriate for sham combinations—should be sufficient grounds for dismissing the sham experiment as a measure of a new synergy framework's validity.

2.5.3 Re-investigating sham compliance claims of previous frameworks

In reviewing the literature, two errors were identified beyond the Hill slope bias (Figure 2.14) pertaining to the sham experiment that merit addressing.

1) Chou, one of the creators of the Combination Index (CI), has strongly argued that satisfaction of the sham experiment is critical. However, there is an error in the derivation of the CI from its underlying model, so that while the CI equation is sham-compliant, the biochemical model

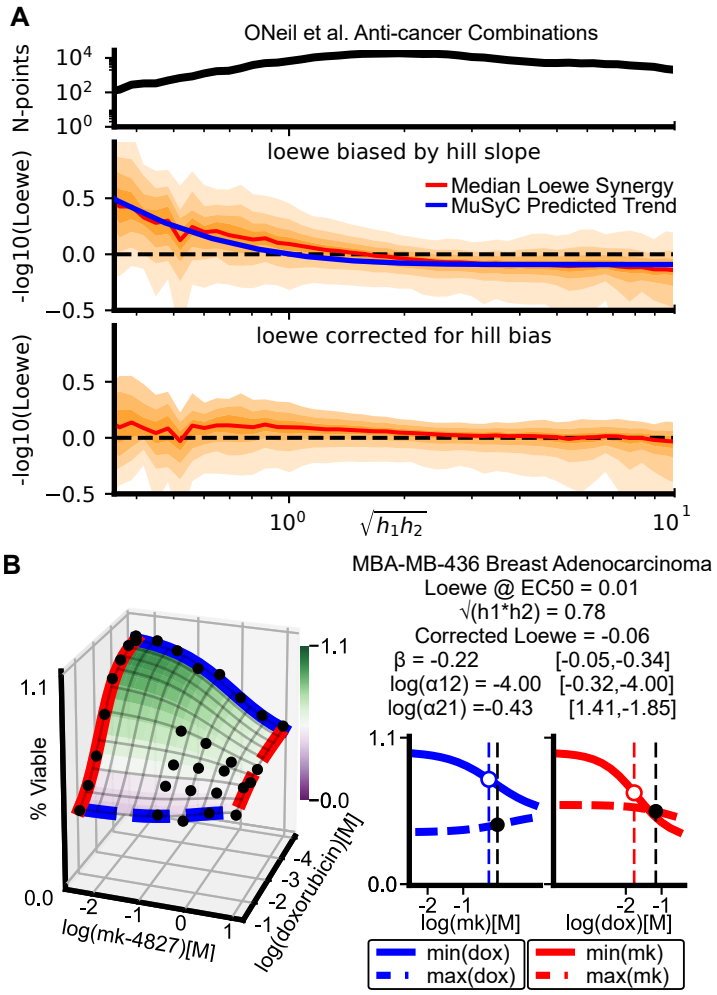

Figure 2.14: Enforcing sham compliance results in Hill-slope dependent bias in DEP frameworks. A) Loewe synergy is biased by Hill slope in the anti-cancer drug screen. The orange shaded regions show moving window percentiles (window width is 0.1) of Loewe (10th through 90th percentiles, in steps of 10). The top panel shows how many data points are present in the window. The blue curve in the middle plot shows the median MuSyC-predicted bias as a function of geometric mean of the Hill slopes (see Methods). Subtracting the MuSyC-estimated bias (calculated for each data point) from Loewe yields the bottom plot. B) The antagonistically efficacious and potent combination of mk-4827 and doxorubicin is misidentified as synergistic by Loewe, because both drugs in isolation have Hill slopes $h < 1$.

proposed by Chou and Talalay is not.

2) ZIP was proposed as a framework that unifies Loewe Additivity (DEP) and Bliss Independence (MSP), much like MuSyC. In support of this, they prove ZIP is sham-compliant; however, again there is an error in their proof. Further, I generate *in silico* sham response data and show that ZIP fails the sham experiment. For this reason, I place ZIP as an MSP method in Figure 2.3C, and not DEP. However, I have contended that satisfying the sham experiment should not be a sought-after standard in drug combinations, so I do not consider it a shortcoming of ZIP that it does not.

Sham Compliance of Combination Index

Chou and Talalay report that the combination index for mutually exclusive drugs satisfies the sham experiment, whereas for MuSyC, I find this is only true when $h = 1$ (eq (2.26)). Because MuSyC's underlying model (Figure 2.3B) is identical to what Chou and Talalay describe (Chou and Talalay, 1981) when $\alpha_{12} = \alpha_{21} = 0$, I sought to discover the source of this discrepancy.

Chou and Talalay's finding comes from "Generalized Equations for the Analysis of Inhibitions of Michaelis-Menten and Higher-Order Kinetic Systems with Two or More Mutually Exclusive and Nonexclusive Inhibitors" (Chou and Talalay, 1981). I found an error in the section *Inhibition of the Higher-Order Kinetic Systems by Mutually Exclusive Inhibitors*. Specifically, the authors correctly solve the n-drug case with $h = 1$

$$\frac{A_{n\,drugs}}{U} = \sum_{j=1}^{n} \frac{d_j}{C_j} \quad \text{Equation 11 from (Chou and Talalay, 1981)}$$

as well as the the 1-drug case with arbitrary h

$$\frac{A_{single\,drug}}{U} = \left(\frac{d}{C}\right)^h \quad \text{Equation 12 from (Chou and Talalay, 1981).}$$

However, they incorrectly extrapolate these two equations to an n-drug, arbitrary h case (though they assume all drugs have the same value of h, *e.g.* all drugs have h binding sites and follow

Hill-type kinetics) by erroneously stating

$$\frac{A_{n\,drugs}}{U} = \left(\sum_{j=1}^{n} \frac{d_j}{C_j}\right)^h \quad \text{Unlabeled equation from (Chou and Talalay, 1981).}$$

In general it is not clear how this would be calculated if each drug has a different value h, as there exists only a single h in their formula. However, in the case of n mutually exclusive drugs following Hill kinetics (a model graphically represented for $n = 2$ in Figure 2.3B), I can say at equilibrium

$$\frac{\mathrm{d}A_j}{\mathrm{d}t} = U r_j d_j^{h_j} - A_j r_{-j} = 0$$

From this I can solve for $\frac{A_j}{U}$ for each drug, arriving at the same equation 12 from Chou (Chou and Talalay, 1981). But applying the constraint that $U + A = 1$, where $A = \sum_{j=1}^{n} A_j$, I instead find the correct form for the multi-drug case with arbitrary h is

$$\frac{A}{U} = \sum_{j=1}^{n} \left(\frac{d_j}{C_j}\right)^{h_j}$$

When $h_j = h = 1$ the discrepancy between these equations vanishes because it does not matter that they place the exponent outside the sum. However Chou and Talalay use the incorrect version to define their Combination Index (Chou and Talalay, 1984), regardless of h.

Sham Compliance of ZIP

ZIP was reported to satisfy the sham experiment (Yadav et al., 2015) based on an argument that if both drugs are the same, then $m_1 = m_2 = m_{1\leftarrow 2} = m_{2\leftarrow 1}$. However, this statement is false for sham experiments, because once some of the drug is added, $m_{1\leftarrow 2}$ is shifted. To demonstrate this, consider their model (equation 13 from (Yadav et al., 2015), without asserting $m_{1\leftarrow 2} = m_1$)

$$y_{1\leftarrow 2} = \frac{y_2 + \left(\frac{x_1}{m_{1\leftarrow 2}}\right)^{h_1}}{1 + \left(\frac{x_1}{m_{1\leftarrow 2}}\right)^{h_1}}$$

$m_{1\leftarrow 2}$ is the amount x_1 of drug 1 that is needed to achieve an effect halfway between y_2 and 1

(the asymptotic value at infinite drug), where y_2 is the effect achieved by adding an amount x_2 of drug 2. Specifically, when $x_1 = m_{1\leftarrow 2}$, $y_{1\leftarrow 2} = \frac{1+y_2}{2}$.

Sham experiments satisfy Equation (2.27), which combined with the above gives

$$y_{1\leftarrow 2} = \frac{\left(\frac{m_{1\leftarrow 2}+x_2}{m_1}\right)^{h_1}}{1+\left(\frac{m_{1\leftarrow 2}+x_2}{m_1}\right)^{h_1}} = \frac{1+y_2}{2}$$

Further I know

$$y_2 = \frac{\left(\frac{x_2}{m_1}\right)^{h_1}}{1+\left(\frac{x_2}{m_1}\right)^{h_1}}$$

This system can be solved to find

$$m_{1\leftarrow 2} = m_1\left[1+2\left(\frac{x_2}{m_1}\right)^{h_1}\right]^{\frac{1}{h_1}} - x_2$$

demonstrating that $m_{1\leftarrow 2} \neq m_1$ for the sham experiment in the ZIP model, contradicting their proof that ZIP is sham-compliant.

To verify ZIP identifies synergy or antagonism for sham combinations, I generated a synthetic sham dose response surface. Sham experiments can be generated exactly for any drug with a pre-defined dose-response by asserting the condition in Equation (2.27). I constructed a synthetic dataset describing a sham dose response surface for a drug with $h = 2$, sampled at 2.5 orders of magnitude above and below the EC50. One drug was sampled at 7 concentrations, the other at 12, defining a 7 x 12 sham dose response matrix. I used the synergyfinder (He et al., 2018) R package to calculate synergy by both Loewe and ZIP (Figure 2.15), and found Loewe reported close to 0 synergy, as expected for a sham combination, but confirms ZIP detects synergy and antagonism at several concentrations.

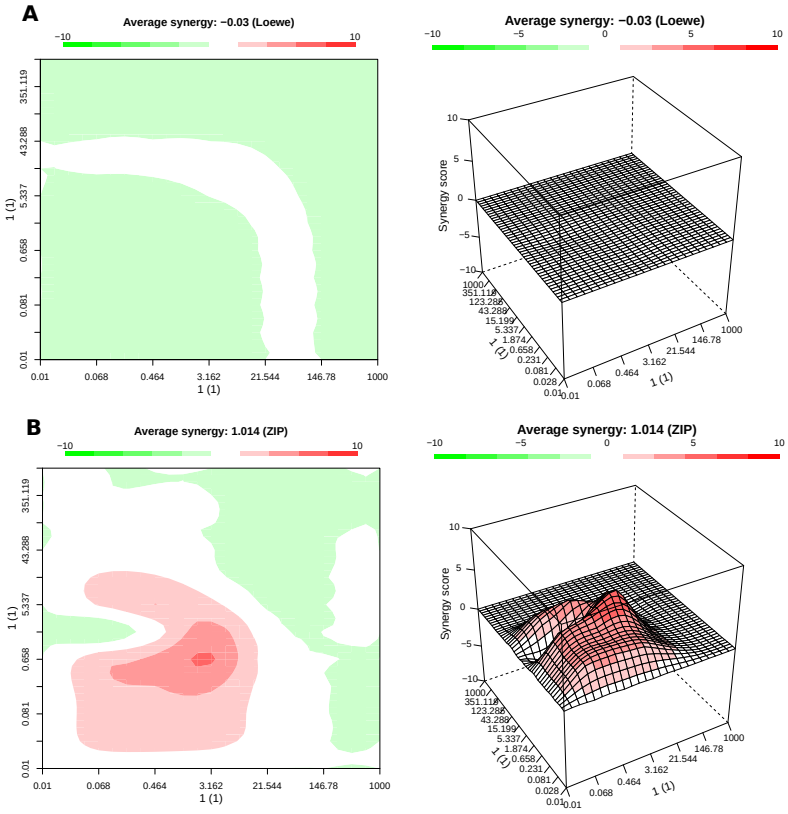

Figure 2.15: The sham compliance of ZIP. A) Loewe synergy calculated by synergyfinder (He et al., 2018) for a synthetic sham dose-response surface with $h = 2$. Loewe correctly identifies the combination as additive. B) ZIP quantifies synergy or antagonism at several concentrations for the sham dataset.

2.6 Concluding remarks: Consensus achieved

Herein, I have demonstrated three key advances of MuSyC particularly germane to the study of combination pharmacology: 1) the unification of the DEP and MSP; 2) the decoupling of three distinct types of synergy; and 3) the revelation of biases emerging from constraints on the single drug pharmacological profile inherent in the DEP and MSP.

In Chapter 3, I expand on the value of distinguishing synergistic potency from synergistic efficacy by applying MuSyC to high throughput drug combination screens which reveal drug class trends otherwise obfuscated using traditional methods. Specifically, I find novel strategies to improve standard of care in EGFR-mutant Non Small Cell Lung Cancer (NSCLC) as well as in BRAF-mutant melanoma. In each system, the decoupling of different types of synergy is critical for guiding the deployment of combination therapy.

Chapter 3

Quantifying Drug Combination Synergy Along Potency and Efficacy Axes

3.1 Synergy of potency and efficacy align with the clinical axes of interest.

As detailed in the previous chapter, MuSyC decouples different types of synergy corresponding to geometric transformations of the dose-response surface. Importantly, these transformations are analogous extensions of classic pharmacologic parameters which govern the shape of the one drug Hill equation (Figure 2.1A). In this chapter, I demonstrate the utility of distinguishing synergy of potency and efficacy to the discovery of novel therapeutic combinations and argue the distinction between synergy of potency and synergy of efficacy is critical for the rational deployment of combination therapy.

Recent decades have witnessed an exponential expansion of available drugs for the treatment of disease (Gong et al., 2017). This expansion has been concomitant with an evolving understanding of disease complexity; complexity commonly necessitating combination therapy (He et al., 2016). However, clinical applications of combination therapy are often limited by tolerable dose ranges, and, therefore, it is desirable to identify combinations that enable dose reduction (Tallarida, 2011), *i.e.*, synergistic potency. Additionally, combining drugs does not guarantee a priori an increase in efficacy over the single agents, and, therefore, it is desirable to identify combinations with effects greater than achievable with either drug alone (Foucquier and Guedj, 2015), *i.e.*, synergistic efficacy. To assess a combination's performance toward these goals, several drug synergy metrics have been proposed (Table 1.1 page 6). However, none of these methods distinguish between synergistic potency and synergistic efficacy. Instead, they either make no distinction or tacitly assume the only form of synergism is through potency.

Nevertheless, this distinction is essential to arrive at an unambiguous definition of synergy and properly rationalize the deployment of drug combinations, *e.g.* in personalized medicine. Indeed, conflating them may mislead drug combination discovery efforts. For instance, a search

for improved efficacy based on traditional synergy frameworks may be confounded by an inability to sort out synergistically potent combinations. Herein, I show how MuSyC addresses this critical shortcoming.

To demonstrate the value of decoupling synergy of potency and efficacy, I investigate a panel of anti-cancer compounds in combination with a third-generation mutant-EGFR inhibitor, osimertinib, in EGFR-mutant non-small cell lung cancer (NSCLC). I find that drugs targeting epigenetic regulators or microtubule polymerization are synergistically efficacious with osimertinib. In contrast, drugs co-targeting kinases in the MAPK pathway affected potency, not efficacy of osimertinib. These conclusions have implications for drug combination deployment in NSCLC where increasing the efficacy of EGFR-inhibitors has historically relied on trial and error with no overarching principles to guide development (Schiffmann et al., 2016).

I also apply MuSyC to study the well-established, clinically-relevant combination targeting RAF and MEK in BRAF-mutant melanoma (Long et al., 2014). I find this combination to be synergistically efficacious, though in several cases at the cost of potency. I then identify NOX5 as a previously unsuspected molecular determinant of sensitivity to BRAF inhibition (BRAFi) in BRAF-mutant melanoma. Applying MuSyC, I find that NOX5 expression levels affect BRAF inhibition efficacy, but not potency.

In direct comparisons, I found that traditional synergy frameworks are ambiguous even for the most synergistically efficacious of the NSCLC and melanoma combination studies, leading to misclassifications of combination synergy.

3.2 MuSyC quantifies synergy of potency and efficacy in a drug combination screen.

I applied MuSyC to evaluate the synergistic potency and efficacy of a 64 drug panel (see Table 3.1 for drugs, drug classes, nominal targets, and tested concentration ranges) in combination with osimertinib, a mutant EGFR-tyrosine kinase inhibitor recently approved for first-line treatment of EGFR-mutant NSCLC (Soria et al., 2018). The selected drugs span a diverse array of cellular targets that can be broadly grouped into four categories: kinases, receptors and channels, epigenetic

regulators, and mitotic check-points (Figure 3.1), each with several sub-categories. The combinations were tested in PC9 cells, a canonical model of EGFR-mutant NSCLC (Jia et al., 2013) using a high-throughput, in vitro, drug-screening assay (Figure 3.2). I quantified drug effect using the DIP rate metric (Harris et al., 2016), a metric which avoids temporal biases characteristic of traditional endpoint assays (see Appendix B.5).

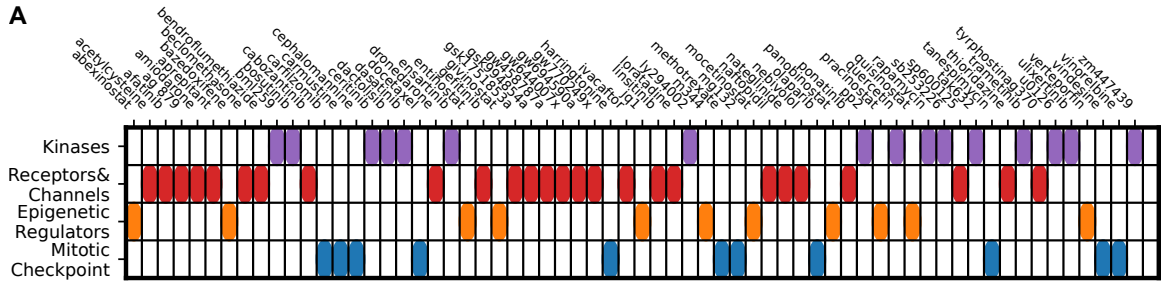

Figure 3.1: High throughput screen of 64 drugs combined with osimertinib (mutant EGFR-TKI) reveals drug class dependence of synergistic potency and efficacy in NSCLC. A) Drug panel used in combination with osimertinib grouped in 4 categories (see Table 3.1 for details).

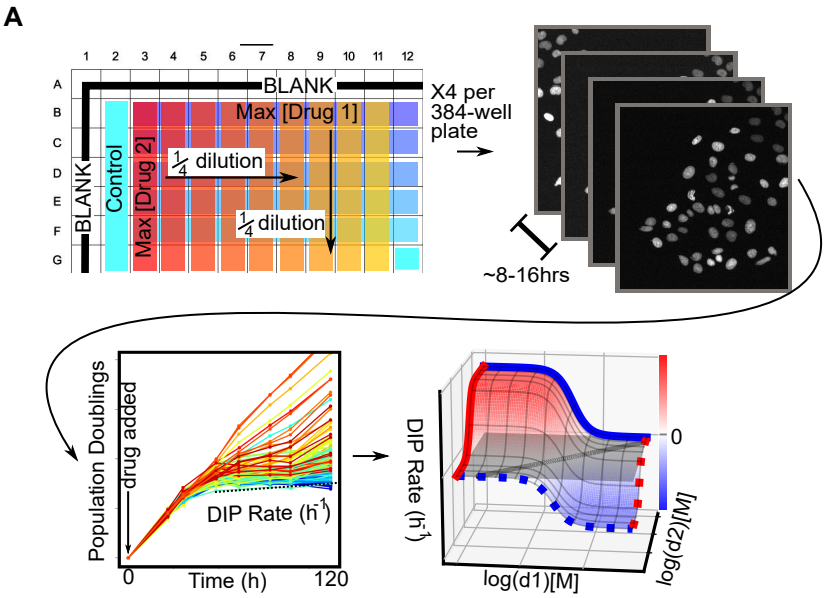

Figure 3.2: High throughput screening pipeline. A) High-throughput pipeline for generating dose-response surfaces. Initial drug matrix is prepared on a 384-well plate and transferred to cells seeded at sub confluent densities. Cells are engineered to express a fluorescently tagged histone (H2B-RFP) allowing for cell counts using automated segmentation software (See Appendix B.5 page 143 for methods). Each condition is imaged every 6-8 hours resulting in growth curves. The growth curves are fit for the DIP rate (slope of dotted line) (Harris et al., 2016) to quantify drug effect. This matrix of DIP Rates is fit to the 2D Hill equation to extract synergy parameters.

Table 3.1: Annotation of anti-cancer drugs used in NSCLC and BRAF-mutant melanoma screens with nominal target and target class.

Class	Subclass	Drug	Tested Range	Nominal Target
NSCLC				
Epigenetic Regulators	BET	jq1	4.0uM-0.1nM	BET bromodomain
	HDACi	abexinostat	0.3uM-0.8nM	HDAC
		entinostat	1.0uM-2.6nM	HDAC
		givinostat	10.0uM-41.1nM	HDAC
		m344	1.0uM-2.6nM	HDAC
		mocetinostat	0.3uM-0.8nM	HDAC
		panobinostat	0.4uM-0.0nM	HDAC
		pracinostat	10.0uM-41.1nM	HDAC
		quisinostat	1.0uM-2.6nM	HDAC
	TF	bazedoxifene	10.0uM-41.1nM	ER
		verteporfin	10.0uM-41.1nM	YAP
Kinases	ALK	ceritinib	4.0uM-0.1nM	ALK/IGF1R
		ensartinib	4.0uM-0.1nM	ALK
	AURK/ CDKs	bml259	1.0uM-2.6nM	CDK
		zm447439	4.0uM-0.1nM	AURK
	MAPK/ PI3K	dactolisib	4.0uM-0.1nM	PI3K/mTOR
		ly294002	10.0uM-41.1nM	PI3K
		rapamycin	0.3uM-0.8nM	mTOR
		sb253226	10.0uM-41.1nM	p38
		tak632	4.0uM-0.1nM	RAF
		trametinib	0.3uM-0.8nM	MEK
		u0126	10.0uM-41.1nM	MEK
		ulixertinib	4.0uM-0.1nM	ERK
	SFK	bosutinib	10.0uM-41.1nM	Bcr-ABL/SFK
		dasatinib	1.0uM-3.9nM	SFK
		pp2	10.0uM-41.1nM	SFK
		quercetin	10.0uM-41.1nM	SFK
Mitotic Checkpoint	DNA Syn/ Dam	carmustine	10.0uM-41.1nM	DNA
		methotrexate	4.0uM-0.1nM	DHFR
		olaparib	20.0uM-0.3nM	PARP
	Protein Syn/Stab	carfilzomib	4.0uM-0.1nM	Proteasome
		harringtonine	10.0uM-41.1nM	Ribosomes

		mg132	4.0uM-0.1nM	Proteasome
		tanespimycin	4.0uM-0.1nM	HSP90
	Tubulin	cephalomannine	10.0uM-41.1nM	Microtubules
		docetaxel	0.3uM-0.8nM	Microtubules
		vindesine	0.3uM-0.8nM	Microtubules
		vinorelbine	10.0uM-41.1nM	Microtubules
Receptors & Channels	Channels	amiodarone	10.0uM-41.1nM	NA Channels
		bendroflume-thiazide	1.0uM-2.6nM	Cl channel
		cabozantinib	4.0uM-0.1nM	C-Met/ Axl/ Ret
		dronedarone	10.0uM-41.1nM	NA Channels
		ivacaftor	10.0uM-41.1nM	CFTR
		nateglinide	1.0uM-2.6nM	ATP-dependent K channels
	GPCRs	acetylcysteine	10.0uM-41.1nM	Glutamate receptor
		aprepitant	10.0uM-41.1nM	Neuromedin receptor
		beclomethas-onedipropionate	1.0uM-2.6nM	Glucocorticoid receptor
		loratadine	10.0uM-41.1nM	Histamine H1-receptors
		naftopidil	10.0uM-41.1nM	B1-adrenergic receptor
		nebivolol	10.0uM-41.1nM	B1 receptor
		sp600125	10.0uM-41.1nM	JNK
		thioridazine	10.0uM-41.1nM	Adrenergic receptor
	MAPK-RTKIs	afatinib	4.0uM-0.1nM	EGFR/HER2
		ag 879	1.0uM-2.6nM	HER2/ RAF-1
		gefitinib	4.0uM-0.1nM	EGFR
		gsk1751853a	10.0uM-41.1nM	IGF1R/ INSR
		gsk994854a	10.0uM-41.1nM	IGF1R/ INSR
		gw458787a	10.0uM-41.1nM	EGFR/ ERBB4
		gw644007x	10.0uM-41.1nM	Ret
		gw694590a	10.0uM-41.1nM	TIE2

		gw770249x	10.0uM-41.1nM	FLT3
		linsitinib	5.0uM-19.5nM	IGF1R
		ponatinib	4.0uM-0.1nM	FGFR
		tyrphostinag 370	10.0uM-41.1nM	PDGFRbeta
BRAF-Mutant Melanoma				
Kinases	MAPK/ PI3K	dabrafenib	0.4nM-0.39nM	BRAFV600
		plx4720	8.0uM-7.8nM	BRAFV600E & CRAF1
		raf265	1.0uM-3.9nM	CRAF,& BRAF
		vemurafenib	8.0uM-7.8nM	BRAFV600
		selumetinib	4.0uM-61pM	MEK1
		trametinib	0.4uM-6.1pM	MEK1/2
		pd98059	0.4uM-6.1pM	MEK1
		cobimetinib	0.8uM-12pM	MEK1

To fit the resulting dose-response surfaces, I developed a Bayesian fitting algorithm, using a Particle Swarm Optimizer (PSO) to seed priors for a Markov Chain Monte Carlo (MCMC) optimization (See Appendix B.4). Applying this algorithm, I extracted synergy parameters (α_{12}, α_{21}, and βobs) from fitted surfaces for all osimertinib combinations (βobs is the observed synergistic efficacy at the maximum tested dose range).

As single agents, the drug panel displays wide ranges of efficacy (E_2) and potency (C) (Figure 3.3A). The efficacy and potency of the single agents have no relationship with the synergistic efficacy and synergistic potency when combined with osimertinib (p-value$>$0.2) (Figure 3.3B) confirming MuSyC's synergy parameters are independent of single-agents' dose-response curve and therefore, as expected, cannot be predicted from the single-agent, pharmacologic profiles.

Inspection of dose-response surfaces from this combination screen, highlight the significance of resolving synergistic potency and efficacy. For instance, the dose-response surface for the osimertinib combination with M344 (a histone deacetylase (HDAC) inhibitor) exhibits synergistic efficacy ($\beta_{obs} = 1.25 \pm 0.03$, reflecting a 125% increase in efficacy over osimertinib alone) (Figure 3.5B,3.6A). However, this improved efficacy comes at the cost of potency ($\log(\alpha_{21})$=-0.90$\pm$0.01)

as observed in the shift in the EC50 of osimertinib in the presence of 1uM M344 (Figure 3.5B red to purple dotted line). In contrast, ceritinib, an ALK inhibitor with off-target effects on IGF1R (Shaw et al., 2014), increases osimertinib's potency ($\log(\alpha_{21})$=6.25±0.50) (Figure 3.5B green to orange dotted line) at 4uM (maximal tested concentration), but with inconsequential improvement of efficacy (βobs=0.28±0.003)

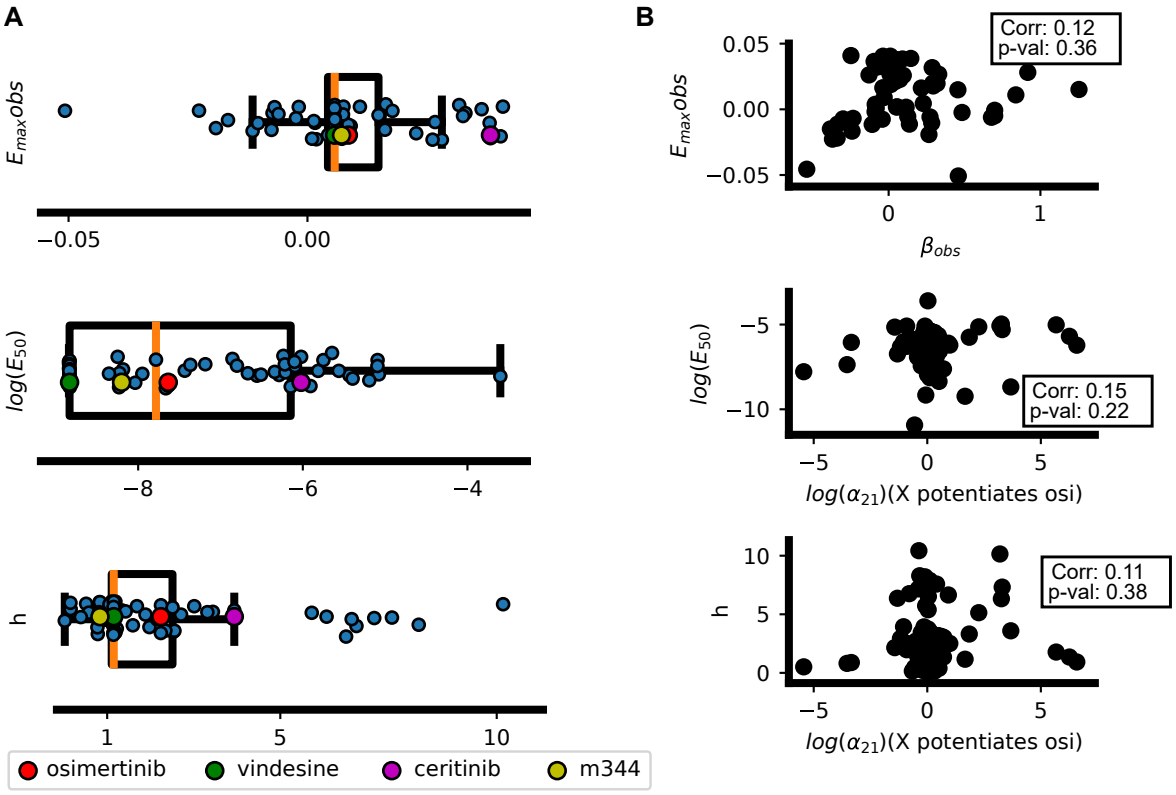

Figure 3.3: Synergistic potency (α_{12}, α_{21}) and efficacy (β) do not depend on the potency and efficacy of the single drugs (C and Emax) and are independent of one another. A) Jitter plot of the 64 surveyed single drug's $E_{max}(obs)$, C [μM], and hill slope h. B) Synergy parameters do not correlate (Pearson-r) with a single drug's potency and efficacy in isolation. (α_{21}=X potentiates osimertinib).

To visualize synergy globally, I plotted drug combinations with observed synergistic efficacy (βobs) and potency on the vertical and horizontal axes, respectively (Figure 3.6). These plots reveal distinguishing trends between the four drug categories tested.

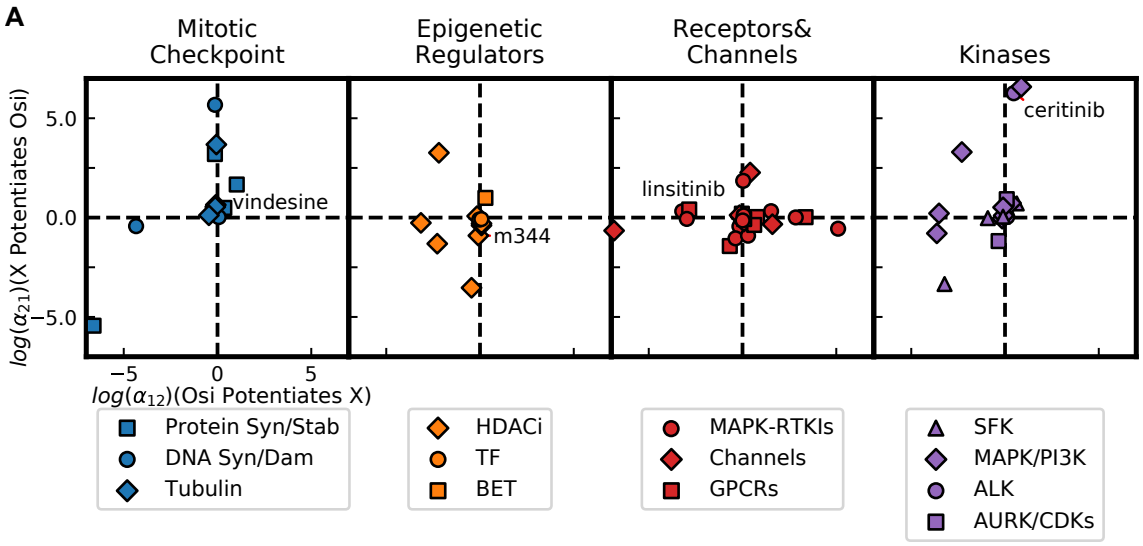

Figure 3.4: Synergistic potency (α_{12}, α_{21}) are independent. A) α_{12} vs. α_{21} by drug class examining the potentiation of drug X by osimertinib (α_{12}) and the potentiation of osimertinib by drug X (α_{21}). Ceritinib is not potentiated by osimertinib (last panel) while osimertinib is potentiated by ceritinib (Figure 3.5B).

Within the mitotic checkpoint drugs, tubulin destabilizers (including vindesine and vinorelbine) showed an upward shift along the axis of synergistic efficacy (Figure 3.6A). The marginal distribution confirmed this trend in comparison to all the drugs (Figure 3.6B, blue versus black vertical distributions). Similar results were obtained for the HDACi subgroup within the epigenetic regulators (Figure 3.6A,B). As expected, I observed limited synergistic/antagonistic efficacy for drugs targeting G-protein coupled receptors (GPCRs) (Figure 3.6A,B red versus black distributions). I also observed limited synergistic efficacy in directly co-targeting kinases in the MAPK pathway suggesting this may be an unproductive avenue in EGFR-mutant NSCLC (Figure 3.6A,B purple to black comparison along vertical axis).

To infer its synergy parameters, MuSyC first quantifies the magnitude of the maximal effects of each drug in isolation and as well as the combination (E1, E2, and E3). In our system, these values relate directly to the rate of regression or expansion of the tumor population for saturating drug conditions. Therefore, I looked for trends between drug classes for these parameters as well (Figure 3.7). Overall, I observed the combination targeting tubulin stability and EGFR achieved the greatest average reduction in DIP rates both in isolation and in combination (Figure 3.7). HDACi

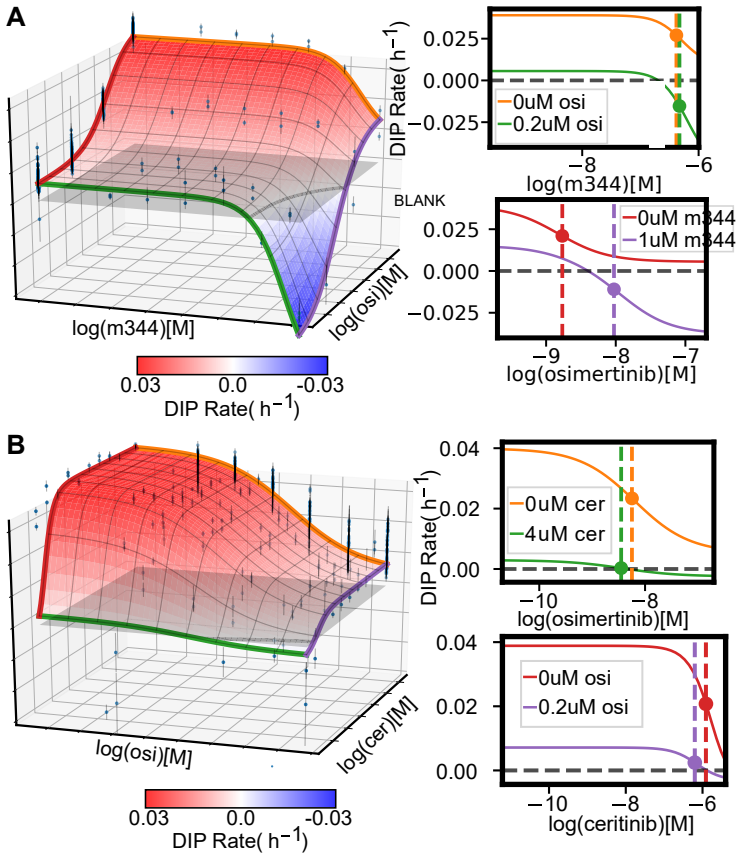

Figure 3.5: Examples dose-response surfaces with different synergy profiles. A) Combination surface of M344, an HDACi, and osimertinib (osi). Grey plane indicates a cytostatic growth rate (*i.e.*, DIP rate=0 h-1). Left are the dose-response curves for each drug alone (orange and red curves) and each drug with the maximum tested concentration of the other (green and purple). Colors correspond to the colored lines on the combination surface. The dotted lines demarcate the EC50 for each curve. B) Combination surface for ceritinib (cer), an ALK, in combination with osimertinib. Ceritinib increases the potency of osimertinib at maximum tested concentration, as observed in the shift of the EC50 between orange and green curves in the top left panel. The shift is proportional to the concentration used and would, therefore, increase at higher concentrations; however, such concentrations are not physiologically realizable due to the low potency of ceritinib in this system (EC50=2.02 uM) highlighting the importance of interpreting synergistic potency in the context of the absolute potency.

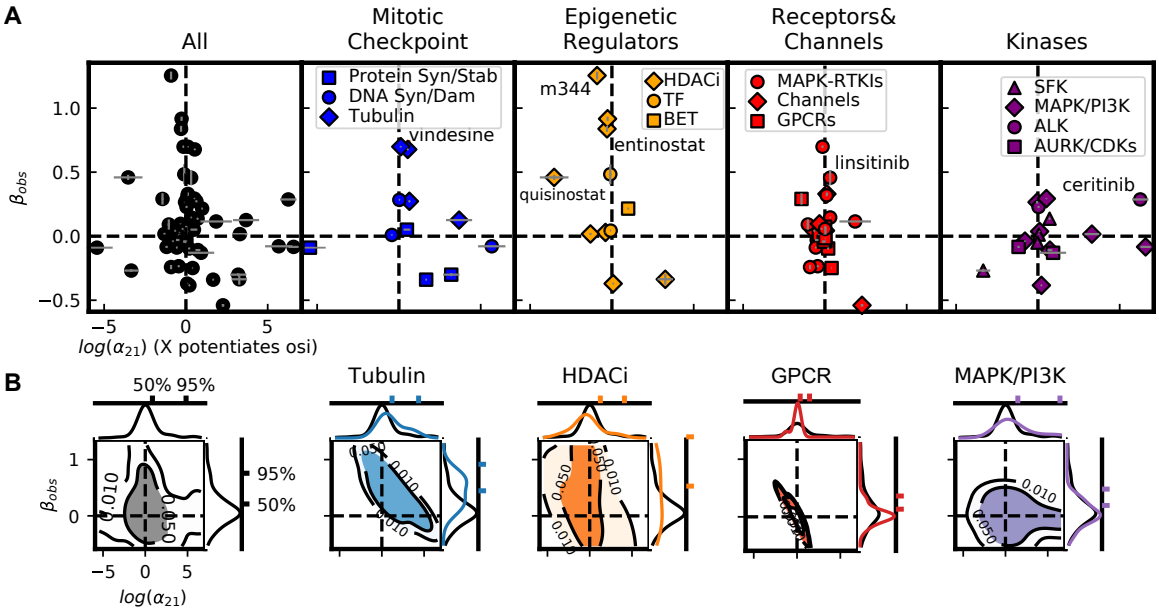

Figure 3.6: High throughput screen of 64 drugs combined with osimertinib (mutant EGFR-TKI) reveals drug class dependence of synergistic potency and efficacy in NSCLC. A) DSDs for drug combinations. The vertical axis quantifies the observed synergistic efficacy, (β_{obs}). The horizontal axis ($log(\alpha_{21})$) quantifies how osimertinib's potency is modulated by each drug (see Figure 3.4 for $\alpha_{12} - \alpha_{21}$ plot). Error bars represent the parameter uncertainty based on the MCMC optimization (See Appendix B.4). B) 2D density plots and associated marginal distributions for βobs (vertical axis) and α2 (horizontal axis) for all drugs (black) and selected category subclasses. Colored tick marks indicate the 50% and 95% probability density intervals for each distribution.

also significantly decreased the DIP rate below zero despite having an average effect less than osimertinib (red line in Figure 3.7) in isolation. Notably, the combination of osimertinib and HDACi quisinostat achieved the lowest E3 (Figure 3.7). The β value for quisinostat is positive; however, as it was significantly efficacious as a single agent it was not the largest observed β. This highlights the importance of interpreting synergistic efficacy in the context of the maximal efficacy (E_3) and exemplifies the necessity of both the drug combination surfaces and the synergy plots (Figure 3.5) because looking exclusively for the most synergistic combination without considering the magnitude of effects can be misleading.

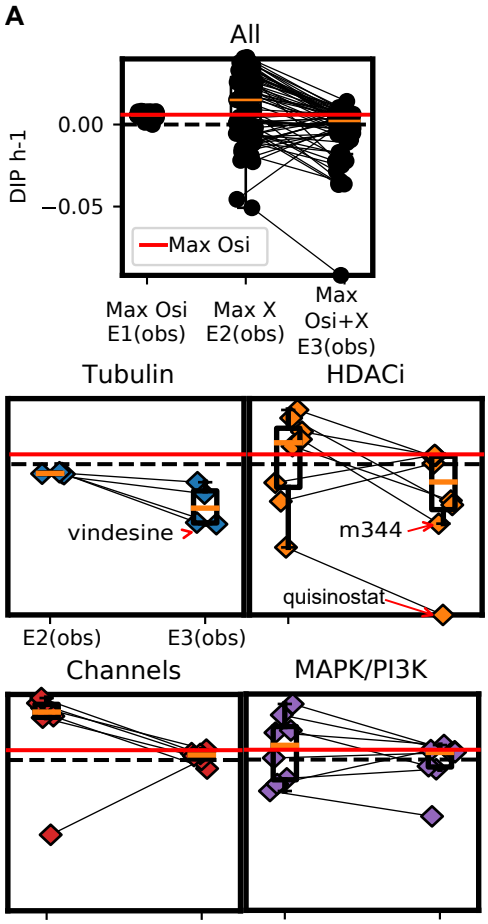

Figure 3.7: Maximal efficacy of drug combinations in NSCLC. A) Distribution of maximal observed effect for drug subclasses in E. The red line signifies maximal effect ofosimertinib alone (E1(obs)) plotted in the first panel. Lines connect the maximal observed effect of the drug alone (E2(obs))and the maximal effect observed in combination with osimertinib (E3(obs)).

In summary, by quantifying synergy of potency separate from synergy of efficacy, MuSyC reveals drug-class trends which can be used to guide subsequent screens and drug combination deployment in NSCLC.

3.3 MuSyC validates co-targeting RAF and MEK in BRAF-mutant melanoma.

The NSCLC drug screen (Section 3.2) suggests combinations targeting molecules within the same signaling pathway may not be productive avenues for increasing efficacy. However, a combination used clinically in BRAF-mutant melanoma co-targets kinases BRAF and MEK in the MAPK pathway (Long et al., 2014; Eroglu and Ribas, 2016). To investigate this combination in more detail, I screened a panel of 8 BRAFV600-mutant melanoma cell lines (Paudel et al., 2018) for cell-line information) against 16 BRAFi/MEKi combinations (see Table 3.1 for drug information and tested dose ranges).

Based on the mean βobs across cell-lines, all 16 combinations were synergistically efficacious (Figure 3.8, 3.9C) indicating MuSyC would have identified this treatment strategy prospectively. In contrast, conventional methods produce ambiguous results (Figure 3.14, top 3 panels in each cell line group), such that this combination strategy could have not been identified. Furthermore, MuSyC detected variations in synergistic efficacy between cell lines (Figure 3.8, 3.9C), underscoring its sensitivity and pointing to heterogeneous, cell-intrinsic mechanisms modulating the efficacy of BRAF/MEK inhibition. In particular, A2058 displayed low average synergistic efficacy, suggesting that its canonical insensitivity to BRAFi does not depend on MEK reactivation, but rather on altered metabolic phenotype (Parmenter et al., 2014; Hardeman et al., 2017). In addition to low synergy, the combination of RAFi+MEKi showed low efficacy in A2058 compared to other cell-lines (Figure 3.10). In several cell lines (A375, SKMEL28, SKMEL5, WM1799, WM983B), the combination was the only way to achieve negative DIP rates (*i.e.* regressing populations) (Figure 3.10) independent of the synergistic efficacy of the combination.

MuSyC also provides information on synergistic potency for these combinations. A clinically deployed combination (dabrafenib and trametinib) is synergistically efficacious, but antagonisti-

cally potent in all cell lines except one (Figure 3.9A), a trade-off that may be relevant in the clinic.

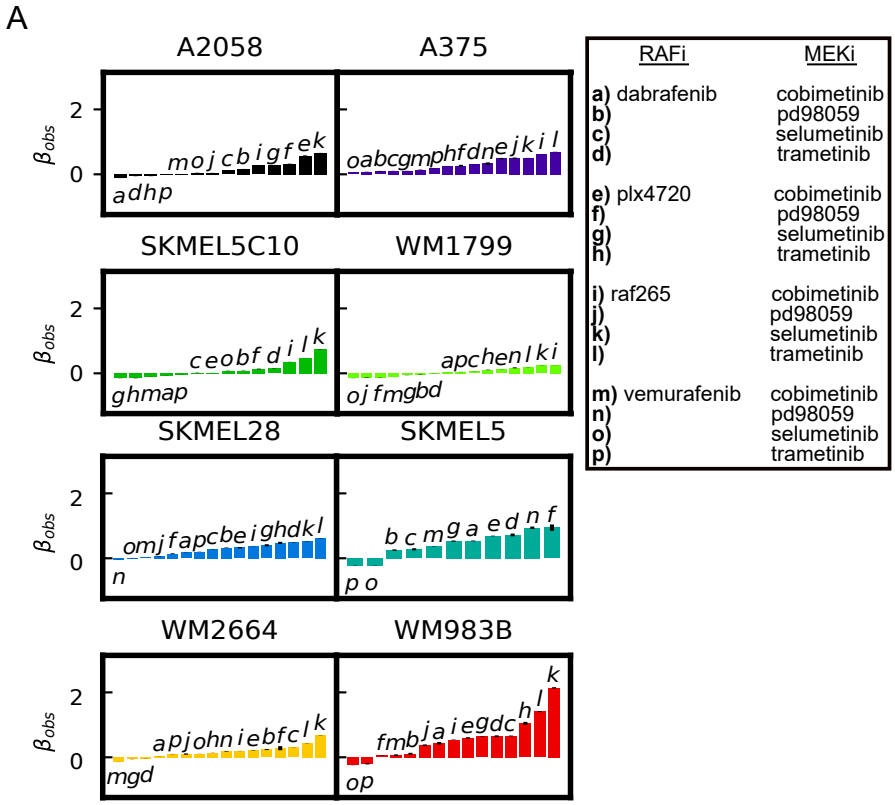

Figure 3.8: Synergistic efficacy and/or potency of drug combinations in BRAF-mutant melanoma. A) 8 BRAF-mutant melanoma cell lines were treated with all possible pairwise combinations of 4 RAF and 4 MEK inhibitors (Table 3.1) for a total of 128 unique combinations. Waterfall plots of βobs for each cell line with all combinations which converged in fitting. Drug combinations noted by letter in the legend to right. (Also see Figure 3.9).

Together, MuSyC analyses of NSCLC and of melanoma combination screens indicate the magnitude of a drug combination's synergistic efficacy depends upon the oncogenetic context, *i.e.*, co-targeting within the MAPK pathway may work for mutant-BRAF melanoma, not for mutant-EGFR NSCLC.

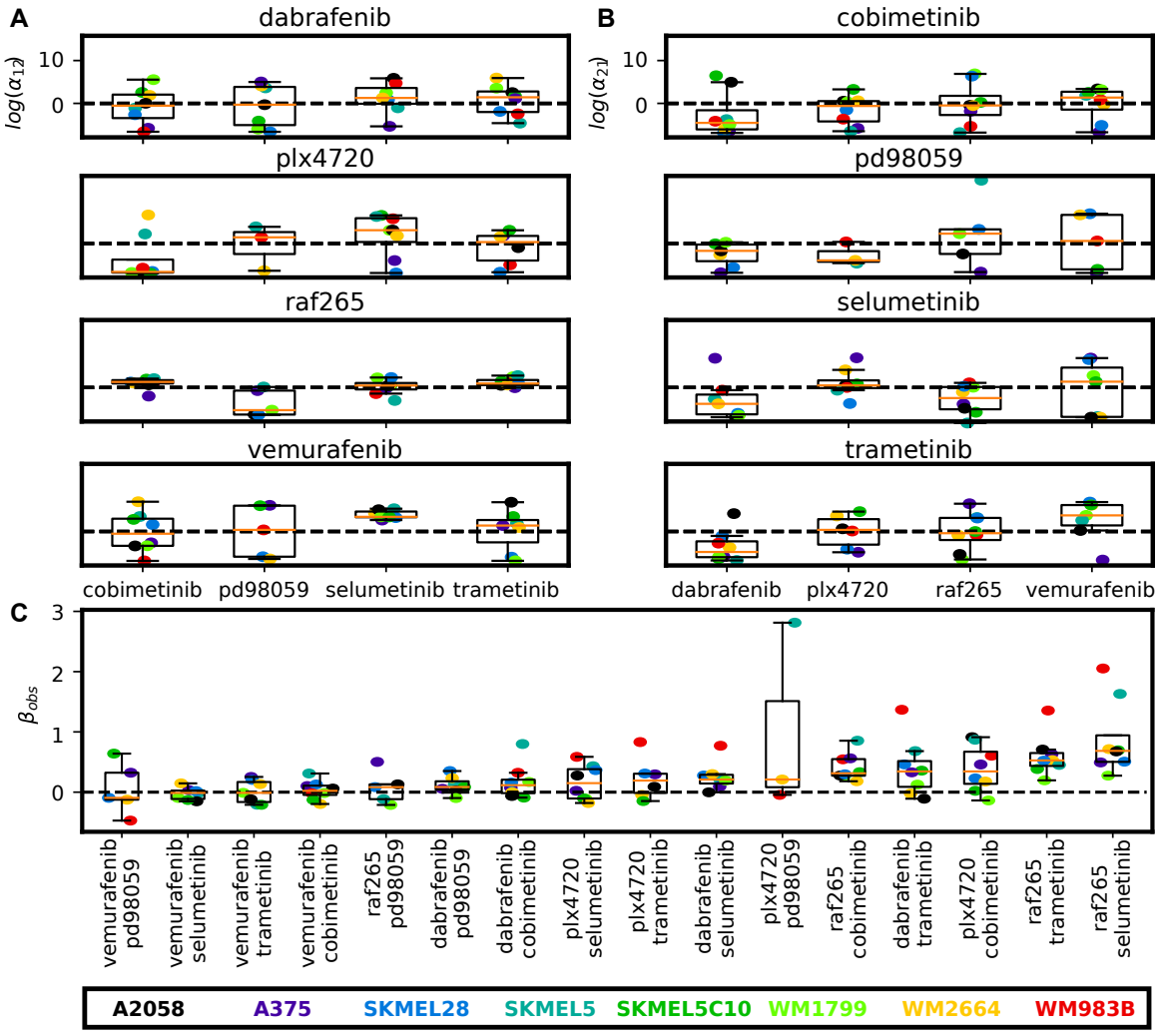

Figure 3.9: Synergistic potency and synergistic efficacy of combined RAFi and MEKi in BRAF-mutant melanoma A) Jitter plots of $\log(\alpha_{12})$ for each RAFi for the 4 MEKi tested. α_{12} corresponds to the alteration in MEKi's effective dose due to the presence of a RAFi. Dashed line denotes zero separating synergistic and antagonistic potency. The color of plotted points is corresponds to the cell line as annotated at the bottom of the figure. B) Jitter plots of $\log(\alpha_{21})$ for each MEKi for the 4 RAFi tested. α_{21} corresponds to the alteration in RAF inhibitor's effective dose due to the presence of a MEK inhibitor. C) Rank ordered jitter plots of the median βobs for each drug combination across all cell lines.

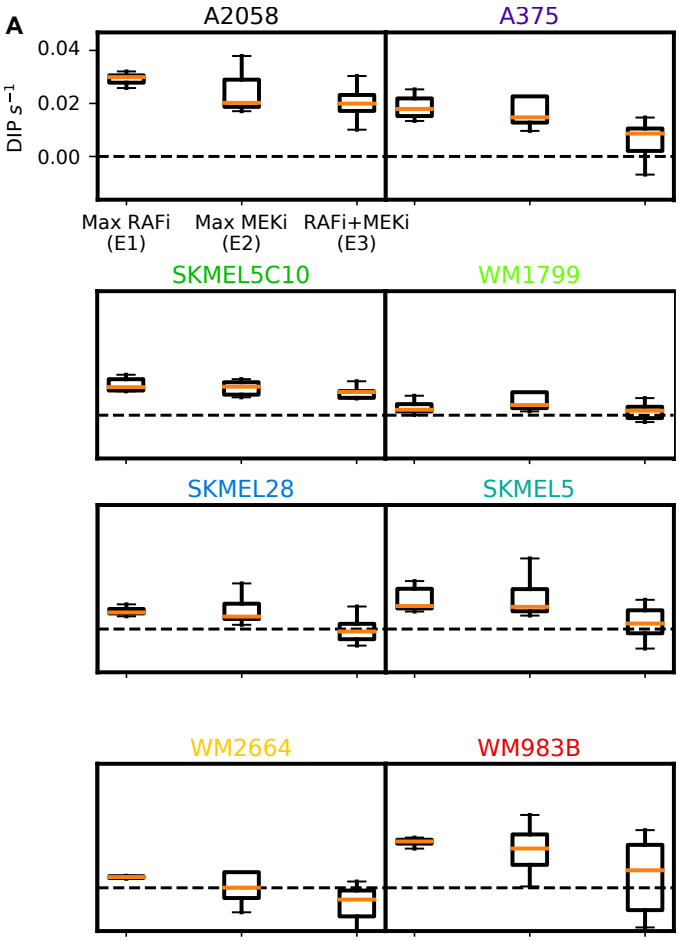

Figure 3.10: Maximal efficacy of combined RAFi and MEKi in BRAF-mutant melanoma. A) Distribution of maximal effects for RAFi alone ($E1$, 4 drugs), MEKi alone ($E2$, 4 drugs), and the combination ($E3$, 16 combinations) for each cell line. Orange bar denotes mean.

3.4 NOX5, a molecular correlate of insensitivity to BRAF inhibition, alters synergistic efficacy, not potency, in BRAF-mutant melanoma.

While drug combinations are commonly identified from top-down approaches, *e.g.*, high throughput drug screens, others, including BRAFi/MEKi, were discovered from a bottom-up approach via investigating molecular correlates of insensitivity. However, these molecular correlates may alter either the potency or the efficacy of the primary drug (or both). MuSyC can distinguish among these possibilities, enabling an informed choice between improving either efficacy or potency. As an example, I looked for molecular correlates of BRAFi insensitivity between subclones of a BRAF-mutant melanoma cell line (SKMEL5) with differential sensitivity to BRAFi (Figure 3.11A). Specifically, I quantified gene expression using RNAseq and identified the top 200 differentially expressed genes (DEGs) (FDR$<$0.001, see Appendix B.1). This gene set was significantly enriched in processes, cellular components, and molecular functions relating to metabolism (Figure 3.11B), aligning with previous reports on the relationship between altered metabolism and resistance to BRAFi (Parmenter et al., 2014; Hardeman et al., 2017). I computed the correlation of the 200 DEGs' expression to BRAFi sensitivity across a 10 cell line panel using expression data from (Subramanian et al., 2017). NADPH oxidase 5 (NOX5) stood out as one of five genes with a significant, positive correlation with BRAFi insensitivity (Pearson r=0.65, p-val=0.042) (Figure 3.11C-D, Table 3.2 for quantification of BRAFi insensitivity and Table 3.3 for genes correlated with BRAFi insensitivity) and was significantly up-regulated in the BRAFi insensitive subclone (SC10) compared with the sensitive subclone (SC01) (Figure 3.11E). Previously unconsidered, NOX5 is an interesting target due to its convergent regulation on metabolic and redox signaling at mitochondria (Lu et al., 2012), processes significantly enriched in the DEGs (Figure 3.11B).

To study NOX5's contribution to the potency or efficacy of BRAF inhibition, I tested PLX4720 in combination with a NOX5 inhibitor, DPI (Jaquet et al., 2011), in a panel of 7 melanoma cell lines selected based on differential NOX5 expression. I found synergistic efficacy correlated with NOX5 expression (Pearson r=0.77, p-value=0.043) (Figure 3.12B,C); however, synergistic potency did not (Pearson r=0.01, p-value=0.96) (Figure 3.12B,D). Of note, A2058, well-known for its

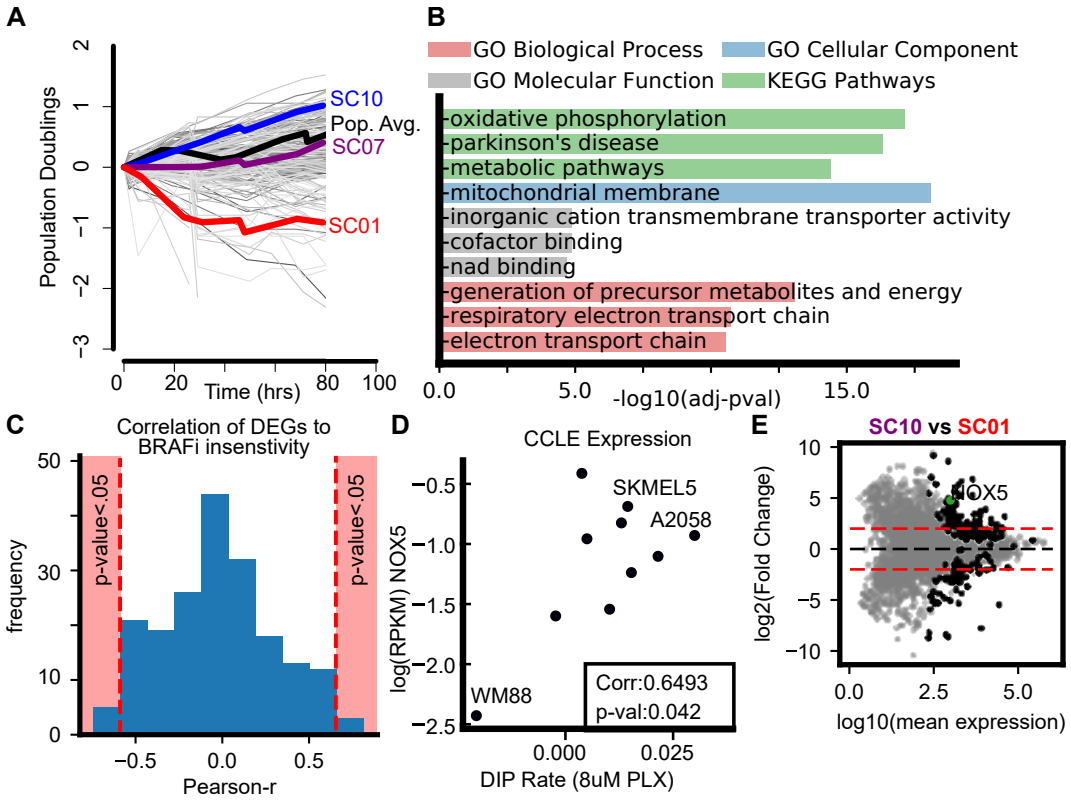

Figure 3.11: NOX5 is a molecular correlate of insensitivity to BRAFi. A) Growth curves of differentially sensitive, single-cell-derived subclones from SKMEL5 treated with 8μM PLX4720. Grey curves represent colony growth according to the clonal fractional proliferation assay (Tyson et al., 2012). The average population response indicated in black curve. SC01, SC07, and SC10 were subsequently used to identify 200 DEGs. B) Top gene set enrichment terms for 200 DEGs. C) Distribution of the correlation between 200 DEGs expression and BRAFi insensitivity. Drug sensitivity was quantified as DIP rate measured in 8μM PLX4720 (Table 3.2). Significance threshold of p-value¡0.05 annotated in pink. D) NOX5 expression correlates with BRAFi sensitivity in 10 BRAF-mutant melanoma cells. E) Pairwise comparison between SC01 and SC10 of DEGs (FDR<0.001) identified using DESeq2 (Love et al., 2014). The 200 identified DEGs (ANOVA between three subclones) are in black. Dotted red lines denote plus/minus 4-fold change.

Table 3.2: BRAFi sensitivity across CCLE BRAF-mutant melanoma cell line panel.

CCLE Cell Line	DIP Rate (h^{-1}) at [8uM] PLX4270
A2058_SKIN	0.030
A375_SKIN	0.005
SKMEL28_SKIN	0.010
SKMEL5_SKIN	0.014
WM115_SKIN	0.013
WM1799_SKIN	-0.002
WM2664_SKIN	0.003
WM793_SKIN	0.015
WM88_SKIN	-0.020
WM983B_SKIN	0.021

Table 3.3: Differentially Expressed Genes (DEGs) between SKMEL5 subclones SC01, SC07, SC10 whose expression significantly correlated to BRAFi insensitivity (Pearson r) across panel of 10 cell-lines (expression data from *Subramanian et al.*). See Table 3.2 for quantification of sensitivity to BRAFi.

+ Correlation with BRAFi insensitivity			- Correlation with BRAFi insensitivity		
Gene symbol	r	p-value	Gene symbol	r	p-value
SLC7A11	0.816	0.004	GRIK3	-0.743	0.014
SLC16A7	0.807	0.005	PRELP	-0.720	0.019
TGFB1	0.666	0.036	CPVL	-0.684	0.029
NOX5	0.649	0.042	ITGA10	-0.659	0.038
LXN	0.646	0.044			

resistance to BRAFi exhibited the highest NOX5 expression among the cell lines and the highest synergistic efficacy ($\beta_{obs} = 1.42 \pm 0.05$) (Figure 3.12A) which was more synergistically efficacious than all tested MEKi/BRAFi combinations (Figure 3.8).

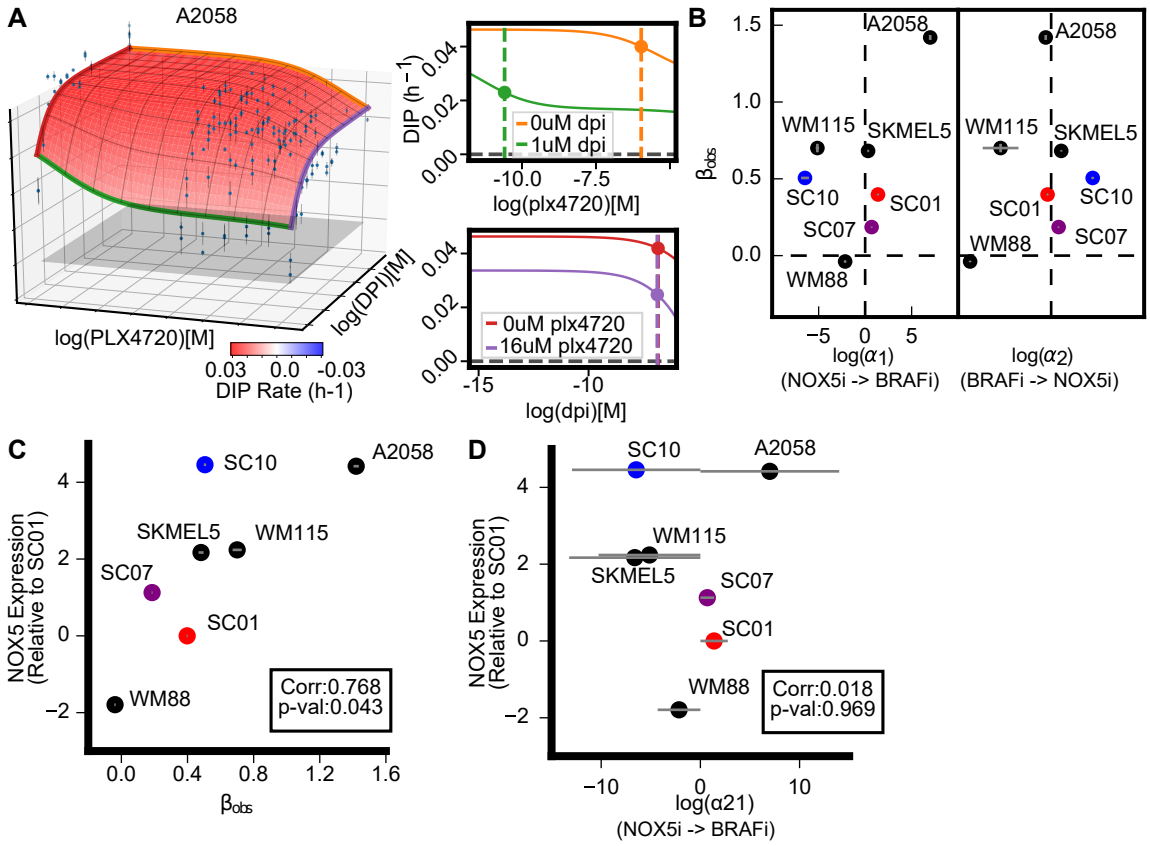

Figure 3.12: NOX5 expression is correlated with synergistic efficacy. A) Dose-response surface for PLX4270+DPI (NOX5 inhibitor) in A2058. A) Scatterplot of β_{obs} vs. $\log(\alpha_{12})$ for NOX5i (DPI) plus BRAFi (PLX4720) in 7 BRAF-mutant melanoma cell lines. H) Correlation (Pearson r) of NOX5 expression with observed synergistic efficacy (β_{obs}). I) Correlation (Pearson r) of NOX5 expression with synergistic potency (α_{21}=DPI's effect on PLX4720 potency).

Taken together, these results suggest co-targeting NOX5 in BRAF-mutant melanoma could lead to improved outcomes for BRAF-mutant melanoma patients with a unique metabolic program for which NOX5 is a biomarker. Furthermore, this study demonstrates the utility of MuSyC for distinguishing a molecular constituent's role in modulating the potency or efficacy of a drug.

3.5 Conflating synergy of potency and efficacy leads to inconclusive classification.

To investigate how results from MuSyC compare with the most frequently used synergy metrics, I calculated synergy using Loewe additivity, Combination Index (CI), and Bliss on data from the NSCLC (Section 3.2) and the melanoma (Section 3.3) screens. Loewe synergy was calculated directly from the DIP rate data, while CI and Bliss, which require percent metrics, were calculated from 72-hour percent viability (Barretina et al., 2012) imputed from the growth curves (see method description Appendix B.6) . Unlike MuSyC, these metrics are evaluated at every concentration resulting in dose-dependent distributions of synergy (Figures 3.13, 3.14) commonly resulting in ambiguous classification of a combination. By the median of each distribution, none of the metrics can statistically discriminate between the quadrants in Figures 3.13, 3.14 (Kruskal-Wallis p-value > 0.05).

Examining the models underlying these metrics revealed several limitations and biases accounting for their ambiguity. For Loewe additivity, synergy is undefinable for many tested concentrations as Loewe cannot be calculated at combination conditions with effects exceeding the maximum effect of the weaker drug (Table 1.1). This is particularly limiting for synergistically efficacious combinations, which, by definition, achieve greater effect than either drug alone. In the NSCLC screen, because osimertinib alone was not sufficient to achieve a negative DIP rate (*i.e.*, regressing population), Loewe is undefinable for all conditions where DIP rate was less than zero (Figure 3.15A). For conditions where Loewe is defined, Loewe contains a Hill slope dependent bias (Section 2.5, page 57) such that when the geometric mean of the hill slopes is less than one ($\sqrt{h1 * h2}$), the linear model of Loewe will overestimate synergy and when, Loewe will underestimate synergy (Figure 2.4). Correspondingly, I found the median value of Loewe synergy was negatively correlated with the geometric mean of the hill coefficients in both the NSCLC and melanoma screens (Figure 3.15B, spearman r= -0.51 and -0.41, p-value=1e-3 and 8e-4 respectively). That is, the synergy of a combination according to Loewe additivity could be estimated based on the hill slope of a single drug alone in contrast to MuSyC where synergistic potency and efficacy are decoupled from the single drug's pharmacologic profile (Figure 3.3B).

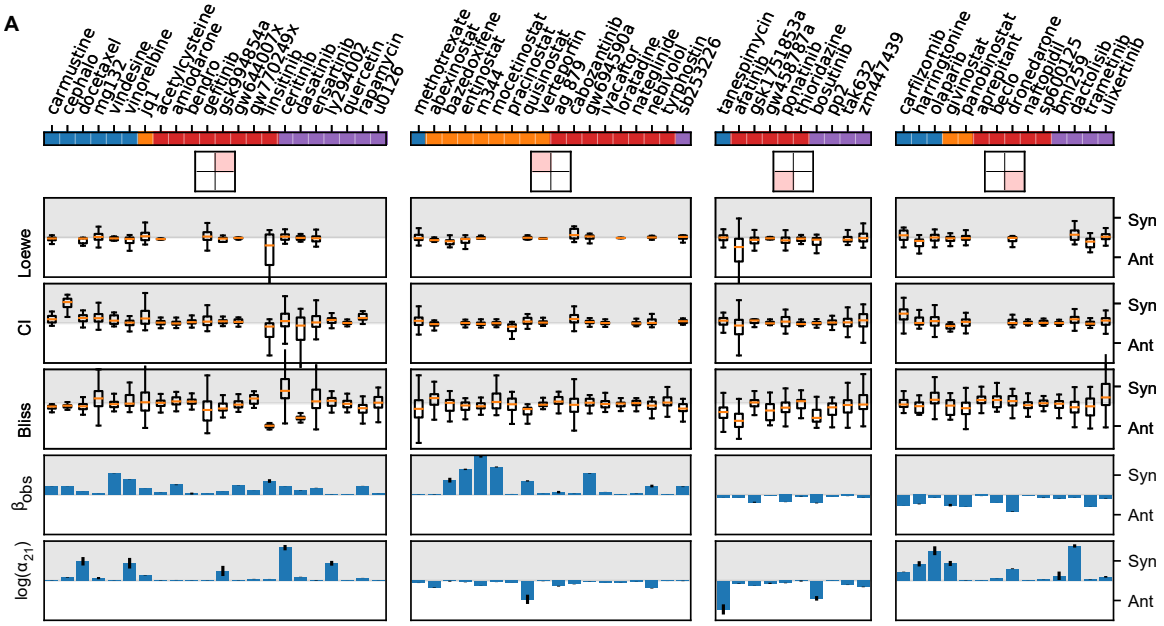

Figure 3.13: Drug combinations against EGFR-mutant NSCLC are ambiguous by Bliss, Loewe, CI, and HSA. A) Drugs are separated based on their quadrant from Figure 3.6, and distributions of synergy calculated by Loewe, CI, and Bliss are shown. Loewe was calculated directly from DIP rates, while CI and Bliss were calculated from 72-hour viability (Appendix B.6). Overall, most combinations span synergism and antagonism when quantified by Loewe, CI, or Bliss. Conditions for which synergy could not be defined were removed. Traditionally, Loewe and CI are synergistic between 0 and 1, and antagonistic for values >1; however, for visualization, I transformed them to -log(Loewe) and -log(CI), so synergism (Syn) corresponds to positive numbers (grey region), antagonism (Ant) to negative (white region). α_{21} is the change in osimertinib's potency due to the other drug. Error bars for β_{obs} and log(α_{21}) calculated from MCMC optimization (Appendix B.4).

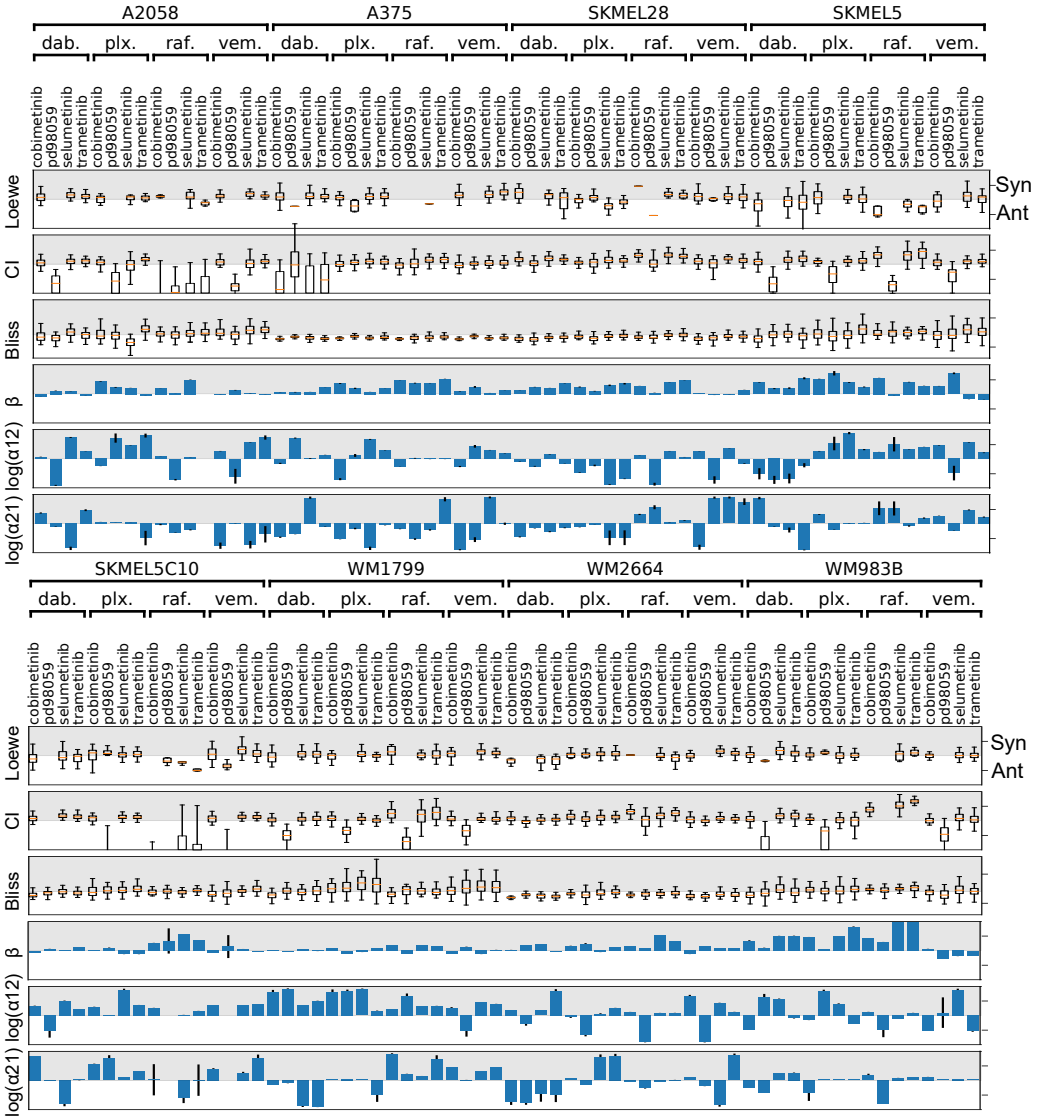

Figure 3.14: Combination of BRAFi+MEKi combinations against BRAF-mutant melanoma are ambiguous by Bliss, Loewe, CI, and HSA. A) Distribution of synergy calculated by Loewe, CI, and Bliss for melanoma dataset. As in the NSCLC data, Loewe was calculated directly from DIP rates, while CI and Bliss were calculated from 72-hour viability. Conditions for which synergy is undefined were not included. By these traditional methods, combinations of BRAF/MEK inhibitors in melanoma are ambiguous, spanning synergy (Syn-gray) and antagonism (Ant-white). $\log(\alpha_{12})$ is the RAFi's effect on the potency of the MEKi and $\log(\alpha_{21})$ is the reverse. Abbreviations of the RAF inhibitors are: dab=dabrafenib, plx=plx4720, raf=raf265, and vem=vemurafenib.

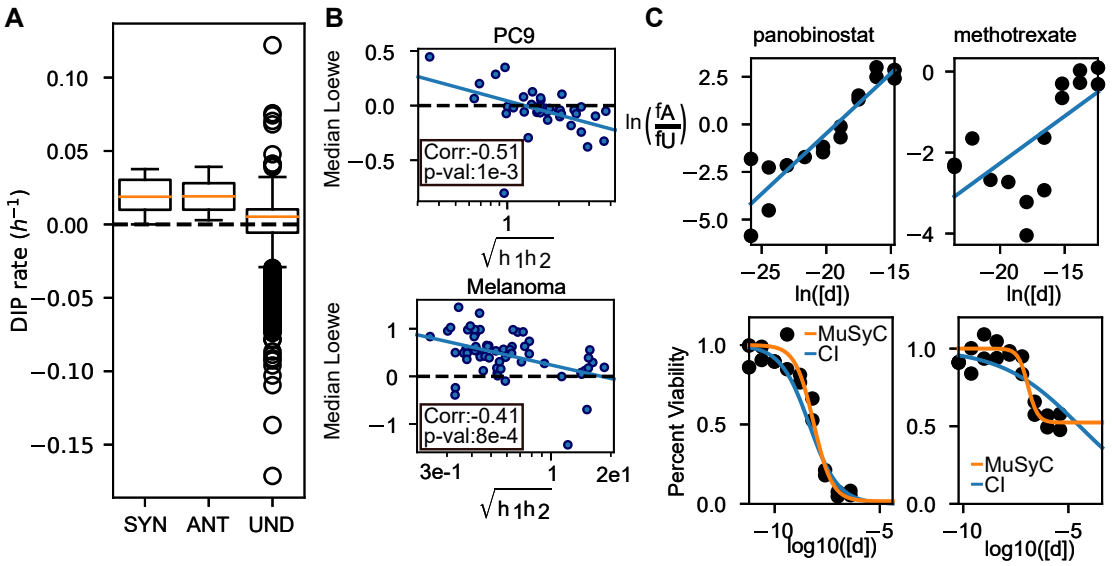

Figure 3.15: Bias and limitations of classic methods applied to the NSCLC drug screen. A) Loewe is undefined (Und) for all concentrations which achieved a net negative DIP rate. B) The median values of synergy calculated by Loewe are anti-correlated with the geometric mean of the hill slope in both the NSCLC and BRAF-mutant melanoma datasets. C) CI poorly fits drugs whose max effect is not equal to 0. The top panel shows linear dose-response fit by the CI algorithm, bottom shows the quality of fit in a standard dose-response view. The CI fit works well for drugs for which Emax = 0, like panobinostat (left, Emax=0.016, C=7.13 nM, h2=0.99 for orange fit, Emax=0, C=4.42 nM, h2=0.63 by CI). However, drugs with Emax ¿¿ 0, like methotrexate (right) lead to poor fits (Emax=0.52, C=0.119 uM, h2=1.88 by orange fit, Emax=0, C=34.7 uM, h2=0.23 by CI).

CI is a special case of Loewe additivity which adds the additional condition that E0=1, E1=E2=E3=0, such that the drug effect is equated with percent inhibition (Chou et al., 1983). As previously discussed, this commonly results in poor fits for data where the maximal effect saturates above 0% (Figure 2.12. I observe poor fits of CI also in the osimertinib screen in these same conditions. For example, methotrexate, which reaches a maximum effect of 52% viability)(Figure 3.15C). CI is thus inappropriate for cell-based assays of drug effect where the correspondence between percent inhibition and cell viability is not one-to-one.

In summary, traditional methods cannot distinguish synergy of potency from synergy of efficacy (Figures 3.13,3.14) leading to ambiguous classifications of the synergistic profile of a combination. This ambiguity is to be expected if synergy is a dose-dependent phenomenon; however, such an assumption precludes a logical method for comparing between drug combinations—a common aim of high throughput drug combination screens.

3.6 Scaling synergy to the genome: combining MuSyC with functional genomics

A persistent challenge in drug combination studies is the combinatorial expansion of conditions required to measure (Section 1.6, page 15). For single dose-response curves, the gold standard is a 13-point dilution series per drug, though in practice as few as 5 to 6 dilutions can still be used to estimate the potency or efficacy of a drug. By comparision, when sampling drug combinations across a matrix, (Figure 3.2) 77 conditions are measured—exceeding a 2^N scaling in number of conditions for N drugs.

A potential work around is suggested by the geometry of the phenomenological model underlying the 2D Hill equation 2.8 (Figure 2.1). As shown in Section 2.1 (page 28), the 2D Hill equation reduces to a 1D Hill equation at the boundaries and, therefore, it is possible to find all parameters of the 2D Hill equation (eq. 2.8, page 31) sampling only on the boundaries. In general, this is not advisable as if there is no difference in the maximal efficacy of the single drug and the combination (for example the combination of osimertinib and ceritinib Figure 3.5B), then estimating α depends on the intermediate doses. However, in special cases such as the binary knockout of a

gene, this sampling strategy which only uses the boundaries could be appropriate. Such a strategy significantly reduce the number of datapoints required to calculate synergy. Here I apply this idea to interpreting the readout of a functional genomics screen in a BRAF-mutant melanoma cell line.

3.6.1 Simplification of the 2D Hill equation and experimental design.

While in general, more doses along the response curve of the RNAi knockdown + drug combination are preferable, it is infeasible to obtain many drug concentrations in high throughput RNAi screens due to cost. However, it remains possible to uniquely compute α and β for only three conditions of drug+RNAi given a well defined dose-response curve for the drug alone (Figure 3.16A). Synergistic potency is then the geometric translations between the dose-response curve with and without the knockdown (Figure 3.16B horizontal axis). Synergistic efficacy is the percent increase in maximal effect of the drug+RNAi combination over the most efficacious of either alone (Figure 3.16B vertical axis).

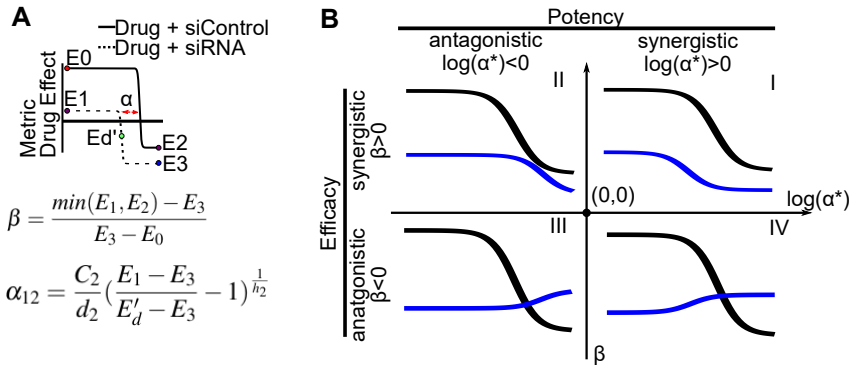

Figure 3.16: Calculating synergistic potency and synergistic efficacy from functional drug plus siRNA combinations. A) Given a well defined dose response curve of a drug by itself (solid black line) with a potency $C2$, efficacy E_2, and Hill slope h_2, then β and α can be calculated uniquely from 3 conditions. Effect of siRNA only (E_1), effect of the siRNA and drug at maximum concentration of drug (E_3), and effect of drug and siRNA at intermediate dose ($d2'$) resulting in effect Ed'. B) As with drug combinations, the knockdown of a gene can change a drug's potency (horizontal axis) and efficacy (vertical axis) independently. Quadrant I is a cartoon of a gene knockdown which increases the potency and the efficacy of the drug (black $\rightarrow$ blue line). Quadrant IV is a gene which antagonizes the efficacy of the drug at low doses.

There are several limitations of this design. First this method precludes fitting asymmetric synergistic potency terms (i.e. the effect of the drug on the potency of the RNAi cannot be estimated). Second is strong antagonistic potency may confound the accuracy of β (Figure 3.17A); however, the converse it not true. Finally, the selected dose dictates the interval where α can be calculated accurately (Figure 3.17B) as the change in Ed' diminishes with increasing absolute value of $log(\alpha)$.

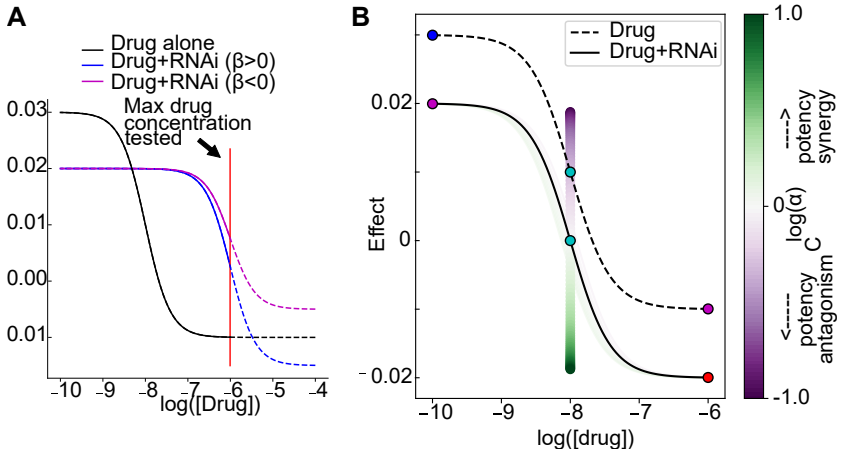

Figure 3.17: EC50 is the optimal dose in siRNA screen. A) Antagonisitic potency increases uncertainty of β. Red line is the maximum drug tested in experiment which is sufficent for the drug alone (black line) to observe the effect saturation; however, when the siRNA shifts the dose response curve, the plateau moves beyond the tested concentration range. As a result, it is not possible to distinguish synergistic from antagonistically efficacious (purple and blue curves respectively), alterations. B) Increasing absolute values of $log(\alpha)$ result in diminishing changes to Ed' such that there is a range of values for which α can be reasonably calculated.

3.6.2 Functional genomics screen reveals key modulators of BRAFi pharmacologic profile.

To test the validity of using siRNA as a "drug" in the MuSyC framework, I tested combinations of a BRAFi (plx4720) with different siRNA over a matrix of concentrations (Figures 3.18,3.19,3.20) in SKMEL5 cells. When combined with a non-targeting control, there is no increase in effect of the BRAF inhibitor and no change in viability for increasing concentrations

of siRNA (Figure 3.18) BRAFi cannot increase the effect (no synergy of efficacy) of the tranfection control (siTOX) which targets essential cell survival genes (Figure 3.19). Interestingly, the combination of an siRNA to BRAF (siBRAF) with a BRAF inhibitor is synergically efficacious ($\beta = 0.44$) (Figure 3.20). This highlights the non-equivalence between molecular inhibition and gene knockout. While the BRAF kinase domain is inhibited, it can still act as a scaffolding molecule to propogate signal through the MAPK cascade; therefore, even a kinase dead BRAF can still drive signal through MAPK (Heidorn et al., 2010). The increase in effect over the gene knockdown due to the drug is either incomplete knockout or polypharmacology.

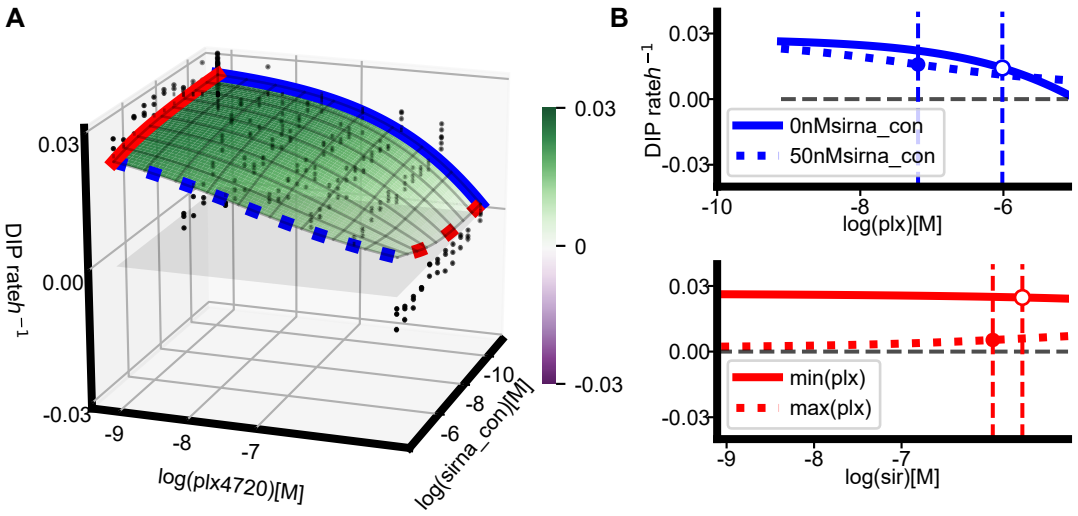

Figure 3.18: Non-targeting siRNA control does not increase the rate of cell killing induced by BRAFi. A) Dose-response surface for the combination of plx4720 combined with non-targeting siRNA control (siCON). B) Boundaries of the dose response surface. Flat lines of red solid and dotted lines signify there is no change in siRNA effect for increasing concentrations of siCON.

Next I ran a functional genomics screen against 1,600 druggable species in SKMEL5 cells in combination with BRAF inhibition (Appendix B.10). The targeted genes spanned multiple molecular families (Figure 3.21) commonly implicated in drug sensitivity. The tested genes spanned a wide range of synergistic efficacy and potency profiles (Figure 3.22A) ranging from strong efficacy synergy (Figure 3.22B PPP1CC) to strong potency synergy (Figure 3.22B RPS6KA4) highlighting

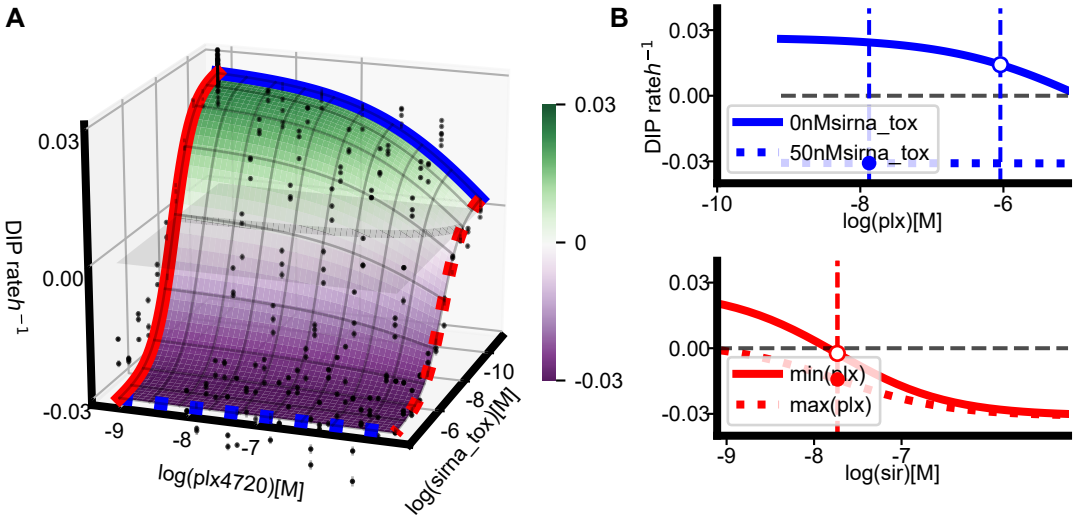

Figure 3.19: BRAFi does not increase the rate of cell killing induced by siTOX. A) Dose-response surface for the combination of plx4720 combined with toxicity control (siTOX, Dharmacon). B) Boundaries of the dose response surface. Flat lines of blue dotted line signifies there is no change in siTOX effect by titrating in BRAFi.

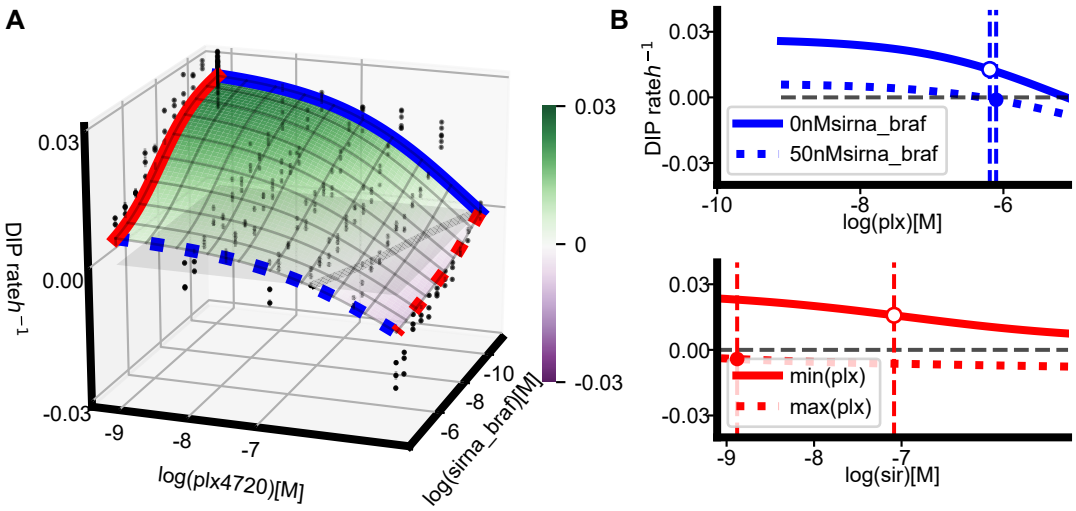

Figure 3.20: Molecular inhibition is synergistically efficacious with gene knockdown. A) Dose-response surface for the combination of plx4720 combined with BRAF-siRNA (siBRAF). B) Boundaries of the dose response surface. Individually, either siBRAF or plx4720 result in near cytostatic growth (gray plane). However, combining them results in a negative DIP rate.

the criticality of distinguishing between different types of synergies when studying the impact of a gene on the pharmacologic properties of a drug. A cluster of genes were strongly antagonistically potent (*e.g.* Figure 3.22B GPR147). Most of these genes had large impacts on the proliferation rate by themselves making estimating β infeasible for reasons detailed in Figure 3.17A.

Of the screen hits, RPS6KA4 is a particularly interesting gene as it is involved in regulating CREB1 and ATF1, which are commonly abnormal in BRAF-mutant melanoma. It also is regulated by MITF which is considered the master transcription factor of melanocyte development (Levy et al., 2006).

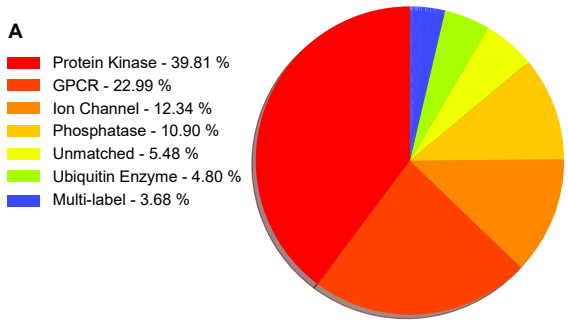

Figure 3.21: Functional genomics screen of 1,600 genes spans multiple molecular families commonly implicated in drug sensitivity. A) Pie chart siRNA targets in each molecular family. Protein kinases are the most abundant followed by GPCRs.

Patients in the TCGA (The Cancer Genome Atlas) who had BRAFV600 mutations and high expression of RPS6KA4 (Figure 3.23A), had lower survival rates (log-rank p-value 3.8e-6) than those with lower expression (Figure 3.23B). While it is unknown whether these patients received targeted BRAF inhibition, it is likely most cases after 2012 where given a targeted agent. Together these results suggest RPS6KA4 as a biomarker of sensitivity to BRAFi.

In summary, combining MuSyC with functional genomics is a potential way of scaling synergy screens to the genomic scale. Such comprehensive maps could be used to guide network motif discovery of targetable gene circuits modulating the potency/efficacy of a drug. However, the non-

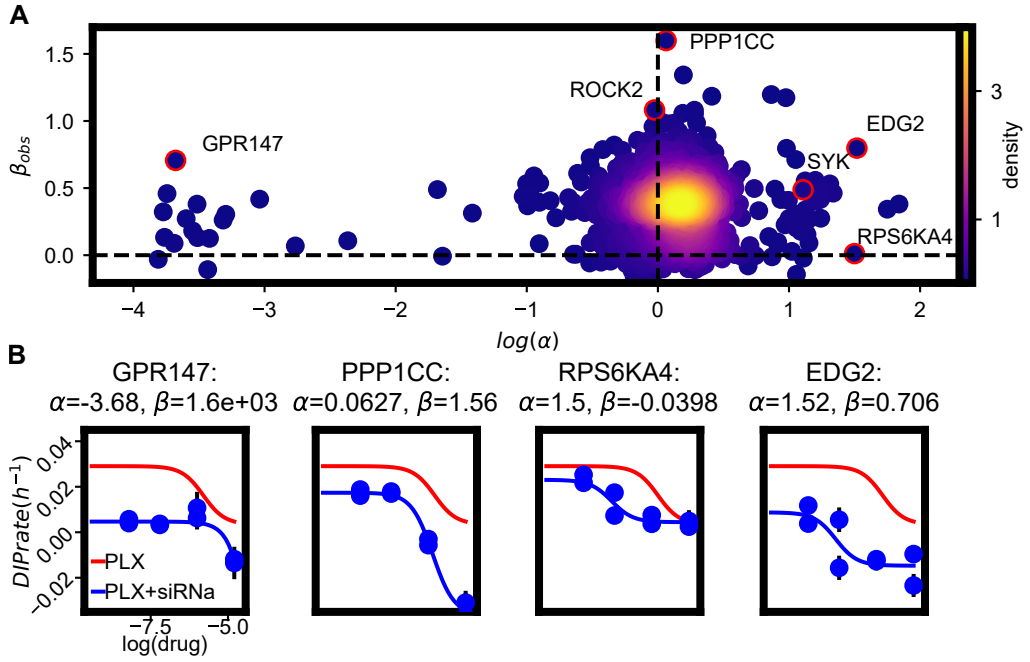

Figure 3.22: Functional genomics screen reveals key gene species which modulate the potency and/or efficacy of BRAF inhibition in BRAF-mutant melanoma. A) 1,600 siRNAs were screened to measure changes in potency (α horizontal axis) and maximal observed efficacy (β_{obs} vertical axis). Color corresponds to density of points. The average β_{obs} and $\log(\alpha)$ was 0.31 and 0.2, respectively. Gene species with $log(\alpha) < -1$ had high uncertainty in calculations of β for reasons demonstrated in Figure 3.17A. B) Four examples highlighted from (A). GPR147 (NPFFR1) is Neuropeptide FF receptor 1 and involved in pain recognition. It had substantial effect singly and only increased further for high concentrations of plx4720 (antagonistic potency, synergistic efficacy). PPP1CC is Protein phosphotase (ser/thr) which is involved in cellular division as well as glycogen metabolism. RPS6KA4 is a ser/thr Kinase regulating CREB1 and ATF1. It is required for mapk activation of CREB1 and ATF1, the latter of which is commonly mutated in melanoma. It has additional interactions with MITF. Finally EDG2 (LPAR1) is a GPCR mediating proliferation, contraction, differentiation, as well as invasion (Muinonen-Martin et al., 2014)

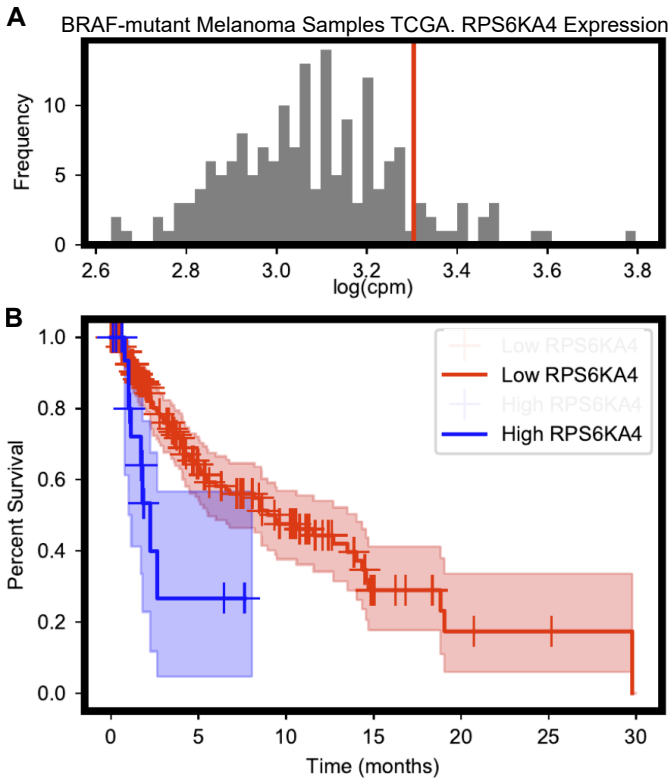

Figure 3.23: RPS6KA4 is a biomarker survival in BRAF-mutant melanoma. A) Expression of RPS6KA4 (log(cpm)) of BRAF-mutant melanoma samples from the TCGA database. While it is unknonw what patients were treated with, since most of the samples come from after the advent of BRAF targeted therapies, it is likely many received BRAF inhibitors. B) Survival curves for populations of high (blue) vs low (red) expression of RPS6KA4. Groups selected based on threshold minimizing the p-value of the log-rank test of significance. (p-value: 3.8e-6) Vertical ticks indicate an event. Confidence interval is plotted as an envelope on the curve.

equivalence between gene knockdown and gene inhibition merits consideration before designing drugs to target screen hits. With the rapid development of targeted degradation strategies (Winter et al., 2015) as well as in vivo RNAi (Adams et al., 2018), the identification of RNAi silencing targets could have increasing clinical applicability.

Chapter 4

Conclusion

"For as I draw closer and closer to the end, I travel in the circle, nearer and nearer to the beginning."
-Dickens, *A Tale of Two Cities*

4.1 A mass action model of combination pharmacology unifies the field of drug synergy

Quantitative models of drug-drug interactions are critical for rationally guiding drug combination discovery and translation in the treatment of complex, multi-factorial diseases. However, the historical fissures in the field have discouraged the wider adoption of formal synergy calculations (Figure 1.1B, page 3). Indeed, recent efforts have only furthered divisions in the field (Section 1.3, page 4). These rifts in the field continue to impact all aspects of modern drug combination discovery, ranging from experimental design (Figure 1.8, page 16) to computational algorithms to predict synergy (Figure 1.9, page 18) to the search for higher order interactions (Figure 1.11, page 22). Therefore the need first identified at the Saariselkä conference (Figure 1.1, page 3)(Greco et al., 1992) still exists, a consensus framework for the quantification of drug synergy.

Herein, I have proposed a mass action model of combination pharmacology (Section 2.1, page 28), termed MuSyC, which subsumes the foundational synergy models in the field (DEP and MSP) into a more general framework (Section 2.2, page 34). The DEP and MSP have formed the foundational principles of most synergy frameworks over the last century; however, the connection between these principles has remained unknown (Greco et al., 1992; Tang et al., 2015). Here, approaching combination pharmacology using the Law of Mass Action unifies both principles in a single framework. By mapping all frameworks on a common landscape (Figure 2.3, page 35), MuSyC facilitates rigorous investigation of oft-cited, contradictory conclusions between existing frameworks (Greco et al., 1995)—contradictions that preclude reproducibility between synergy studies. Specifically, as is seen in Figure 2.3C, there is no combination which can simultaneously

satisfy the conditions required by both DEP and MSP synergy frameworks.

This unification of the MSP and DEP brings to light several key insights germane to the field of drug synergy. In particular, the connections between MuSyC and the classic frameworks predict biases emerging from constraints on the single drug pharmacological profile inherent in the DEP and MSP (Sections 2.4 and 2.5, pages 51 and 57, respectively). As shown in Figure 2.3, the relationship between MuSyC and the MSP and DEP frameworks is constrained by the single-drug parameters (E_1, E_2 for MSP, h for DEP). These constraints suggested systematic biases in MSP and DEP frameworks contingent on a single drug's efficacy (MSP) and Hill slope (DEP)—biases subsequently demonstrated in large drug combination databases. These systematic biases merit consideration when using these frameworks for drug discovery in large screens. Additionally, the constraint on h highlighted a discrepancy between the biochemistry of true sham experiments and real combinations. The centrality of the sham experiment in the drug synergy literature cannot be overstated; however, I argue enforcing sham compliance comes at the cost of improperly modeling real combinations, leading to a predictable Hill-dependent bias.

4.2 Decoupling synergy of potency and efficacy to guide drug combination discovery and deployment

The goal of using synergistic drugs is to achieve more with less. It is therefore intuitive that at least two types of synergy exist: one corresponding to how much more is achievable (synergistic efficacy), the other to how much less is required (synergistic potency). Finding such combinations is vital for optimizing therapeutic windows, as there exists a fundamental trade-off between clinical efficacy and tolerable doses (Figure 4.1). However, I envision distinguishing synergies of potency, efficacy, and cooperativity will be of differential consequence in different contexts. Diseases for which single-drug efficacy is sufficient would benefit from synergistically potent combinations to drive down toxicity and/or side effects. Diseases with treatments of insufficient efficacy are in pressing need of synergistically efficacious combinations in order to improve depth and durability of response. By stratifying synergy along distinct axes of potency and efficacy using MuSyC,

informed choices can be made about this trade-off.

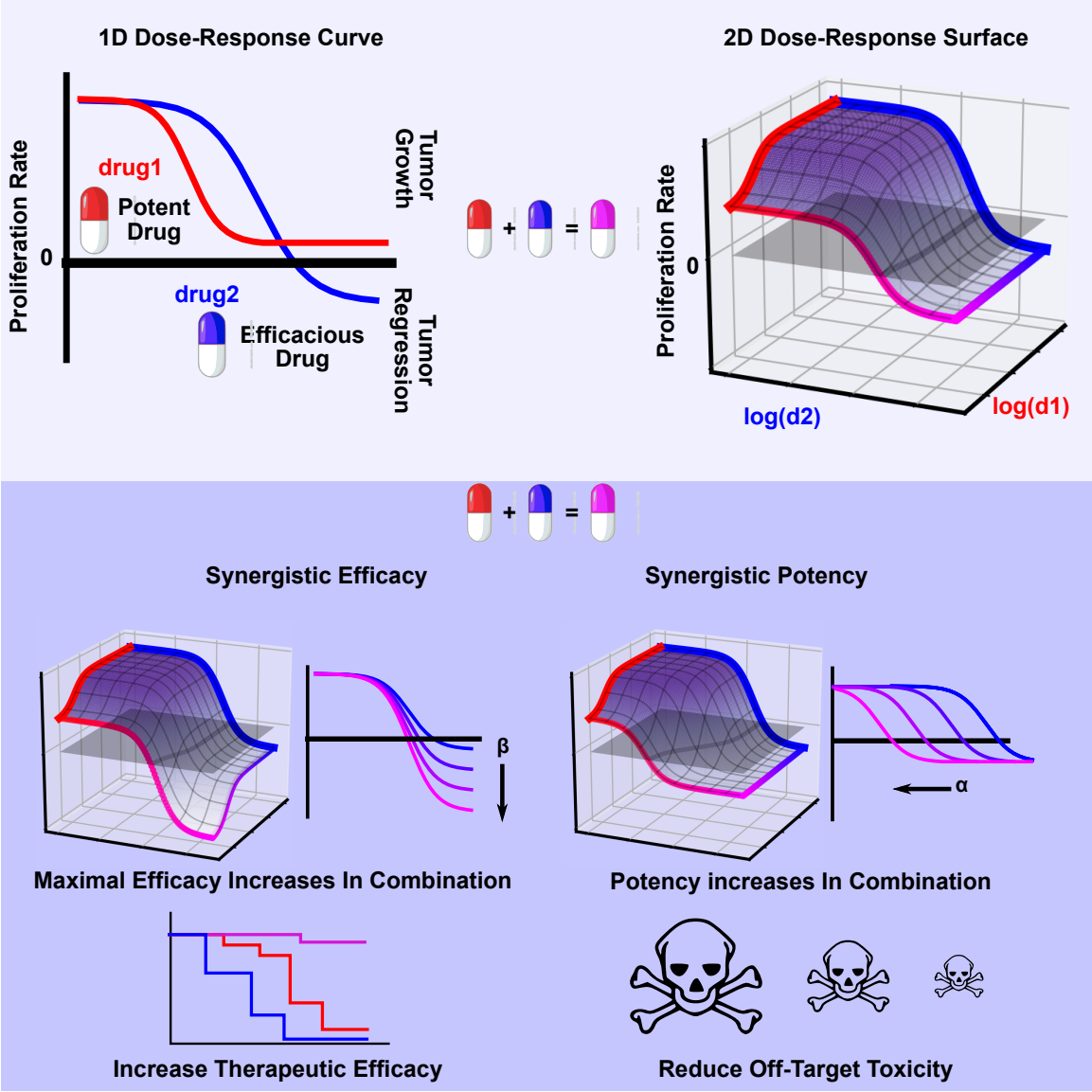

Figure 4.1: The goal of combination therapy is two-fold: more effect for less drug. MuSyC distinguishes different types of synergistic interactions which correspond to these clinical goals.

There has been much critical analysis over the past twenty-five years on the term 'synergy' (Greco et al., 1992), arguably rooted in the practice of defining synergy with respect to arbitrary expectations of drug additivity implicitly codified in previous methods' foundational principles.

In contrast, ambiguity about the meaning of 'synergy' disappears in MuSyC, because its synergy parameters relate directly to the textbook pharmacology concepts of efficacy and potency. By calculating synergy in this way, its interpretation does not depend on arbitrary expectations or thresholds. Rather, an α of 10 corresponds to a 10-fold increase in a compound's potency, as a result of the other drug, regardless of whether I define $\alpha = 1$ or $\alpha = 10$ as the "threshold" for synergy. Indeed, a major advance of MuSyC is the decisive shift toward synergy calculations directly related to an observable change in efficacy and/or potency. Thus, ambiguous questions, such as "is there synergy?" can be recast into more precise questions, such as "How much does efficacy/potency of drug X change when drug Y is added?" Such precise language should promote a move away from arbitrary cut-offs for "significant synergy" which are context dependent.

I have shown how distinguishing between synergy of potency and efficacy facilitates identifying drug-class trends that can be iteratively expanded in future screens to optimize synergistic efficacy or synergistic potency, whichever is desirable for a particular disease. Specifically in this work, MuSyC revealed a subclass of epigenetic regulators as potentially interesting targets for combination therapy in an EGFR-oncogene addicted background (Section 3.2, page 69). Epigenetic regulators have previously been suggested to prime NSCLC for sensitivity to EGFRi (Schiffmann et al., 2016)and the HDACi entinostat in combination with erlotinib (first generation EGFR-TKI) has been shown to increase overall survival in EGFR-mutant, NSCLC cases with high expression of E-cadherin (Witta et al., 2012, 2006). Consistent with this, I also observe entinostat was synergistically efficacious with osimertinib ($\beta_{obs} = 0.84 \pm 0.027$) in PC9 cells, an E-cadherin high expressing cell line (Shimoyama et al., 1992). As is typical of high-throughput screens, there were results of undetermined significance, including dronedarone (an anti-arrhythmic sodium channel inhibitor) and GW694590a (an anti-angiogenesis compound targeting the TIE2 receptor) which were the most antagonistic and synergistically efficacious compounds out of the Receptors and Channels drug class respectively. Further studies are needed to verify these results. Nonetheless, MuSyC provides a quantitative foundation to further investigate unsuspected combinations.

The global views provided by the MuSyC also reveal synergistic trends that vary according

to disease context. For example, co-targeting the MAPK pathway in NSCLC or BRAF-mutant melanoma yields different outcomes: in the former, only synergistic potency is observed, while in the latter synergistic efficacy, and sometimes potency, is registered (Section 3.3, page 80). The disparity emphasizes that synergistic trends require data-driven metrics that distinguish between synergy of efficacy and potency.

MuSyC dose-response surfaces facilitate evaluating the significance that combination synergy should be assigned. That is, MuSyC's synergy parameters quantify the relative increase in efficacy or potency of the combination, with respect to single agents, and therefore the improvements should be interpreted in the context of the absolute potency and efficacy. This information is directly conveyed in the topology of the dose-response surface. As an example, in the NSCLC screen, the combination of osimertinib with quisinostat exhibited the greatest total efficacy. However, since quisinostat is already significantly efficacious on its own, that combination ranks lower than the M344-osimertinib combination along the axis of synergistic efficacy (Figure 3.7, page 3.7). Thus, consideration of both the synergy and the absolute efficacy is critical in assessing new combinations.

MuSyC is also useful for investigating a molecular species' contribution to the potency and efficacy of a compound. Here I demonstrated NOX5 activity modulates the efficacy, but not the potency, of BRAFi (Section 3.4, page 84). However, the NOX5i used, DPI, is known to have off-target effects (Altenhöfer et al., 2015); therefore, further evidence for the role of NOX5 in BRAFi efficacy will require extending MuSyC to studies combining drugs and gene silencing technology (*e.g.*, RNAi or CRISPR).

Finally, I have shown how drug synergy screens can bypass some of the burdensome data requirements for calculating synergy by leveraging the geometry of the MuSyC model (Section 3.6, page 92) when a binary effect is expected such as in the case of a gene knockout. This approximation was used to measure the impact of 1,600 genes on the potency and efficacy of a BRAFi in BRAF-mutant melanoma. This screen demonstrated the criticality of distinguishing between synergy of potency and efficacy when studying a gene's role in drug sensitivity. Follow-

up studies will be necessary to assess the potential of the identified genes for biomarkers of drug sensitivity (*e.g.* RPS6KA4 Figure 3.23, page 99) and targetability for combination therapy. Note such efforts should carefully distinguish between impact of molecular knockdown and molecular inhibition (Figure 3.20, page 96).

4.3 Future directions and limitations

The prospects of higher order synergies (*i.e.*, interactions beyond pairwise) and scaling laws for drug mixtures, while provocative, have remained contentious (Wood et al., 2014; Zimmer et al., 2016; Tekin et al., 2018) (Section 1.6.3, page 20). MuSyC's cubic geometry allows it to be easily extended to three or more drugs (Figure 2.2, page 2.2), and I expect MuSyC will enable a more refined search for higher order interactions. For instance, combinations that mix different synergy profiles (*e.g.*, drugs 1 and 2 are synergistically potent, and drugs 2 and 3 are synergistically efficacious) may exhibit different higher order interactions than combinations all sharing a single synergy type. However, the number of synergy parameters in MuSyC scales poorly, and the commensurate data necessary to fully constrain MuSyC hyper-surfaces invokes a parameter identifiability problem. MuSyC's geometry could be leveraged to guide sampling schemes to constrain the boundaries, allowing the solution to be built up step-wise as was done for the functional genomics work (Section 3.6, page 92).

MuSyC expects single-drug dose-response curves to be sigmoids well fit by the 1D Hill equation (eq (2.3)), and dose-response surfaces to be well fit by the 2D Hill equation (eq (2.8)). In my experience, these expectations are met by real data, as most single drugs have monotonic, sigmoidal responses, and even complex drug interactions can be modeled using various mixtures of α, β, and γ (96% and 88% of combinations in anti-cancer (O'Neil et al., 2016) and anti-malarial (Mott et al., 2015) datasets had $R^2 > 0.7$, respectively). However, it is possible for drugs to have multiphasic responses due to poly-pharmacology which is not well fit by a Hill curve. It may be possible to extend MuSyC to encompass such drugs —for instance by including a multiphasic Hill model (Di Veroli et al., 2015) or modeling effects of "partially affected" states (Figure

2.13 page 60). In extreme cases, it may only be possible to apply non-parametric frameworks such as Bliss, Loewe, or HSA. Additionally, MuSyC assumes all drugs are administered concurrently, whereas patient treatments are often staggered. New theory and experimental methods are needed to address the synergy of combinations which are staggered temporally, bridging the synergy of pharmacodynamics with the synergy of pharmacokinetics (Koplev et al., 2017). Finally, in the datasets I analyzed here, I did not find a role for γ. Future studies in other systems, such as neuronal modulators, are needed to better understand situations when synergistic cooperativity is expected.

Substantial effort was made to reliably calculate the confidence interval for fitted parameters (Appendix A.1). This was an unexpected difficulty arising from the multi-collinearity between parameters in the Hill equation which caused standard regression estimates of uncertainty to be unstable. The recommended algorithm for fitting dose-response surfaces at present is described in Appendix A.1.

While I focused on the DIP rate as the metric of effect, MuSyC may be applied to any quantifiable phenotype whose dose-response is suitable to be fit by a Hill equation. In contrast, all other synergy models I surveyed impose strict constraints on the type and/or magnitude of the drug effect metric. Thus, MuSyC opens up the potential to study synergy of drug effects previously impossible to address by existing methods. Examples of metrics include immune activation, growth in three dimensional culture, or second messenger efflux. The flexibility is particularly critical in translating drug combinations to the clinic by using models of increasing complexity, such as organoids, which better represent drug sensitivity of a patient (Jabs et al., 2017). Indeed, that most clinical combinations can be explain by patient-to-patient variability (Palmer and Sorger, 2017) is strong rationale for translating combination screens to more complex, pre-clinical models. Subsequent work will be devoted to scaling the combination drug screening pipeline developed here to pre-clinical experimental models of increasing complexity, such as organoids.

4.4 Concluding Remarks

By viewing the landscape of drug synergy through the lens of mass-action, I have demonstrated the underlying assumptions, limitations, and biases of commonly applied synergy methods. I have shown how MuSyC unifies the DEP and MSP thus providing a consensus framework for the study of combination pharmacology. These findings provide much needed clarity to the field and should promote the reproducibility of drug synergy studies across drug combination discovery efforts. I showed this framework allows for a richer understanding of drug interactions, with practical, translational consequences. I foresee this approach will streamline drug combination discovery and facilitate the deployment of precision approaches to therapeutic combinations. In doing so, MuSyC will open the door to the discovery of new and previously discarded avenues for therapeutic mixtures.

BIBLIOGRAPHY

D. Adams, A. Gonzalez-Duarte, W. D. O'Riordan, C.-C. Yang, M. Ueda, A. V. Kristen, I. Tournev, H. H. Schmidt, T. Coelho, J. L. Berk, K.-P. Lin, G. Vita, S. Attarian, V. Planté-Bordeneuve, M. M. Mezei, J. M. Campistol, J. Buades, T. H. Brannagan, B. J. Kim, J. Oh, Y. Parman, Y. Sekijima, P. N. Hawkins, S. D. Solomon, M. Polydefkis, P. J. Dyck, P. J. Gandhi, S. Goyal, J. Chen, A. L. Strahs, S. V. Nochur, M. T. Sweetser, P. P. Garg, A. K. Vaishnaw, J. A. Gollob, and O. B. Suhr. Patisiran, an RNAi Therapeutic, for Hereditary Transthyretin Amyloidosis. *New England Journal of Medicine*, 379(1):11–21, jul 2018. doi: 10.1056/NEJMoa1716153.

S. Altenhöfer, K. A. Radermacher, P. W. M. Kleikers, K. Wingler, and H. H. H. W. Schmidt. Evolution of NADPH Oxidase Inhibitors: Selectivity and Mechanisms for Target Engagement. *Antioxidants & redox signaling*, 23(5):406–27, aug 2015. doi: 10.1089/ars.2013.5814.

A. Amzallag, S. Ramaswamy, and C. H. Benes. Statistical assessment and visualization of synergies for large-scale sparse drug combination datasets. *BMC BIOINFORMATICS*, 20(1):83, feb 2019. doi: 10.1186/s12859-019-2642-7.

B. Anchang, K. L. Davis, H. G. Fienberg, B. D. Williamson, S. C. Bendall, L. G. Karacosta, R. Tibshirani, G. P. Nolan, and S. K. Plevritis. DRUG-NEM: Optimizing drug combinations using single-cell perturbation response to account for intratumoral heterogeneity. *Proceedings of the National Academy of Sciences of the United States of America*, 115(18):E4294–E4303, may 2018. doi: 10.1073/pnas.1711365115.

J. C. Ashton. Drug Combination Studies and Their Synergy Quantification Using the Chou–Talalay Method—Letter. *Cancer Research*, 75(11):2400–2400, jun 2015. doi: 10.1158/0008-5472.CAN-14-3763.

M. Bansal, J. Yang, C. Karan, M. P. Menden, J. C. Costello, H. Tang, G. Xiao, Y. Li, J. Allen, R. Zhong, B. Chen, M. Kim, T. Wang, L. M. Heiser, R. Realubit, M. Mattioli, M. J. Alvarez,

Y. Shen, N.-D. NCI-DREAM Community, D. Gallahan, D. Singer, J. Saez-Rodriguez, Y. Xie, G. Stolovitzky, A. Califano, and NCI-DREAM Community. A community computational challenge to predict the activity of pairs of compounds. *Nature biotechnology*, 32(12):1213–22, dec 2014. doi: 10.1038/nbt.3052.

C. Beppler, E. Tekin, Z. Mao, C. White, C. McDiarmid, E. Vargas, J. H. Miller, V. M. Savage, and P. J. Yeh. Uncovering emergent interactions in three-way combinations of stressors. *Journal of The Royal Society Interface*, 13(125):20160800, dec 2016. doi: 10.1098/rsif.2016.0800.

M. C. Berenbaum. What is synergy? *Pharmacological reviews*, 41(2):93–141, jun 1989.

A. Berg, R. Meyer, and J. Yu. Deviance Information Criterion for Comparing Stochastic Volatility Models. *Journal of Business & Economic Statistics*, 22(1), 2004. doi: 10.1198/073500103288619430.

C. I. Bliss. The Toxicity of Poisons Applied Jointly. *Annals of Applied Biology*, 26(3):585–615, aug 1939. doi: 10.1111/j.1744-7348.1939.tb06990.x.

Z. P. Bulman, R. C. Dillon, and B. T. Tsuji. Pharmacodynamic Issues in Antibiotic Combinations. In Rotschafer, JC and Andes, DR and Rodvold, KA, editor, *ANTIBIOTIC PHARMACODYNAMICS*, Methods in Pharmacology and Toxicology, pages 89–108. 2016. ISBN 978-1-4939-3323-5; 978-1-4939-3321-1. doi: 10.1007/978-1-4939-3323-5_4.

K. C. Bulusu, R. Guha, D. J. Mason, R. P. I. Lewis, E. Muratov, Y. Kalantar Motamedi, M. Cokol, and A. Bender. Modelling of compound combination effects and applications to efficacy and toxicity: state-of-the-art, challenges and perspectives. *Drug discovery today*, 21(2):225–238, sep 2015. doi: 10.1016/j.drudis.2015.09.003.

E. Chantzi, M. Jarvius, M. Niklasson, A. Segerman, and M. G. Gustafsson. COMBImage: a modular parallel processing framework for pairwise drug combination analysis that quantifies temporal changes in label-free video microscopy movies. *BMC Bioinformatics*, 19(1):453, dec 2018. doi: 10.1186/s12859-018-2458-x.

E. Chantzi, M. Jarvius, M. Niklasson, A. Segerman, and M. G. Gustafsson. COMBImage2: a parallel computational framework for higher-order drug combination analysis that includes automated plate design, matched filter based object counting and temporal data mining. *BMC Bioinformatics*, 20(1):304, dec 2019. doi: 10.1186/s12859-019-2908-0.

T.-C. Chou. Drug Combination Studies and Their Synergy Quantification Using the Chou-Talalay Method. *Cancer Research*, 70(2):440–446, jan 2010. doi: 10.1158/0008-5472.CAN-09-1947.

T. C. Chou and P. Talalay. Generalized equations for the analysis of inhibitions of Michaelis-Menten and higher-order kinetic systems with two or more mutually exclusive and nonexclusive inhibitors. *European journal of biochemistry*, 115(1):207–16, mar 1981.

T. C. Chou and P. Talalay. Quantitative analysis of dose-effect relationships: the combined effects of multiple drugs or enzyme inhibitors. *Advances in enzyme regulation*, 22:27–55, 1984.

T.-C. T.-C. T.-C. Chou, P. Talalay, M. Bowie, T.-C. T.-C. T.-C. Chou, J. Budinger, K. Watanabe, J. Fox, and F. Philips. Analysis of combined drug effects: a new look at a very old problem. *Trends in Pharmacological Sciences*, 4:450–454, jan 1983. doi: 10.1016/0165-6147(83)90490-X.

M. Cokol, H. N. Chua, M. Tasan, B. Mutlu, Z. B. Weinstein, Y. Suzuki, M. E. Nergiz, M. Costanzo, A. Baryshnikova, G. Giaever, C. Nislow, C. L. Myers, B. J. Andrews, C. Boone, and F. P. Roth. Systematic exploration of synergistic drug pairs. *Molecular systems biology*, 7(1):544, nov 2011. doi: 10.1038/msb.2011.71.

M. Cokol, N. Kuru, E. Bicak, J. Larkins-Ford, and B. B. Aldridge. Efficient measurement and factorization of high-order drug interactions in Mycobacterium tuberculosis. *Science Advances*, 3(10):e1701881, oct 2017. doi: 10.1126/sciadv.1701881.

M. Cokol-Cakmak, F. Bakan, S. Cetiner, and M. Cokol. Diagonal Method to Measure Synergy Among Any Number of Drugs. *JOVE-JOURNAL OF VISUALIZED EXPERIMENTS*, (136), jun 2018. doi: 10.3791/57713.

Z. Dean, J. Maltas, and K. B. Wood. Antibiotic interactions shape short-term evolution of resistance in E. faecalis. *bioRxiv*, page 641217, may 2019. doi: 10.1101/641217.

K. der Borght, A. Tourny, R. Bagdziunas, O. Thas, M. Nazarov, H. Turner, B. Verbist, and H. Ceulemans. BIGL: Biochemically Intuitive Generalized Loewe null model for prediction of the expected combined effect compatible with partial agonism and antagonism. *SCIENTIFIC REPORTS*, 7, dec 2017. doi: 10.1038/s41598-017-18068-5.

G. Y. Di Veroli, C. Fornari, I. Goldlust, G. Mills, S. B. Koh, J. L. Bramhall, F. M. Richards, and D. I. Jodrell. An automated fitting procedure and software for dose-response curves with multiphasic features. *Scientific Reports*, 5(1):14701, dec 2015. doi: 10.1038/srep14701.

G. Y. Di Veroli, C. Fornari, D. Wang, S. Mollard, J. L. Bramhall, F. M. Richards, and D. I. Jodrell. Combenefit: an interactive platform for the analysis and visualization of drug combinations. *BIOINFORMATICS*, 32(18):2866–2868, sep 2016. doi: 10.1093/bioinformatics/btw230.

J. R. Dry, M. Yang, and J. Saez-Rodriguez. No Title. 8(1):125, dec 2016. doi: 10.1186/s13073-016-0379-8.

F. Eduati, V. Doldàn-Martelli, B. Klinger, T. Cokelaer, A. Sieber, F. Kogera, M. Dorel, M. J. Garnett, N. Blüthgen, and J. Saez-Rodriguez. Drug Resistance Mechanisms in Colorectal Cancer Dissected with Cell Type-Specific Dynamic Logic Models. *Cancer research*, 77(12):3364–3375, jun 2017. doi: 10.1158/0008-5472.CAN-17-0078.

Z. Eroglu and A. Ribas. Combination therapy with BRAF and MEK inhibitors for melanoma: latest evidence and place in therapy. *Therapeutic advances in medical oncology*, 8(1):48–56, jan 2016. doi: 10.1177/1758834015616934.

M. Fallahi-Sichani, S. Honarnejad, L. M. Heiser, J. W. Gray, and P. K. Sorger. Metrics other than potency reveal systematic variation in responses to cancer drugs. *Nature Chemical Biology*, 9 (11):708–714, sep 2013. doi: 10.1038/nchembio.1337.

H.-B. Fang, X. Chen, X.-Y. Pei, S. Grant, and M. Tan. Experimental design and statistical analysis for three-drug combination studies. *Statistical Methods in Medical Research*, 26(3):1261–1280, jun 2017. doi: 10.1177/0962280215574320.

Å. Flobak, M. Vazquez, A. Lægreid, and A. Valencia. CImbinator: a web-based tool for drug synergy analysis in small- and large-scale datasets. *Bioinformatics*, 33(15):2410–2412, aug 2017. doi: 10.1093/bioinformatics/btx161.

J. Foucquier and M. Guedj. Analysis of drug combinations: current methodological landscape. *Pharmacology research & perspectives*, 3(3):e00149, jun 2015. doi: 10.1002/prp2.149.

J. H. Gaddum. *Pharmacology*. Oxford University Press, London, 1940.

N. Geary. Understanding synergy. *AJP: Endocrinology and Metabolism*, 304(3):E237–E253, feb 2013. doi: 10.1152/ajpendo.00308.2012.

C. Gilvary, J. R. Dry, and O. Elemento. Multi-task learning predicts drug combination synergy in cells and in the clinic. *bioRxiv*, page 576017, mar 2019. doi: 10.1101/576017.

Z. Gong, G. Hu, Q. Li, Z. Liu, F. Wang, X. Zhang, J. Xiong, P. Li, Y. Xu, R. Ma, S. Chen, and J. Li. Compound Libraries: Recent Advances and Their Applications in Drug Discovery. *Current Drug Discovery Technologies*, 14(4):216–228, oct 2017. doi: 10.2174/1570163814666170425155154.

W. Greco, H.-D. Unkelbach, G. Poch, J. Suhnel, M. Kundi, W. Bodeker, M. Kunki, and W. Bodeker. Consensus on Concepts and Terminology for Combined-action Assessment: The Saariselka Agreement. *Archives of Complex Environmental Studies*, 4(3):65–69, 1992.

W. R. Greco, G. Bravo, and J. C. Parsons. The search for synergy: a critical review from a response surface perspective. *Pharmacological reviews*, 47(2):331–85, jun 1995.

V. Gupta and N. M. Dixit. Trade-off between synergy and efficacy in combinations of HIV-1

latency-reversing agents. *PLoS computational biology*, 14(2):e1006004, 2018. doi: 10.1371/journal.pcbi.1006004.

M. Hafner, M. Niepel, M. Chung, and P. K. Sorger. Growth rate inhibition metrics correct for confounders in measuring sensitivity to cancer drugs. *Nature Methods*, 13(6):521–527, may 2016. doi: 10.1038/nmeth.3853.

K. Han, E. E. Jeng, G. T. Hess, D. W. Morgens, A. Li, and M. C. Bassik. Synergistic drug combinations for cancer identified in a CRISPR screen for pairwise genetic interactions. *Nature Biotechnology*, 35(5):463–474, mar 2017. doi: 10.1038/nbt.3834.

K. N. Hardeman, C. Peng, B. B. Paudel, C. T. Meyer, T. Luong, D. R. Tyson, J. D. Young, V. Quaranta, and J. P. Fessel. Dependence On Glycolysis Sensitizes BRAF-mutated Melanomas For Increased Response To Targeted BRAF Inhibition. *Scientific reports*, 7:42604, feb 2017. doi: 10.1038/srep42604.

L. A. Harris, P. L. Frick, S. P. Garbett, K. N. Hardeman, B. B. Paudel, C. F. Lopez, V. Quaranta, and D. R. Tyson. An unbiased metric of antiproliferative drug effect in vitro. *Nature Methods*, 13(6):497–500, may 2016. doi: 10.1038/nmeth.3852.

B. He, C. Lu, G. Zheng, X. He, M. Wang, G. Chen, G. Zhang, and A. Lu. Combination therapeutics in complex diseases. *Journal of cellular and molecular medicine*, 20(12):2231–2240, 2016. doi: 10.1111/jcmm.12930.

L. He, E. Kulesskiy, J. Saarela, L. Turunen, K. Wennerberg, T. Aittokallio, and J. Tang. Methods for High-throughput Drug Combination Screening and Synergy Scoring. *Methods in molecular biology (Clifton, N.J.)*, 1711:351–398, 2018. doi: 10.1007/978-1-4939-7493-1_17.

S. J. Heidorn, C. Milagre, S. Whittaker, A. Nourry, I. Niculescu-Duvas, N. Dhomen, J. Hussain, J. S. Reis-Filho, C. J. Springer, C. Pritchard, and R. Marais. Kinase-Dead BRAF and Oncogenic RAS Cooperate to Drive Tumor Progression through CRAF. *Cell*, 140(2):209–221, jan 2010. doi: 10.1016/j.cell.2009.12.040.

T. Horn, S. Ferretti, N. Ebel, A. Tam, S. Ho, F. Harbinski, A. Farsidjani, M. Zubrowski, W. R. Sellers, R. Schlegel, D. Porter, E. Morris, J. Wuerthner, S. Jeay, J. Greshock, E. Halilovic, L. A. Garraway, G. Caponigro, and J. Lehár. High-Order Drug Combinations Are Required to Effectively Kill Colorectal Cancer Cells. *Cancer Research*, 76(23):6950–6963, dec 2016. doi: 10.1158/0008-5472.CAN-15-3425.

H. Huang, H.-B. Fang, and M. T. Tan. Experimental design for multi-drug combination studies using signaling networks. *Biometrics*, 74(2):538–547, 2018. doi: 10.1111/biom.12777.

J. D. Hunter. Matplotlib: A 2D Graphics Environment. *Computing in Science & Engineering*, 9 (3):90–95, 2007. doi: 10.1109/MCSE.2007.55.

A. Ianevski, L. He, T. Aittokallio, and J. Tang. SynergyFinder: a web application for analyzing drug combination dose–response matrix data. *Bioinformatics*, 33(15):2413–2415, aug 2017. doi: 10.1093/bioinformatics/btx162.

J. Jabs, F. M. Zickgraf, J. Park, S. Wagner, X. Jiang, K. Jechow, K. Kleinheinz, U. H. Toprak, M. A. Schneider, M. Meister, S. Spaich, M. Sütterlin, M. Schlesner, A. Trumpp, M. Sprick, R. Eils, and C. Conrad. Screening drug effects in patient-derived cancer cells links organoid responses to genome alterations. *Molecular Systems Biology*, 13(11):955, nov 2017. doi: 10.15252/msb.20177697.

M. Jafarnejad, R. J. Sové, L. Danilova, A. C. Mirando, Y. Zhang, M. Yarchoan, P. T. Tran, N. B. Pandey, E. J. Fertig, and A. S. Popel. Mechanistically detailed systems biology modeling of the HGF/Met pathway in hepatocellular carcinoma. *npj Systems Biology and Applications*, 5(1):29, dec 2019. doi: 10.1038/s41540-019-0107-2.

V. Jaquet, J. Marcoux, E. Forest, K. G. Leidal, S. McCormick, Y. Westermaier, R. Perozzo, O. Plastre, L. Fioraso-Cartier, B. Diebold, L. Scapozza, W. M. Nauseef, F. Fieschi, K.-H. Krause, and K. Bedard. NADPH oxidase (NOX) isoforms are inhibited by celastrol with

a dual mode of action. *British journal of pharmacology*, 164(2b):507–20, sep 2011. doi: 10.1111/j.1476-5381.2011.01439.x.

P. Jia, H. Jin, C. B. Meador, J. Xia, K. Ohashi, L. Liu, V. Pirazzoli, K. B. Dahlman, K. Politi, F. Michor, Z. Zhao, and W. Pao. Next-generation sequencing of paired tyrosine kinase inhibitor-sensitive and -resistant EGFR mutant lung cancer cell lines identifies spectrum of DNA changes associated with drug resistance. *Genome research*, 23(9):1434–45, sep 2013. doi: 10.1101/gr.152322.112.

E. O. Johnson, E. LaVerriere, E. Office, M. Stanley, E. Meyer, T. Kawate, J. E. Gomez, R. E. Audette, N. Bandyopadhyay, N. Betancourt, K. Delano, I. Da Silva, J. Davis, C. Gallo, M. Gardner, A. J. Golas, K. M. Guinn, S. Kennedy, R. Korn, J. A. McConnell, C. E. Moss, K. C. Murphy, R. M. Nietupski, K. G. Papavinasasundaram, J. T. Pinkham, P. A. Pino, M. K. Proulx, N. Ruecker, N. Song, M. Thompson, C. Trujillo, S. Wakabayashi, J. B. Wallach, C. Watson, T. R. Ioerger, E. S. Lander, B. K. Hubbard, M. H. Serrano-Wu, S. Ehrt, M. Fitzgerald, E. J. Rubin, C. M. Sassetti, D. Schnappinger, and D. T. Hung. Large-scale chemical–genetics yields new M. tuberculosis inhibitor classes. *Nature*, 571(7763):72–78, jul 2019. doi: 10.1038/s41586-019-1315-z.

E. Jones, T. Oliphant, and P. Peterson. SciPy: Open Source Scientific Tools for Python, 2001.

I. Katzir, M. Cokol, B. B. Aldridge, and U. Alon. Prediction of ultra-high-order antibiotic combinations based on pairwise interactions. *PLOS COMPUTATIONAL BIOLOGY*, 15(1), jan 2019. doi: 10.1371/journal.pcbi.1006774.

D. Kim, B. Langmead, and S. L. Salzberg. HISAT: a fast spliced aligner with low memory requirements. *Nature Methods*, 12(4):357–360, apr 2015. doi: 10.1038/nmeth.3317.

A. Kononov, S. Timonen, T. Aittokallio, and A. K. Giri. SynToxProfiler: an approach for top drug combination selection based on integrated profiling of 1 synergy, toxicity and efficacy 2 3 Aleksandr Ianevski. doi: 10.1101/693010. URL http://dx.doi.org/10.1101/693010.

S. Koplev, J. Longden, J. Ferkinghoff-Borg, M. Blicher Bjerregård, T. R. Cox, J. T. Erler, J. T. Pedersen, F. Voellmy, M. O. Sommer, and R. Linding. Dynamic Rearrangement of Cell States Detected by Systematic Screening of Sequential Anticancer Treatments. *Cell Reports*, 20(12): 2784–2791, sep 2017. doi: 10.1016/J.CELREP.2017.08.095.

M. V. Kuleshov, M. R. Jones, A. D. Rouillard, N. F. Fernandez, Q. Duan, Z. Wang, S. Koplev, S. L. Jenkins, K. M. Jagodnik, A. Lachmann, M. G. McDermott, C. D. Monteiro, G. W. Gundersen, and A. Ma'ayan. Enrichr: a comprehensive gene set enrichment analysis web server 2016 update. *Nucleic Acids Research*, 44(W1), jul 2016. doi: 10.1093/nar/gkw377.

E. O. Lebigot. Uncertainties: a Python package for calculations with uncertainties, 2011.

C. Levy, M. Khaled, and D. E. Fisher. MITF: master regulator of melanocyte development and melanoma oncogene. *Trends in Molecular Medicine*, 12(9):406–414, sep 2006. doi: 10.1016/j.molmed.2006.07.008.

Y. Liao, G. K. Smyth, and W. Shi. featureCounts: an efficient general purpose program for assigning sequence reads to genomic features. *Bioinformatics*, 30(7):923–930, apr 2014. doi: 10.1093/bioinformatics/btt656.

S. Loewe. über Kombination swirkungen. *Arch fur Exp Pathology*, 114:313–326, 1926.

S. Loewe. Versuch einer allgemeinen Pharmakologie der Arznei- kombinationen. *Klinische Wochenschrift*, 6(23):1078–1085, 1927.

G. V. Long, D. Stroyakovskiy, H. Gogas, E. Levchenko, F. de Braud, J. Larkin, C. Garbe, T. Jouary, A. Hauschild, J. J. Grob, V. Chiarion Sileni, C. Lebbe, M. Mandalà, M. Millward, A. Arance, I. Bondarenko, J. B. Haanen, J. Hansson, J. Utikal, V. Ferraresi, N. Kovalenko, P. Mohr, V. Probachai, D. Schadendorf, P. Nathan, C. Robert, A. Ribas, D. J. DeMarini, J. G. Irani, M. Casey, D. Ouellet, A.-M. Martin, N. Le, K. Patel, and K. Flaherty. Combined BRAF and MEK Inhibition versus BRAF Inhibition Alone in Melanoma. *New England Journal of Medicine*, 371(20):1877–1888, nov 2014. doi: 10.1056/NEJMoa1406037.

M. I. Love, W. Huber, and S. Anders. Moderated estimation of fold change and dispersion for RNA-seq data with DESeq2. *Genome biology*, 15(12):550, 2014. doi: 10.1186/s13059-014-0550-8.

W. Lu, Y. Hu, G. Chen, Z. Chen, H. Zhang, F. Wang, L. Feng, H. Pelicano, H. Wang, M. J. Keating, J. Liu, W. McKeehan, H. Wang, Y. Luo, and P. Huang. Novel Role of NOX in Supporting Aerobic Glycolysis in Cancer Cells with Mitochondrial Dysfunction and as a Potential Target for Cancer Therapy. *PLoS Biology*, 10(5):e1001326, may 2012. doi: 10.1371/journal.pbio.1001326.

S. M. Lundberg and S.-I. Lee. A Unified Approach to Interpreting Model Predictions, 2017.

J. Ma, M. K. Yu, S. Fong, K. Ono, E. Sage, B. Demchak, R. Sharan, and T. Ideker. Using deep learning to model the hierarchical structure and function of a cell. *Nature Methods*, 15(4):290–298, apr 2018. doi: 10.1038/nmeth.4627.

J. Maltas and K. B. Wood. Pervasive and diverse collateral sensitivity profiles inform optimal strategies to limit antibiotic resistance. *bioRxiv*, page 241075, jan 2018. doi: 10.1101/241075.

A. Malyutina, M. M. Majumder, W. Wang, A. Pessia, C. A. Heckman, and J. Tang. Drug combination sensitivity scoring facilitates the discovery of synergistic and efficacious drug combinations in cancer. *PLOS Computational Biology*, 15(5):e1006752, may 2019. doi: 10.1371/journal.pcbi.1006752.

W. McKinney. Data Structures for Statistical Computing in Python, 2010.

M. P. Menden, D. Wang, M. J. Mason, B. Szalai, K. C. Bulusu, Y. Guan, T. Yu, J. Kang, M. Jeon, R. Wolfinger, T. Nguyen, M. Zaslavskiy, I. S. Jang, Z. Ghazoui, M. E. Ahsen, R. Vogel, E. C. Neto, T. Norman, E. K. Y. Tang, M. J. Garnett, G. Y. D. Veroli, S. Fawell, G. Stolovitzky, J. Guinney, J. R. Dry, and J. Saez-Rodriguez. Community assessment to advance computational prediction of cancer drug combinations in a pharmacogenomic screen. *Nature Communications*, 10(1):2674, dec 2019. doi: 10.1038/s41467-019-09799-2.

B. T. Mott, R. T. Eastman, R. Guha, K. S. Sherlach, A. Siriwardana, P. Shinn, C. McKnight, S. Michael, N. Lacerda-Queiroz, P. R. Patel, P. Khine, H. Sun, M. Kasbekar, N. Aghdam, S. D. Fontaine, D. Liu, T. Mierzwa, L. A. Mathews-Griner, M. Ferrer, A. R. Renslo, J. Inglese, J. Yuan, P. D. Roepe, X.-z. Su, and C. J. Thomas. High-throughput matrix screening identifies synergistic and antagonistic antimalarial drug combinations. *Scientific Reports*, 5(1):13891, nov 2015. doi: 10.1038/srep13891.

H. Motulsky and A. Christopoulos. *Fitting Models to Biological Data using Linear and Nonlinear Regression A practical guide to curve fitting Contents at a Glance*. GraphPad Software Inc., San Diego, 2003.

A. J. Muinonen-Martin, O. Susanto, Q. Zhang, E. Smethurst, W. J. Faller, D. M. Veltman, G. Kalna, C. Lindsay, D. C. Bennett, O. J. Sansom, R. Herd, R. Jones, L. M. Machesky, M. J. O. Wakelam, D. A. Knecht, and R. H. Insall. Melanoma Cells Break Down LPA to Establish Local Gradients That Drive Chemotactic Dispersal. *PLoS Biology*, 12(10):e1001966, oct 2014. doi: 10.1371/journal.pbio.1001966.

S. Nelander, W. Wang, B. Nilsson, Q.-B. She, C. Pratilas, N. Rosen, P. Gennemark, and C. Sander. Models from experiments: combinatorial drug perturbations of cancer cells. *Molecular systems biology*, 4:216, 2008. doi: 10.1038/msb.2008.53.

R. J. Nichols, S. Sen, Y. J. Choo, P. Beltrao, M. Zietek, R. Chaba, S. Lee, K. M. Kazmierczak, K. J. Lee, A. Wong, M. Shales, S. Lovett, M. E. Winkler, N. J. Krogan, A. Typas, and C. A. Gross. Phenotypic Landscape of a Bacterial Cell. *CELL*, 144(1):143–156, jan 2011. doi: 10.1016/j.cell.2010.11.052.

M. Niepel, M. Hafner, Q. Duan, Z. Wang, E. O. Paull, M. Chung, X. Lu, J. M. Stuart, T. R. Golub, A. Subramanian, A. Ma'ayan, and P. K. Sorger. Common and cell-type specific responses to anti-cancer drugs revealed by high throughput transcript profiling. *Nature Communications*, 8 (1):1186, dec 2017. doi: 10.1038/s41467-017-01383-w.

M. Niepel, M. Hafner, C. E. Mills, K. Subramanian, E. H. Williams, M. Chung, B. Gaudio, A. M. Barrette, A. D. Stern, B. Hu, J. E. Korkola, C. E. Shamu, G. Jayaraman, E. U. Azeloglu, R. Iyengar, E. A. Sobie, G. B. Mills, T. Liby, J. D. Jaffe, M. Alimova, D. Davison, X. Lu, T. R. Golub, A. Subramanian, B. Shelley, C. N. Svendsen, A. Ma'ayan, M. Medvedovic, J. W. Gray, M. R. Birtwistle, L. M. Heiser, and P. K. Sorger. A Multi-center Study on the Reproducibility of Drug-Response Assays in Mammalian Cell Lines. *Cell Systems*, jul 2019. doi: 10.1016/J.CELS.2019.06.005.

T. E. Oliphant. Guide to NumPy. 2006.

J. O'Neil, Y. Benita, I. Feldman, M. Chenard, B. Roberts, Y. Liu, J. Li, A. Kral, S. Lejnine, A. Loboda, W. Arthur, R. Cristescu, B. B. Haines, C. Winter, T. Zhang, A. Bloecher, and S. D. Shumway. An Unbiased Oncology Compound Screen to Identify Novel Combination Strategies. *Molecular Cancer Therapeutics*, 15(6):1155–1162, jun 2016. doi: 10.1158/1535-7163.MCT-15-0843.

A. C. Palmer and P. K. Sorger. Combination Cancer Therapy Can Confer Benefit via Patient-to-Patient Variability without Drug Additivity or Synergy Theory Combination Cancer Therapy Can Confer Benefit via Patient-to-Patient Variability without Drug Additivity or Synergy. *Cell*, 171, 2017. doi: 10.1016/j.cell.2017.11.009.

T. J. Parmenter, M. Kleinschmidt, K. M. Kinross, S. T. Bond, J. Li, M. R. Kaadige, A. Rao, K. E. Sheppard, W. Hugo, G. M. Pupo, R. B. Pearson, S. L. McGee, G. V. Long, R. A. Scolyer, H. Rizos, R. S. Lo, C. Cullinane, D. E. Ayer, A. Ribas, R. W. Johnstone, R. J. Hicks, and G. A. McArthur. Response of BRAF-mutant melanoma to BRAF inhibition is mediated by a network of transcriptional regulators of glycolysis. *Cancer discovery*, 4(4):423–33, apr 2014. doi: 10.1158/2159-8290.CD-13-0440.

B. P. B. Paudel, L. A. Harris, K. N. Hardeman, A. A. Abugable, C. E. Hayford, D. R. Tyson,

and V. Quaranta. A Nonquiescent "Idling" Population State in Drug-Treated, BRAF-Mutated Melanoma. *Biophysical Journal*, 114(6):1499–1511, mar 2018.

K. Preuer, R. P. I. Lewis, S. Hochreiter, A. Bender, K. C. Bulusu, and G. Klambauer. DeepSynergy: predicting anti-cancer drug synergy with Deep Learning. *Bioinformatics*, 34(9):1538–1546, may 2018. doi: 10.1093/bioinformatics/btx806.

D. Russ and R. Kishony. Additivity of inhibitory effects in multidrug combinations. *NATURE MICROBIOLOGY*, 3(12):1339–1345, dec 2018. doi: 10.1038/s41564-018-0252-1.

J. Salvatier, T. V. Wiecki, and C. Fonnesbeck. Probabilistic programming in Python using PyMC3. *PeerJ Computer Science*, 2:e55, apr 2016. doi: 10.7717/peerj-cs.55.

M. Santolini and A.-L. Barabási. Predicting perturbation patterns from the topology of biological networks. *Proceedings of the National Academy of Sciences of the United States of America*, 115(27):E6375–E6383, jul 2018. doi: 10.1073/pnas.1720589115.

I. Schiffmann, G. Greve, M. Jung, and M. Lübbert. Epigenetic therapy approaches in non-small cell lung cancer: Update and perspectives. *Epigenetics*, 11(12):858–870, dec 2016. doi: 10.1080/15592294.2016.1237345.

M. Schindler. Theory of synergistic effects: Hill-type response surfaces as 'null-interaction' models for mixtures. *Theoretical Biology and Medical Modelling*, 14(1):15, dec 2017. doi: 10.1186/s12976-017-0060-y.

P. Sen, A. Saha, and N. M. Dixit. You Cannot Have Your Synergy and Efficacy Too. *Trends in pharmacological sciences*, 0(0), oct 2019. doi: 10.1016/j.tips.2019.08.008.

A. T. Shaw, D.-W. Kim, R. Mehra, D. S. Tan, E. Felip, L. Q. Chow, D. R. Camidge, J. Vansteenkiste, S. Sharma, T. De Pas, G. J. Riely, B. J. Solomon, J. Wolf, M. Thomas, M. Schuler, G. Liu, A. Santoro, Y. Y. Lau, M. Goldwasser, A. L. Boral, and J. A. Engelman.

Ceritinib in ALK -Rearranged Non–Small-Cell Lung Cancer. *New England Journal of Medicine*, 370(13):1189–1197, mar 2014. doi: 10.1056/NEJMoa1311107.

Y. Shimoyama, A. Nagafuchi, S. Fujita, M. Gotoh, M. Takeichi, S. Tsukita, and S. Hirohashi. Cadherin dysfunction in a human cancer cell line: possible involvement of loss of alpha-catenin expression in reduced cell-cell adhesiveness. *Cancer research*, 52(20):5770–4, oct 1992.

M. Sinzger, J. Vanhoefer, C. Loos, and J. Hasenauer. Comparison of null models for combination drug therapy reveals Hand model as biochemically most plausible. *Scientific Reports*, 9(1):3002, dec 2019. doi: 10.1038/s41598-019-38907-x.

J.-C. Soria, Y. Ohe, J. Vansteenkiste, T. Reungwetwattana, B. Chewaskulyong, K. H. Lee, A. Dechaphunkul, F. Imamura, N. Nogami, T. Kurata, I. Okamoto, C. Zhou, B. C. Cho, Y. Cheng, E. K. Cho, P. J. Voon, D. Planchard, W.-C. Su, J. E. Gray, S.-M. Lee, R. Hodge, M. Marotti, Y. Rukazenkov, S. S. Ramalingam, and FLAURA Investigators. Osimertinib in Untreated EGFR -Mutated Advanced Non–Small-Cell Lung Cancer. *New England Journal of Medicine*, 378(2):113–125, jan 2018. doi: 10.1056/NEJMoa1713137.

A. Subramanian, R. Narayan, S. M. Corsello, D. D. Peck, T. E. Natoli, X. Lu, J. Gould, J. F. Davis, A. A. Tubelli, J. K. Asiedu, D. L. Lahr, J. E. Hirschman, Z. Liu, M. Donahue, B. Julian, M. Khan, D. Wadden, I. C. Smith, D. Lam, A. Liberzon, C. Toder, M. Bagul, M. Orzechowski, O. M. Enache, F. Piccioni, S. A. Johnson, N. J. Lyons, A. H. Berger, A. F. Shamji, A. N. Brooks, A. Vrcic, C. Flynn, J. Rosains, D. Y. Takeda, R. Hu, D. Davison, J. Lamb, K. Ardlie, L. Hogstrom, P. Greenside, N. S. Gray, P. A. Clemons, S. Silver, X. X. Wu, W.-N. Zhao, W. Read-Button, X. X. Wu, S. J. Haggarty, L. V. Ronco, J. S. Boehm, S. L. Schreiber, J. G. Doench, J. A. Bittker, D. E. Root, B. Wong, and T. R. Golub. A Next Generation Connectivity Map: L1000 Platform and the First 1,000,000 Profiles. *Cell*, 171(6):1437–1452.e17, nov 2017. doi: 10.1016/j.cell.2017.10.049.

R. J. Tallarida. Drug synergism: its detection and applications. *The Journal of pharmacology and experimental therapeutics*, 298(3):865–72, sep 2001.

R. J. Tallarida. Quantitative methods for assessing drug synergism. *Genes & cancer*, 2(11):1003–8, nov 2011. doi: 10.1177/1947601912440575.

J. Tang. Informatics Approaches for Predicting, Understanding, and Testing Cancer Drug Combinations. In *Methods in molecular biology (Clifton, N.J.)*, volume 1636, pages 485–506. 2017. doi: 10.1007/978-1-4939-7154-1_30.

J. Tang, K. Wennerberg, and T. Aittokallio. What is synergy? The Saariselkä agreement revisited. *Frontiers in pharmacology*, 6:181, 2015. doi: 10.3389/fphar.2015.00181.

J. Tang, P. Gautam, A. Gupta, L. He, S. Timonen, Y. Akimov, W. Wang, A. Szwajda, A. Jaiswal, D. Turei, B. Yadav, M. Kankainen, J. Saarela, J. Saez-Rodriguez, K. Wennerberg, and T. Aittokallio. Network pharmacology modeling identifies synergistic Aurora B and ZAK interaction in triple-negative breast cancer. *npj Systems Biology and Applications*, 5(1):20, dec 2019. doi: 10.1038/s41540-019-0098-z.

O. Tange. GNU Parallel: The Command-Line Power Tool. *;login;*, 36(1):42–47, 2011.

E. Tekin, V. M. Savage, and P. J. Yeh. Measuring higher-order drug interactions: A review of recent approaches. *Current Opinion in Systems Biology*, 4:16–23, aug 2017. doi: 10.1016/J.COISB.2017.05.015.

E. Tekin, C. White, T. M. Kang, N. Singh, M. Cruz-Loya, R. Damoiseaux, V. M. Savage, and P. J. Yeh. Prevalence and patterns of higher-order drug interactions in Escherichia coli. *npj Systems Biology and Applications*, 4(1):31, dec 2018. doi: 10.1038/s41540-018-0069-9.

A. Tendler, A. Zimmer, A. Mayo, and U. Alon. Noise-precision tradeoff in predicting combinations of mutations and drugs. *PLOS COMPUTATIONAL BIOLOGY*, 15(5), may 2019. doi: 10.1371/journal.pcbi.1006956.

Z.-B. Tong, R. Huang, Y. Wang, C. A. Klumpp-Thomas, J. C. Braisted, Z. Itkin, P. Shinn, M. Xia, A. Simeonov, and D. L. Gerhold. The Toxmatrix: Chemo-Genomic Profiling Identifies Interactions That Reveal Mechanisms of Toxicity. *Chemical Research in Toxicology*, 31(2):127–136, feb 2018. doi: 10.1021/acs.chemrestox.7b00290.

N. R. Twarog, E. Stewart, C. V. Hammill, and A. A. Shelat. BRAID: A Unifying Paradigm for the Analysis of Combined Drug Action. *Scientific Reports*, 6(1):25523, jul 2016. doi: 10.1038/srep25523.

S. van der Walt, J. L. Schönberger, J. Nunez-Iglesias, F. Boulogne, J. D. Warner, N. Yager, E. Gouillart, and T. Yu. scikit-image: image processing in Python. *PeerJ*, 2:e453, jun 2014. doi: 10.7717/peerj.453.

A. H. Vlot, N. Aniceto, M. P. Menden, G. Ulrich-Merzenich, and A. Bender. Applying synergy metrics to combination screening data: agreements, disagreements and pitfalls. *Drug Discovery Today*, sep 2019. doi: 10.1016/J.DRUDIS.2019.09.002.

H. Wang, N. Kubica, L. W. Ellisen, L. S. Jefferson, and S. R. Kimball. Dexamethasone represses signaling through the mammalian target of rapamycin in muscle cells by enhancing expression of REDD1. *The Journal of biological chemistry*, 281(51):39128–34, dec 2006. doi: 10.1074/jbc.M610023200.

J. L. Webb. *Enzyme and metabolic inhibitors*. Ney York, Academic Press, 1963.

J. N. Weiss'. The Hill equation revisited: uses and misuses. Technical report. URL https://pdfs.semanticscholar.org/e3c7/47d79dae8f346754852a64e5d28c18ad2cf0.pdf.

S. G. Wicha, C. Chen, O. Clewe, and U. S. H. Simonsson. A general pharmacodynamic interaction model identifies perpetrators and victims in drug interactions. *Nature Communications*, 8(1):2129, dec 2017. doi: 10.1038/s41467-017-01929-y.

G. E. Winter, D. L. Buckley, J. Paulk, J. M. Roberts, A. Souza, S. Dhe-Paganon, and J. E. Bradner. DRUG DEVELOPMENT. Phthalimide conjugation as a strategy for in vivo target protein degradation. *Science (New York, N.Y.)*, 348(6241):1376–81, jun 2015. doi: 10.1126/science.aab1433.

S. E. Witta, R. M. Gemmill, F. R. Hirsch, C. D. Coldren, K. Hedman, L. Ravdel, B. Helfrich, R. Dziadziuszko, D. C. Chan, M. Sugita, Z. Chan, A. Baron, W. Franklin, H. A. Drabkin, L. Girard, A. F. Gazdar, J. D. Minna, and P. A. Bunn. Restoring E-Cadherin Expression Increases Sensitivity to Epidermal Growth Factor Receptor Inhibitors in Lung Cancer Cell Lines. *Cancer Research*, 66(2):944–950, jan 2006. doi: 10.1158/0008-5472.CAN-05-1988.

S. E. Witta, R. M. Jotte, K. Konduri, M. A. Neubauer, A. I. Spira, R. L. Ruxer, M. Varella-Garcia, P. A. Bunn, and F. R. Hirsch. Randomized phase II trial of erlotinib with and without entinostat in patients with advanced non-small-cell lung cancer who progressed on prior chemotherapy. *Journal of Clinical Oncology*, 30(18):2248–55, jun 2012. doi: 10.1200/JCO.2011.38.9411.

K. Wood, S. Nishida, E. D. Sontag, and P. Cluzel. Mechanism-independent method for predicting response to multidrug combinations in bacteria. *Proceedings of the National Academy of Sciences of the United States of America*, 109(30):12254–9, jul 2012. doi: 10.1073/pnas.1201281109.

K. K. K. Wood, K. K. K. Wood, S. Nishida, and P. Cluzel. Uncovering Scaling Laws to Infer Multidrug Response of Resistant Microbes and Cancer Cells. *Cell Reports*, 6(6):1073–1084, mar 2014. doi: 10.1016/j.celrep.2014.02.007.

B. Yadav, K. Wennerberg, T. Aittokallio, and J. Tang. Searching for Drug Synergy in Complex Dose–Response Landscapes Using an Interaction Potency Model. *Computational and Structural Biotechnology Journal*, 13:504–513, jan 2015. doi: 10.1016/J.CSBJ.2015.09.001.

B. Zagidullin, J. Aldahdooh, S. Zheng, W. Wang, Y. Wang, J. Saad, A. Malyutina, M. Jafari, Z. Tanoli, A. Pessia, and J. Tang. DrugComb: an integrative cancer drug combination data portal. *Nucleic acids research*, 47(W1):W43–W51, jul 2019. doi: 10.1093/nar/gkz337.

A. Zimmer, I. Katzir, E. Dekel, A. E. Mayo, and U. Alon. Prediction of multidimensional drug dose responses based on measurements of drug pairs. *Proceedings of the National Academy of Sciences of the United States of America*, 113(37):10442–7, sep 2016. doi: 10.1073/pnas.1606301113.

A. Zimmer, A. Tendler, I. Katzir, A. Mayo, and U. Alon. Prediction of drug cocktail effects when the number of measurements is limited. *PLOS BIOLOGY*, 15(10), oct 2017. doi: 10.1371/journal.pbio.2002518.

GLOSSARY

- **Cooperativity:** Also known as the Hill slope, this is a measure of the steepness of the dose-response curve (Figure 1.2).
- **Curse of dimensionality:** The name given to a large class of problems arising from the combinatorial expansion of considering higher dimensions.
- **CyTOF:** Mass Cytometry uses heavy-metal tagged antibodies to quantify single-cell expression of up to 50 target proteins.
- **Dose-response curve:** To assay drug effect, drugs are commonly titrated across several concentrations and the resulting effect measured. Commonly the dose-response is sigmoidal well fit by a Hill equation.
- **Dose-response surface:** The measured effect of a combination of two drugs over a range of different concentrations. Commonly plotted as either a heatmap (*e.g.* Figure 1.6) or 3D surface plot (Figure 2.1) where the X-Y axes are drug concentration and the color or Z-axis is the measured effect, respectively.
- **Efficacy** The degree to which a drug can produce a beneficial effect. Classically quantified as the maximal effect (E_{max}) (Figure 1.2).
- **Higher-order combinations:** Combinations of three or more drugs.
- **Isobols:** Contours of equal effect. For all pairs of drug 1 and drug 2 concentrations along an isobol, the resulting effect (e.g. percent of viable cells) is the same.
- **Mutually Exclusive:** Two inhibitors are mutually exclusive if binding to one precludes the binding of the other.
- **Parametric equations:** Equations with parameters which are fit to the data. An example is the Hill equation (Figure 1.2) which varies E0, Em, h, and C to fit dose-response data. An

example of a non-parametric equation is the Bliss equation (U12=U1*U2) as there are no values to fit.

- **Percent Affect vs. Percent Effect:** For historical reasons, these are often used interchangeably, but they are fundamentally different. Affect measures whether there is a discrete change in phenotype (live vs. dead). The percent of affected cells, eggs, etc. can never exceed 100%. Percent effect is the relative change compared to control and is commonly measured in phenotypic assays. In contrast to percent affect, it can exceed 100% (Figure 1.2).

- **Potency:** The concentration of drug required to achieve a particular effect. Commonly quantified by the EC50. the drug concentration is required to achieve a half-maximal effect (Figure 1.2).

- **Sham Experiment:** A thought experiment in which a combination of drugs is tested for synergy; however, the combination is actually two of the same drug. The sham principle states no combination should be synergistic with itself. Classically, DEP frameworks are sham compliant while MSP frameworks are not.

- **Synergistic Coopertivity:** The magnitude of change in a drug's Hill slope, due to the presence of another drug (Figure 2.1).

- **Synergistic Efficacy:** The percent change in the maximal efficacy of the combination compared to the most efficacious single agent (Figure 2.1).

- **Synergistic Potency:** The magnitude of the change in the drug potency, due to the presence of another drug (Figure 2.1).

APPENDIX A: Methods for studies in Chapter 2.

Note the analyses conducted were not necessarily the same as those used in the original paper. Indeed the limitations of the current frameworks forced customized analysis for each publication highlighting the need for a consensus framework. Here I describe fitting protocol for drug metrics where the metric of drug effect *decreases* as dose increases ($E_0 > E_3$) *(e.g.*, anti-proliferative drugs); however, the framework is equally valid if increasing the drug corresponds to increases the effect ($E_0 < E_3$) (*e.g.*, percent effect)

A.1 Fitting 2D Hill equation

The following packages were used for fitting, data analysis, or visualization: GNU parallel (Tange, 2011), SciPy (Jones et al., 2001), Numpy (Oliphant, 2006), Pandas (McKinney, 2010), Matplotlib (Hunter, 2007), uncertainties (Lebigot, 2011). Fitting was done using a custom library written in Python2.

For the fitting the 2D Hill equation in this study, I adopted a Monte Carlo sampling approach to calculate the fit parameter uncertainty. This is significantly faster than my previous method (PSO+MCMC) (Appendix B). while maintaining reasonable calculations of the parameter uncertainties accounting for the multi-collinearities described above. The Monte Carlo algorithm for fitting the 2D Hill equation is as follows. First, the 4-parameter 1D Hill equation (eq. 2.3) is fit to the dose-response of each drug in isolation. The fit uses the Trust Region Reflective (TRF) algorithm implemented in the $curve\_fit()$ module of the scipy.optimization package. h and C were unconstrained while E_{max} and E_0 are constrained for each dataset as annotated in the methods section *Data acquisition, preparation, and analysis*. The initial 1D Hill fits provide estimates for $(E_0, E_1, E_2, C_1, C_2, h1, h2)$. Next the 2D Hill equation (eq. 2.8) is fit using the TRF algorithm with initial values based on the 1D Hill equation fits and with bounds based on the parameter uncertainty calculated for the 1D Hill fits. The initial values for parameters unique to the 2D Hill equation, $E_3, \alpha_{21}, \alpha_{12}, \gamma_{12}, \gamma_{21}$ are ($min(E_1, E_2)$,1,1,1,1). For all combinations $r_1 = r_2 = 100$. The bounds

for $\log(\alpha_{21}), \log(\alpha_{12})$ are set to [-4,4]. From this initial fit, 100 Monte Carlo samples are used to calculate the parameter uncertainty as described by Motulsky and Christopoulos (Motulsky and Christopoulos, 2003), (*Chapter 17: Generating confidence intervals by Monte Carlo, pg. 104*). Specifically, noise, with a distribution N(0,σ), where σ is equal to the root mean square (RMS) of the best fit, is added to best-fit values of the 2D Hill equation for all drug doses. The data plus noise is then fit again initializing the optimization from the best fit parameters of the original data. This is done 100 times. From this ensemble of fits, the 95% confidence interval of each parameter can be calculated. This Monte Carlo approach results in asymmetric confidence intervals which better captures the non-Gaussian distribution of uncertainty for many fits (*e.g.* the distribution of h is log-normal) as well as being robust to the co-linear parameters in the 2D Hill equation. The asymmetric confidence interval is particularly salient when the dose-range is insufficient to observe the lower plateau of the dose-response. Only combinations for which $R^2 > 0.7$ and the fitted EC50s of both drugs was less than maximum tested dose for each ($C_1 < max(d1)$,$C_2 < max(d2)$) were included for subsequent analysis.

A.2 Data acquisition, preparation, and analysis

A.2.1 ONeil et al. anti-cancer screen

The anti-cancer drug combination data was downloaded from the supplemental materials of (O'Neil et al., 2016). Single agent and combination datasets were merged. Drug effect was the mean normalized percent viability (X/X_0 column) calculated as detailed in (O'Neil et al., 2016). The minimum and maximum bounds for $[E_0, E_1, E_2, E_3]$ during 2D Hill equation fits were [.99,0.,0.,0.,0.] and [1.01,2.5,2.5,2.5] respectively.

A.2.2 Mott et al. anti-malarial screen

The anti-malarial drug combination data was downloaded from https://tripod.nih.gov/matrix-client/ from the **Malaria Matrix** project. Blocks downloaded for analysis were: [1601,1602,1603,1701,1702,1703,1761,1764]. Only blocks with a *mqcConfidence* of greater than

0.9 were included. The drug effect was calculated as described in (Mott et al., 2015). Effects less than -20% and greater than 120% were removed. The minimum and maximum bounds for $[E_0, E_1, E_2, E_3]$ during 2D Hill equation fits were [90.,0.,0.,0.] and [110,200,200,200] respectively.

A.3 Calculation of other synergy metrics

A.3.1 Bliss, Loewe, and HSA

Bliss, Loewe, and HSA depend on the concentration of drugs so a combination can be synergistic at one dose, but antagonistic at another dose. Several methods have been proposed for extracting a single synergy metric per combination from these frameworks to enable comparisons between combinations (Ianevski et al., 2017; O'Neil et al., 2016; Flobak et al., 2017; He et al., 2018). For our analysis, I calculate the synergy score at the combination of each drug's EC50 (as done in Figures 2.6,2.8,2.9, and 2.14) or at the maximum tested concentration of each drug (Figure 2.11 and 2.10). The EC50 of each drug was calculated from the fits to the 2D Hill equation ((2.8)) which I have observed to be more robust to noise when estimating the single drug pharmacologic profile. Assuming the notation for the 1D Hill equation and inverse Hill equation—which calculate effect (E given a dose (d) and a dose given an effect, respectively—are given by

$$Hx(d) = E_x + \frac{(E_0 - E_x)}{1 + \left(\frac{d_x}{C_x}\right)^h_x} \tag{A.1}$$

$$Hx_{inv}(E) = C_x * \left(\frac{(E_0 - E_x)}{(E - E_x)} - 1\right)^{\frac{1}{h_x}} \tag{A.2}$$

where $E_x < E_0$, then equations for Bliss, Loewe,and HSA at the EC50 are:

$$Bliss = H1(C_1) * H2(C2) \tag{A.3}$$

$$Loewe = \frac{C1}{H1_{inv}(Ed(C_1, C_2))} + \frac{C2}{H2_{inv}(Ed(C_1, C_2))} \tag{A.4}$$

$$HSA = E(C_1, C_2) - min\,(H1(C_1), H2(C_2)) \tag{A.5}$$

where $Ed(C_1,C_2)$ is the measured effect of combining C_1 of d_1 and C_2 of d_2. And equations for Bliss at the max of each drug is:

$$Bliss = H1(max(d_1)) * H2(max(d_2) \tag{A.6}$$

These equations assume the metric of drug effect decreases as the dose increases. Because many single agents did not reach 0% maximum efficacy, the EC50s (C_1,C_2) were not necessarily 50% (Figure 2.12). If $E(C_1,C_2) < E_1,E_2$ then Loewe was undefined. I apply a $-\log_{10}$ transformation the scale Loewe to match the ranges Bliss and HSA are synergistic; therefore, f $-\log_{10}(Loewe) > 0$ the combination is synergistic and if $-\log_{10}(Loewe) < 0$ the combination is antagonistic. Additionally, for Figure 2.6 and Figure 2.14 I had to calculate the Hill-dependent bias in Loewe. For Figure 2.6, I subtracted the Hill slope bias to only study the impact of conflating synergistic potency and efficacy. To calculate the bias, Loewe was calculated as in equation (A.4) where Hx_{inv} was was evaluated at the MuSyC-predicted $Ed(d1,d2)$ for the combination retaining all the single drug parameters ($E_0,E_1,E_2,C_1,C_2,h1,h2$) and assuming ($\alpha_{12} = \alpha_{21} = 0$). This resulted in an estimate of the bias purely due to the Hill slope in the Loewe calculation.

A.3.2 ZIP and BRAID

Both ZIP and BRAID were calculated for each combination using the R packages available for each method: (ZIP's R code is in the supplemental file 1 of the manuscript (Yadav et al., 2015) and BRAID's package is available from:https://cran.r-project.org/web/packages/braidReports/braidReports.pdf).

A.3.3 Effective Dose Model (EDM)

To fit Zimmer et al.'s Effective Dose Model I used the *scipy.optimization.curve_fit* module in Python 2.7. Specifically, the Effective Dose Model, equation 2 in (Zimmer et al., 2016) (eq. (2.20) in Supplement), contains parameters (C_1, C_2, a_{12}, a_{21}, h_1, h_2) where the a parameters are the synergy values. In the model, there are no parameters for efficacy because it is assumed the drug

effect ranges between zero and one. When this is not true, the Effective Dose Model results in poor fits to the data (Figure 2.12).

A.3.4 Schindler's Hill PDE model

The Hill PDE model has no parameters to fit as the dose-response surface is derived the single dose-response curves. In fact, Schindler does not propose a method to estimate synergy from experimental data, but postulates some implementation of perturbation theory could be used to fit experimental data (Schindler, 2017). Therefore, to calculate the synergy of this model, I defined the sum of residuals between the null surface and the experimental data to the metric of synergy.

A.3.5 Combination Index (CI)

Following the CI fitting algorithm in the CompuSyn software, I fit the median-effect equation, a 2-parameter, log-linearized form of the Hill equation obtained by assuming $E_0 = 1$ and $E_1 = 0$ (Chou et al., 1983). C and h were then obtained from the slope and y-intercept of the log-linearized data using the *scipy.stats.linregress* module in Python 2.7. While CI assumes the drug effect is scaled between (0,1), when this is not the case, a poor fit results (Figure 2.12A). All data points with percent viability greater than 1 were excluded from the CI fit because the median-effect equation becomes complex in those cases. For some drugs, this left too few points to fit a line, such that CI was undefined. In other cases, the fitted value for h was less than zero, a physically unrealistic result; therefore, those combinations were also considered undefined. After that, CI was calculated as

$$CI(d_1, d_2) = \frac{d_1}{f_1(E(d_1, d_2))} + \frac{d_2}{f_2(E(d_1, d_2))} \tag{A.7}$$

where $f_i(E)$ is obtained by solving the Hill equation for d, and is given by

$$f_i(E) = \left(\frac{E}{(1-E)}\right)^{\frac{1}{h_i}} C_i \tag{A.8}$$

As with Loewe, I apply a $-\log_{10}$ transformation to scale CI synergy such that $-\log_{10}(CI) > 0$ the combination is synergistic and if $-\log_{10}(CI) < 0$ the combination is antagonistic.

APPENDIX B: Methods for studies in Chapter 3.

B.1 Combination experiments protocol

Experiments were conducted in the Vanderbilt High Throughput Screening Facility. Cells were seeded at approximately 300 cells per well in 384-well plates and allowed to adhere overnight. A preliminary image of each plate was taken approximately 8 hours after seeding to verify sufficient numbers of cells for each experiment. Images were taken on either the ImageXpress Micro XL (Molecular Devices) or CellaVista. The matrix of drug concentrations was prepared using a row-wise and column-wise serial 2X or 4X dilution in 384 well plates using a Bravo Liquid Handling System (Agilent) or manually in 96-well plates. See Table S2 for dose ranges tested. After allowing to adhere overnight, medium containing drugs and 5 nM Sytox Green (to detect dead cells) was added (time = 0) and replaced after 72 hours. Images were obtained at intervals ranging from every 4 to 8 h, depending on the experiment, for $>$120 hours. Cell counts were determined using custom-image segmentation software developed in Python using scikit-image package (van der Walt et al., 2014) and run in parallel using RabbitMQ/Celery (http://www.celeryproject.org/).

B.2 RNA-seq of melanoma cell lines

Total RNA was isolated from untreated SKMEL5 single-cell derived sublines, each in triplicate, using Trizol isolation method (Invitrogen) according to the manufacturer's instructions. RNA samples were submitted to Vanderbilt VANTAGE Core services for quality check, where mRNA enrichment and cDNA library preparation were done with Illumina Tru-Seq stranded mRNA sample prep kit. Sequencing was done at Paired-End 75 bp on the Illumina HiSeq 3000. Reads were aligned to the GRCh38 human reference genome using HISAT2 (Kim et al., 2015) and gene counts were obtained using featureCounts (Liao et al., 2014). All downstream analyses were performed in R (https://www.r-project.org) using the Bioconductor framework (https://www.bioconductor.org)

B.3 RT-qPCR quantification of NOX5 expression

Total RNA was extracted using Trizol isolation method (Invitrogen) according to the manufacturer's instructions. cDNA synthesis was performed with QuantiTect Reverse Transcription Kit (Cat# 205311) from Qiagen. RT-qPCR was performed using the IQTM SYBR Green Supermix from BioRad (Cat# 1708880). Amplifications were performed in BioRad CFX96 TouchTM Real-Time PCR Detection System. All experiments were done at least in 3+ technical replicates. Log2 of the transcript expressions were normalized to SKMEL5 subline SC01. HPRT or 36B4 were used as housekeeping gene in all the experiments. Primers used in RT-qPCR are in Table A.1.

NOX5_Forward Primer	GGCTCAAGTCCTACCACTGGA
NOX5_Reverse Primer	GAACCGTGTACCCAGCCAAT
HPRT_Forward Primer	TGCTCGAGATGTGATGAAGGAG
HPRT_Reverse Primer	TGATGTAATCCAGCAGGTCAGC
36B4_Forward Primer	CATGTTGCTGGCCAATAAGG
36B4_Reverse Primer	TGGTGATACCTAAAGCCTGGAA
PGC1a_Forward Primer	TGCCCTGGATTGTTGACATGA
PGC1a_Reverse Primer	TTTGTCAGGCTGGGGGTAGG

Table A.1: Primers for qRT-PCR

B.4 Fitting Dose-response Surfaces

NOTE:

The algorithm used for fitting the dose response surfaces in Chapter 3, has been replaced with the algorithm described in Appendix A which is faster than the algorithm described below and more consistent in quantifying uncertainty.

I developed a fitting algorithm, implemented in Python, to fit the combinations experiments to the 2D Hill equation. The fitting is done in three steps, first estimates of the single dose-response parameters (C1,C2,h1,h2,E0,E1,E2) are extracted from fits to the single dose-response

curves using the Pythonic implementation of a Levenburg-Marquart (LM) least squares optimization (*scipy.optimize.curve_fit*). The fit uncertainty (σ) is then the square root of the covariance matrix which is approximated as the inverse of the Hessian matrix (equal to JTJ in LM where J is the Jacobian) at the solution. In the second step, a Particle Swarm Optimizer (10,000 particles, 100 iterations) fits the full 2D Hill equation using the single parameter fits and uncertainties as initial values and bounds ($\pm 2\sigma$). In the last step, the PSO optimized values are used to construct priors for a Metropolis-Hastings Monte-Carlo Markov Chain (MCMC) Optimization (Metropolis Hastings 10,000 iterations). Convergence is tested by checking all parameters' Geweke Z-score. If the Z-score range is (-2,2) over the sampling time frame, the optimization is considered to converge (Figure A.2). I found it necessary to use both the PSO and MCMC in order to fit a wide range of dose-response surfaces (Figure A.1).

I found it necessary to use a Metropolis Hastings Monte Carlo (MCMC) seeded with a particle swarm optimization (PSO) to fit the 2D Hill equation. This was prompted by the inconsistent performance of standard non-linear least squares (NLLS) regression. In particular, I observed instances of calculated uncertainties in NLLS which were several orders of magnitude greater than the parameter value. This, I have discovered, is because the multi-collinearity between the Hill slope and the EC50 (C) inherent in the structure of the Hill equation—collinearities which are amplified when extending the Hill equation to 2D. The correlation between variable h and C is easiest to observe in a linearized 1D Hill equation (eq. B.9).

$$log(\frac{E_0 - E_m}{E - E_m} - 1) = h * log(d) - h * log(C) \tag{B.9}$$

In eq. B.9, the intercept of the line ($h * log(C)$) depends on the slope of the line (h). This correlation is problematic when trying to estimate the parameter uncertainty (σ) from NLLS regression because σ is estimated as the square root of the inverse Hessian, approximated to be $J^T J$ (where J

is the Jacobian at the solution). J of the 4 parameter Hill equation is

$$J = \begin{bmatrix} \frac{\partial}{\partial E_0} & \frac{\partial}{\partial E_m} & \frac{\partial}{\partial h} & \frac{\partial}{\partial C} \end{bmatrix} \tag{B.10}$$

$$= \begin{bmatrix} 1 - \frac{1}{\frac{d}{C}^h + 1} & \frac{1}{\frac{d}{C}^h + 1} & -\frac{(E_0 - E_m)\left(\frac{d}{C}\right)^h log\left(\frac{d}{C}\right)}{\left(\left(\frac{d}{C}\right)^h + 1\right)^2} & -\frac{h(E_m - E_0)\left(\frac{d}{C}\right)^h}{C\left(\left(\frac{d}{C}\right)^h + 1\right)^2} \end{bmatrix} \tag{B.11}$$

When the Hill slope is large (*e.g.*, h>5), the second two terms of the J cause the inverse of the Hessian matrix to be undefined. This problem is compounded in the 2D Hill equation where, in addition to h and C, the parameters α and γ are co-linear. However, this does not affect the accuracy of the fitted parameter values from the NLLS regression—only the parameter uncertainty (Motulsky and Christopoulos, 2003).

To test the sensitivity of our fitting algorithm, I generated in silico data for 125 different dose-response surfaces at different data densities. The density of data tested were square matrices of rank 5, 7, 10, 15, and 25. At each density 25 different dose-response surfaces were sampled across a 5X5 grid of log(α) and β values ranging from [-2,2] and from [-0.5,0.5], respectively. The parameters for E0, the single drug hill slope, EC50, and maximal effects were held constant at (0.3, 1, 10e-5, and 0.0), respectively. Random noise equal to the average uncertainty in the DIP Rate fits from the NSCLC screen was added to the data (0.001). In all conditions I observed a PSO particle count of 10,000 converged to a minimum in <60 iterations (Figure A.1A). However, this minimum was not the optimal solution. The addition of an MCMC walk further improved fits (Figure A.1B) (Pymc3 package). The MCMC walk calculates the posterior distribution for each parameter from which each parameter's value (mean of trace) and uncertainty (standard deviation of trace) is calculated. Uncertainty in (E0, E1, E2, and E3) was propagated when calculating β using the equation:

$$\sigma\beta = \sqrt{\left(\left(\frac{E_0 - E_3}{(E_0 - E_x)^2}\sigma E_x\right)^2 + \left(\frac{-\sigma E_3}{E_0 - E_x}\right)^2 \left(\frac{E_3 - E_x}{(E_0 - E_x)^2}\sigma E_0\right)^2\right)^2} \tag{B.12}$$

Where Ex and Ex are min(E1,E2) and respectively. All other uncertainty propagations were

handled with python package uncertainties (Lebigot, 2011). By calculating the uncertainty in the synergy parameters from the posterior distributions, the significance of synergy can be assessed in an unbiased way. Multiple factors contribute to increasing uncertainty in the fitted parameters. Dose-selection, an important consideration in all drug response profiling, changes the certainty of the fits (Figure A.2). While I are unable to observe saturating effects implicit in the model for some of our drug combinations – due to limited solubility or potency of the drug – by keeping careful account of the uncertainty in our synergy calculations I can still interpret the synergy of non-optimal dose-regimes. To demonstrate this, I generated the same 25 dose-response surfaces with varying $\log(\alpha)$ and β values ranging from [-2,2] and from [-0.5,0.5] respectively but at different coverage of the dose-response curve. The uncertainty in the synergy parameters increases for decreased dose range (Figure A.2A). It is important to note that in general the uncertainty is a function of many different aspects other than data density including the hill slope of the single curves (high hill slopes can result in higher uncertainty in $\log(\alpha)$), noise of experimental data, and quality of priors resulting from the single-drug fits. I posit the rigorous approach taken here accounts for all these sources resulting in a true estimate of confidence in a particular synergy value.

To prevent over fitting the data, I have defined six different model tiers which have increasing degrees of freedom (Table A.2). To select the correct model tier, I penalize models with higher degrees of freedom by selecting the model based on minimizing the deviance information criterion (DIC) (Berg et al., 2004). Fits for each nest are used to inform priors for subsequent nests. **Only drug combinations which converged to the full model (tier 5 with fits for all 12 parameters) were used for subsequent analysis.** The MCMC optimization additionally allows for quantification of parameter confidence given the data. The following packages were used for fitting, data analysis, or visualization: GNU parallel (Tange, 2011), SciPy (Jones et al., 2001), Numpy (Oliphant, 2006), Pandas (McKinney, 2010), Matplotlib (Hunter, 2007). Pymc3 (Salvatier et al., 2016).

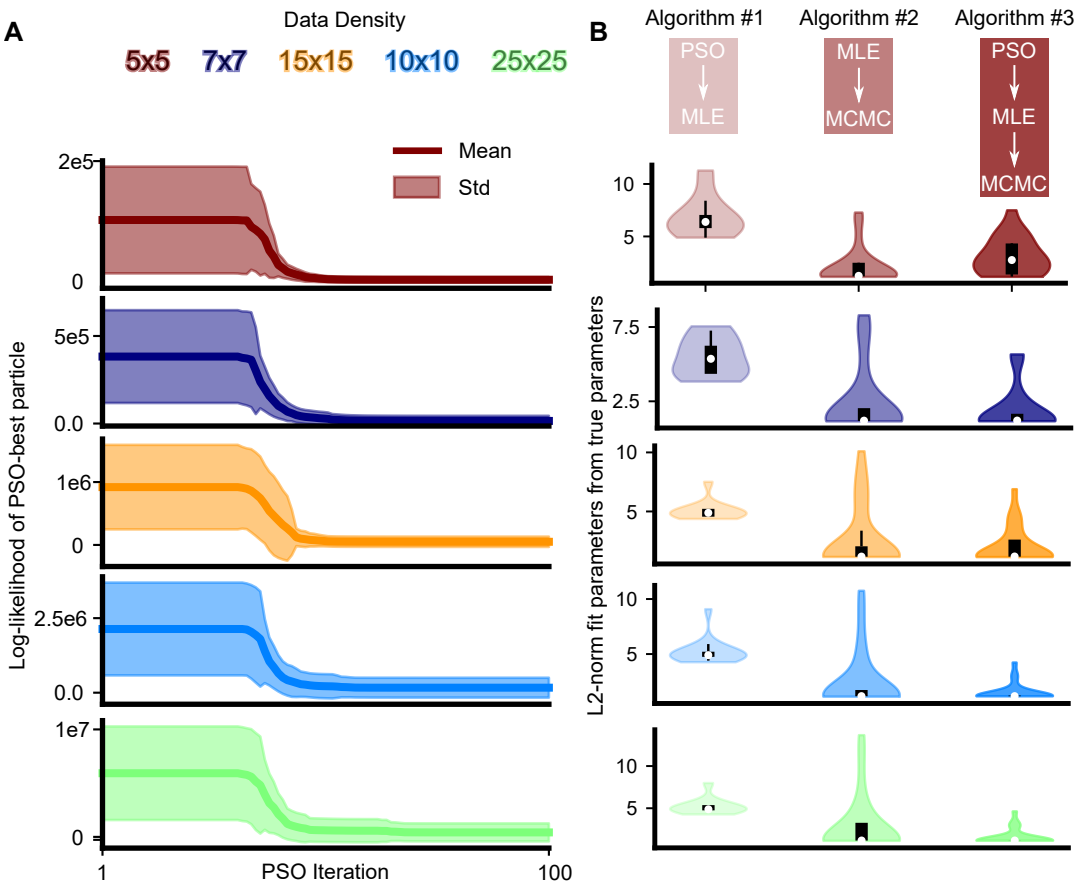

Figure A.1: Bayesian synergy parameter estimation to fit dose-surfaces accounts for density of data-sampling. A) A particle swarm optimizer (PSO) was tested for convergence across several different data densities ranging from 5X5 to 25X25 grids. Within each density range, 25 different dose-response surfaces were fit. At all tested densities for all conditions, a minimum in the log-likelihood was observed after approximately 60 iterations. B) Comparison of the error in final fits of the parameters between three methods PSO alone followed by a non-linear least squares (NLLS) optimizer (Levenberg-Marquardt), Markov Chain Monte Carlo (MCMC) posterior estimation, and PSO seeded MCMC optimization. Y-axis is the L2-norm of the fitted parameters to the true parameters. Across all data densities, PSO seeded MCMC had the highest fit accuracy across different dose-response surface topologies.

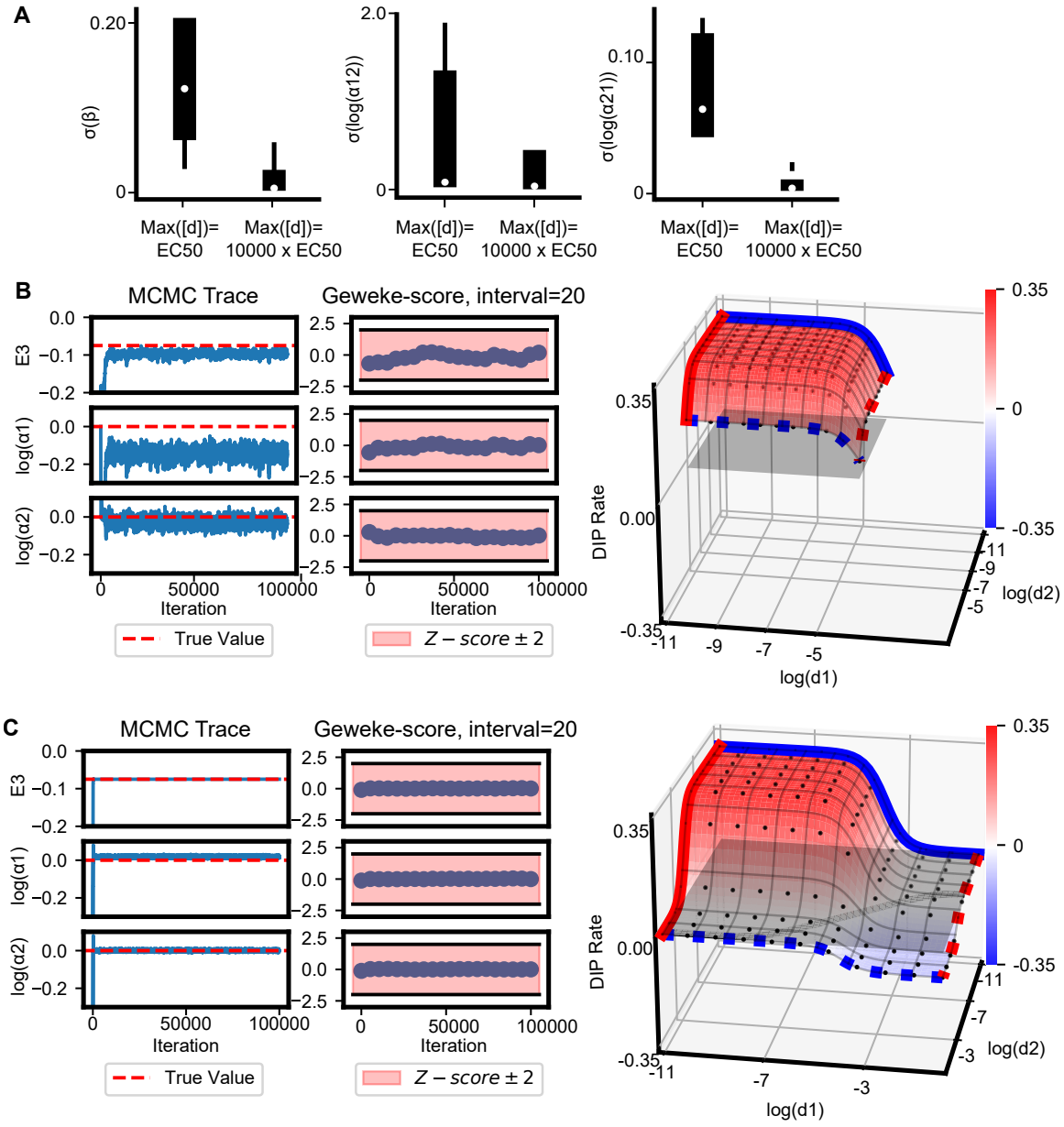

Figure A.2: Bayesian synergy parameter estimation to fit dose-surfaces accounts for dose-response surface coverage. A) Synergy parameter uncertainty as a function of dose coverage. σ is the standard deviation of the MCMC trace. As the dose coverage decreases, there is a commensurate increase in the uncertainty of in the fit across different dose-response surfaces. B) Trace-plots and posterior distributions of $\log(\alpha_{12})$, $\log(\alpha_{21})$, and $E3$ for a surface where max dose is equal to the EC50 (bottom). Red line demarcates the true value. Middle plot is the z-score of 20 segments from the overall sample ordered by trace number. Parameters which have absolute z-scores >2 at any point in the trace are considered not to have converged. C) Trace-plots and posterior distributions of $\log(\alpha_{12})$, $\log(\alpha_{21})$, and $E3$ for a surface where max dose is 10,000 times the EC50 fully capturing the drug effect saturation. Posterior distributions are narrower than for the surface with less coverage corresponding to an increase in uncertainty. However, other factors than dose-selection can contribute to fit uncertainty including experimental noise, density of data, steepness of single drug curves (i.e., the hill coefficient), and quality of priors in the MCMC fit

Table A.2: Description of nested model tiers used in MCMC fit.

Model Tier	Fit Parameters	Approximations
#5	α_{12}, α_{21}, E_3, E_1, E_2, C_1, C_2, h1, h2, E_0, r_1, r_2	1. Rate of transition (r1,r2) $>>$ 1.
#4	α_{21}, E_3, E_1, E_2, C_1, C_2, h1, h2, E_0	1. System obeys detail balance.
#3	α_{21}, E_3, E_1, E_2, C_1, C_2, h1, h2	1. All conditions tier 4 2. E0 is the minimally observed effect.
#2	α_{21}, E_3, E_1, E_2, C_1, C_2	1. All conditions tiers 3,4 2. h1,h2 are from single drug fits or 1 if single fits failed to converge.
#1	α_{21}, E_3, E_1, E_2	1. All conditions tiers 2-4 2. C1,C2 are from single drug fits or the median concentration if single fits failed to converge.
#0	α_{21}, E_3	1. All conditions tiers 1-4 2. E1, E2 are assumed to be the maximally observed effect at maximum concentration of d1 and d2 respectively.

B.5 Calculating the DIP Rate

Traditionally, the efficacy of an anti-proliferative compound is measured as the percent of viable cells (relative to control) after a treatment interval (Fallahi-Sichani et al., 2013); however, it has been recently shown this metric is subject to temporal biases (Hafner et al., 2016; Harris et al., 2016). To address these biases, I previously developed an unbiased metric of drug effect termed the drug-induced proliferation (DIP) rate (Harris et al., 2016). The DIP rate is defined as the steady state proliferation rate after drug equilibration. A positive DIP rate indicates an exponentially growing population, while a negative DIP rate indicates a regressing one. A rate of zero indicates a cytostatic effect, which may result from cells entering a non-dividing state or from balanced death and division (Paudel et al., 2018) I used the available findDIP R package for calculating DIP rates from growth curves which automatically selects the interval after drug equilibration ($https://github.com/QuLab-VU/DIP_rate_NatMeth2016.git$).

B.6 Calculating Loewe, CI, Bliss, and HSA

To compare our method to the prevailing methods for computing synergy, I calculated Loewe, CI, Bliss for the data from the osimertinib screen in Figure 2 and melanoma BRAF/MEK data of Figure 3. Loewe is agnostic to effect metric, and so I applied it directly to the DIP rate. To calculate CI and Bliss, I imputed the percent viability at 72 hours from the DIP rate for each condition. Percent viability is defined as in equation:

$$\%-viable = \frac{Cell\,Count(t = 72hr)_{Treated}}{Cell\,Count(t = 72hr)_{Control}} \tag{B.13}$$

Estimates of percent viability are sensitive to even small differences between initial cell counts in the control and treated wells due to exponential amplification (Harris et al., 2016). To correct for this the bias, a 'matching' control cell count at 72-hours for each treated condition was calculated using equation

$$Cell\,Count(t = 72hr)_{Control} = Cell\,Count(t = 0hr)_{Treated} * 2^{Control\,Growth\,Rate * 72hr} \tag{B.14}$$

where Control Growth Rate is the median of the fitted growth rates for all control wells. Because the automated microscope did not image all the conditions at exactly zero or seventy two hours, I extrapolate and interpolate respectively the cell count at these times from the measured time series.

The Bliss metric only requires marginal data. For each experiment, individually, I calculated a Bliss score as

$$Bliss = PV_1(d_1) * PV_2(d_2) - PV_{1,2}(d_1, d_2) \tag{B.15}$$

where $PV_i(d_i)$ is the %-viability measured for treatment with drug i alone at dose d_i, and $Pv_{1,2}(d_1, d_2)$ is the %-viability measured for the combination treatment. The first term corresponds to the expected viability, assuming independence, while the second term is the measured viability. By this definition, Bliss>0 is synergistic, and Bliss<0 is antagonistic.

Loewe and CI require parameterization of a 1D Hill equation for each drug alone.

$$E = E_m + \frac{E_0 - E_m}{\left(\frac{d}{C}\right)^h + 1} \tag{B.16}$$

CI, as per standard calculations (Chou and Talalay, 1984), further requires that $E_0 = 1$ and $E_m = 0$ and is fit to a linearized, log-transformed version of the hill equation (Chou, 2010) which has been previously critiqued for artificial compression of uncertainty in experimental data leading to poor model fits compared with nonlinear regression (Ashton, 2015). CI dose-response curves were fit using the *scipy.stats.linregress* module. All data points with percent viability greater than 1 were excluded from the CI fit, as $log(\frac{1-pervia}{pervia})$ becomes complex. For some drugs, this left too few points to fit a line, such that CI was undefined for combinations with those drugs. In other drugs,

the fit hill coefficient was negative, and likewise all CI values were undefined for those drugs. For Loewe, I used the single-drug parameters fit by MuSyC.

From these parameterized hill equations, Loewe and CI were calculated using

$$S = -log_{10}\left(\frac{d_1}{D_1} + \frac{d_2}{D_2}\right) \tag{B.17}$$

where D_i is the amount of drug i which, alone, achieves an effect equal to the combination effect, and is calculated from the Hill equation fit for that drug. I take the negative log to transform the synergy values to match Bliss, such that $S > 0$ is synergistic, while $S < 0$ is antagonistic. Because Loewe allows the two drugs to have different Emax, Loewe synergy cannot be calculated for measurements which exceed the weaker drug's Emax because no amount of the weaker drug alone would be sufficient to achieve that effect; therefore, those conditions are undefined.

For calculating HSA, I calculate the difference between the observed effect at each combination concentration and the most efficacious single agent effect at those doses. This difference is integrated across the surface to yield a single value for a particular combination.

B.7 Fitting ZIP, BRAID, Schindler's Hill PDE, and Effective Dose Models

Both ZIP and BRAID were calculated using the R packages available for each method (ZIP's R code is in the supplemental file 1 of the manuscript (Yadav et al., 2015) and BRAID's package is available from:https://cran.r-project.org/web/packages/braidReports/braidReports.pdf). Schindler's Hill PDE model contains no fitting parameters as the dose-response surface is derived purely from the marginal data. In fact, Schindler does not propose a method to estimate synergy from experimental data, but postulates some implementation of perturbation theory could be used to fit experimental data (Schindler, 2017). Therefore, to calculate the synergy of this model, I defined the sum of residuals between the null surface and the experimental data to the metric of synergy. Finally, to fit Zimmer et al.'s Effective Dose Model I used the curve_fit() module of the scipy.optimization package in python. Specifically, the Effective Dose Model, equation 2 in (Zim-

mer et al., 2016) contains parameters for C1,C2, a12, a21, h1, and h2 where the C parameters are the EC50 of the single agents, the parameters are the synergy values corresponding to a change in potency, and the h parameters are the hill slopes of the single agents. In the model, there are no parameters for efficacy because it is assumed the drug effect ranges between zero and one. When this is not true, the Effective Dose Model results in poor fits to the data (Figure 2.12) similar to CI (Figures 2.12,3.15C).

B.8 Identifying DEGs for GO Enrichment Analysis

Differentially Expressed Genes (DEGs) were selected by ANOVA on baseline gene expression data on three clones based on a statistical cutoff of Likelihood Ratio Test (LRT) (p-values < 0.001). Functional enrichment analyses, including GO Term Enrichment and Pathway Enrichment Analysis were done using CRAN Package "Enrichr" (https://cran.r-project.org/web/packages/enrichR/index.html), based on a web-based tool for analyzing gene sets and enrichment of common annotated biological functions (Kuleshov et al., 2016). The enriched GO terms and enriched KEGG pathways were restricted to those with p-values corrected for multiple testing less than 0.001. The top GO Biological Processes included generation of precursor metabolites and energy, electron transport chain, inorganic cation transmembrane transport, and metabolic process. The top GO Molecular Function terms included inorganic cation transmembrane transporter activity, cofactor binding, NAD binding, and ATPase activity. The top GO Cellular Component term was the mitochondria membrane. Top KEGG pathways enriched in the DEGs included metabolic pathways, oxidative phosphorylation, carbon metabolism and TCA cycle (Figure 3.11). Overall, these enriched GO terms and pathways point toward differences in the regulators of metabolic function in the three subclones. This is consistent with previous reports that suggest altered metabolism is implicated in drug sensitivity and melanoma resistance to BRAFi (Parmenter et al., 2014; Hardeman et al., 2017).

Correlation of BRAFi insensitivity was computed for each identified DEG according to DIP Rate at 8μM PLX-4720 for a 10 cell line panel (Table 3.2) Pair-wise comparisons of DEGs was

performed on genes (after low count genes were removed) using DESeq2 pipeline (Love et al., 2014).

B.9 Data Availability

All raw cell counts, calculated DIP rates, DEGs between subclones, and expression data are available in the github repo: https://github.com/QuLab-VU/MuSyC_Cell.git in the folder Data. Additionally, the repo contains all the code required to reproduce all the figures and supplemental figures from the data and is found in the Code_Paper_Figures folder. The subfolders Fig2 and Fig3 contain html folders with interactive plots of all the screened combinations. Open the .html files using a browser. The raw RNAseq is available from GEO at the accession number GSE122041. The software for interactive manipulation of the different parameters to study their contribution to the contours of the dose-response surface is also available in the github repo in the folder MuSyC_App. This folder contains both the matlab source code and a compiled application for the different operating systems. A copy of the github repo at the time of publication is also available from Mendeley Data via the following http://dx.doi.org/10.17632/n8bp8db5ff.

B.10 Functional Genomics Screen

Five siRNA plates from Dharmacon Whole Genome siRNA library (pooled) were used. Plates are 16,17,18,19,22 which comprise the GPCR (16), Protein Kinase (17,18), Phosphatase (19) and Ion Channels (22) drug classes (Figure 3.21). Each siRNA was tested in replicate at 4 unique doses of PLX4720. Each siRNA is pre-stamped into 384-well plate at 500nM concentration. The final concentration of siRNA on cells was 25nM. Concentration of siRNA and RNAiMax during incubation was 0.0125uL lipid/uL and 175nM siRNA. Catalog numbers for siCON (#D-001810-10-05) and siTOX (#D-001500-01-05).

siRNA was added when plating the cells. First 5uL siRNA+lipid in optimem was added to the bottom of plate then 30uL cell mixture was added after 20 minutes of siRNA+lipid incubation time. 600 SKMEL5 cells were plated per well. 24 hours later the drug was added (5uL of 8X

concentration) for a total volume of 40uL. Plates were imaged every 8 hours continously for 96 hours from intitial seeding. DIP rates were calculated according to B.5.